Polymorph Selective Crystallization Using Organized Organic Assemblies as Templates

by

Changzai Chi

A Dissertation submitted to the Graduate Faculty in Engineering in partial fulfillment of the requirements for the degree of Doctor of Philosophy,
The City University of New York

2003

This manuscript has been read and accepted for the Graduate Faculty in Engineering in satisfaction of the dissertation requirement for the degree of Doctor of Philosophy

1/30/2003
Date

Alexander Couzis
Prof. Alexander Couzis
Chair of the Examining Committee

1/30/2003
Date

Charles Maldarelli
Prof. Charles Maldarelli
Co- Chair of the Examining Committee

1/30/2003
Date

Mumtaz Kasir
Prof. Mumtaz Kasir
Executive Officer

Prof. Leslie Isaacs

Prof. Lane Gilchrist

Dr. Daniel A. Green

Supervisory Committee

THE CITY UNIVERSITY OF NEW YORK

To my wife Hua Tan and our son Alan

Abstract

Polymorph selective crystallization using organized organic assemblies as templates

By

Changzai Chi

Advisors: Professor Alexander Couzis and Professor Charles Maldarelli

The size, crystalline phase (polymorphism) and morphology of particles greatly affect the chemical and physical properties of particulate materials. In many applications, such as agrochemical, pharmaceutical and material industries, it is very important to obtain a desired crystalline phase which may exist as several polymorphs. In this research, we have used organized organic assemblies as templates to control the polymorphism of crystals. Compared to the traditional crystallization methods, this approach utilizes the potential of controlling the molecular recognition events which may exist between the incipient nuclei and organized organic assemblies. By using Langmuir monolayers at the air/liquid interfaces and Self-Assembled Monolayers (SAMs) at the solid/liquid interfaces as templates, we have successfully controlled the polymorphism of $CaCO_3$ crystals. Vaterite crystals, which are the thermodynamically unfavored from homogeneous crystallization, have been nucleated by carefully choosing the functional groups of organic assemblies.

Several Langmuir monolayers and SAMs with various properties have been investigated as templates for polymorph selective crystallization of $CaCO_3$. Our experimental results have clearly shown that the electrostatic interaction and stereochemical correspondence between incipient nuclei and organized organic assemblies are the predominant factors in determining the specific nucleation face and the polymorphism of the crystals, while exact geometric matching is not necessary for template directed nucleation of calcium carbonate.

In situ ATR-FTIR was used to investigate the interactions between the templates and the moieties of crystals. The calcium ion binding to the stearic acid headgroups was evident from the increase of carboxylate asymmetric stretching band intensity. Atomic force microscopy (AFM) was used to investigate the morphology development and crystal growth of nuclei on the solid surface at the early stage of template crystallization. The results of AFM showed that nucleation only happened at the very beginning of the process. The frequency of nuclei on the functionalized surfaces is extremely high at the early stage of nucleation. However, only a very small portion of these nuclei (one out of 0.96×10^5) survived and grew into micron-sized particle during crystal growth process.

Acknowledgements

I would like to express my deepest gratitude to my advisors Prof. Alexander Couzis and Prof. Charles Maldarelli for the continuous encouragement, guidance and support during my doctoral study. Without their guidance and inspiration, I would have achieved very little. I am very much in debt to both of my advisors for the numerous helps and advice, not only professionally but also personally.

I would also like to express my great thanks to Dr. Daniel Green from DuPont Central R&D experimental station for his helps and valuable comments and suggestions upon this research. It is always a great pleasure to work with him. I would also like to thank Dr. Paul Meenan, Dr. Sean Dalziel and Dr. Arthur Boxman for all kinds of helps.

I would also like to thank Chandra Sekhar Palla for all kinds of helps and discussions during the past four and half years. Special thanks to Nitin Kumar whose helps are always available when needed. Many thanks to Dr. Fengqiu Fan, Ravi Palaparthi, Hongjie Liu, Ashish Taneja, Jose Lorenzo, and Qing Song,

I would also like to thank Zhen Rong Xu and Andy Eng for all kinds of help and encouragement during the course of my Ph.D.

I would also like to thank my parents for their constant support and sacrifice.

Finally, I would like to thank my wife Hua Tan for her constant support, patience, and encouragement during my thesis preparation.

Table of Contents

List of figures

List of tables

Chapter 1

Template directed nucleation

1. 1 Introduction

Crystals, such as diamond and quartz, are familiar to everyone because of their external beauty. Below such beauty lies a regular repeating internal structure. A crystal is a solid composed of a regularly periodic repeated arrangement of atoms in three dimensions. This regular arrangement is the reason for the development of faces on diamonds or quartz [1,2]. Polymorphism is the ability of a substance to exist as two or more crystalline phases that have different arrangement of the atoms or molecules in the crystal lattice [3]. The most familiar example of polymorphism is diamond and graphite, which are both composed of carbon atom but arranged in a different way. This results in the totally different properties of diamond and graphite (see figure 1.1).

Remarkably, differences in properties of different polymorphs arise from the different ways the atoms or molecules arrange inside the crystal. If polymorphs of a given substance have unrelated lattice structures, they will have the most striking difference in properties. Change from one crystalline state to another will require a change in the state of chemical bonding. For example, completely different chemical bonding exists for the diamond/graphite and white/red phosphorus polymorphic pairs. Polymorphism also can

arise from structurally related lattices. For this latter kind of polymorphism, the rearrangement of the units from one lattice type to another is much easier compared to the previous one. For the polymorphism among molecular lattices, which is very common in agrochemical and pharmaceutical products, polymorphism can results from conformationally similar molecules or conformationally different molecules. Harry G. Brittan and Stephen R. Byrn have summarized several pharmaceutical examples for both cases in their book [4].

It is very important to obtain a desired crystalline form in many industries. Traditional methods, such as seeding [5,6], change of solvent [7], sublimation, vapor diffusion, thermal treatment, crystallization from melt, changing solution pH, thermal desolvation of crystalline solvates, growth in the presence of additives, grinding are difficult to control and sometime unsuccessful [8-12]. An alternative new method for selective polymorph crystallization is highly demanded.

Traditional crystallization methods have utilized the different interactions between the moieties of the crystals and the solvent in the bulk solution to control polymorphs by varying the crystallization parameters. But the interfacial interactions between the faces of crystals and the foreign nucleation agents, which are especially important for the heterogeneous nucleation, have not been explored by the traditional methods. In contrast, the template directed crystallization utilizes the specific molecular recognition events,

which may exist between the incipient nuclei and organized organic assemblies. In this research, we used Langmuir monolayer and SAMs as nucleation agents to control the polymorphs of the crystals. By modifying the functional groups of the engineering templates, we were able to adjust the interaction between the incipient nuclei and the organized organic assemblies and thus control the polymorphs of crystals.

1.2 Background

Polymorphism is a widespread phenomenon for both organic and inorganic substances. Different polymorphs of a substance can exhibit a variety of different physical properties. In the agrochemical and pharmaceutical industry, it is very important to obtain a desired crystal form, which can exist in several different polymorphs. The Food and Drug Administration's(FDA's) drug substance guideline states that appropriate analytical procedure should be used to detect polymorphic and amorphous forms of the drug substance. The choice of the polymorphs to be produced is governed both by the properties of the solid state form and its relevance to the anticipated application. Table 1.1[13] lists possible property differences among polymorphs for a substance. For pharmaceutical and agrochemical applications, properties such as dissolution rate, stability and absorption profile are very important, which can affect the physicochemical activity of the active compound.

Table 1.1 Different physical properties among various polymorphs

• Packing properties a. Molar volume and density b. Reflective index c. Conductivity, electrical and thermal d. Hygroscopicity
• Thermodynamic properties a. melting and sublimation temperatures b. Internal energy (i.e., Structural energy) c. Enthalpy (i.e., Heat content) d. Heat capacity e. Entropy f. Free energy and chemical potential g. Thermodynamic activity h. Vapor pressure i. Solubility
• Spectroscopic properties a. Electronic transitions (i.e., ultraviolet-visible absorption spectra) b. Vibration transitions (i.e., infrared absorption spectra and Raman spectra) c. Rotation transitions (i.e., far infrared or microwave absorption spectra) d. Nuclear spin transitions (i.e., nuclear magnetic resonance spectra)
• Kinetic properties a. Dissolution rate b. Rate of solid state reactions c. Stability
• Surface properties a. Surface free energy b. Interfacial tensions c. Habit (i.e., shape)
• Mechanical properties a. Hardness b. Tensile strength c. Compactibility, tableting d. Handling, flow, and blending

Source: Ref. [13]

Example drug substances include the antibiotic ampicillin (bioactivity differences due to the different solubility and absorption rate), the steriod prednisolone(dissolution rate) and more recently the anti-AIDS drug protease inhibitor "Ritanovir" (different dissolution rate and possible absorption profile)[9]. Also compactibility for tableting is an important consideration. For example, Paracetamol (acetaminophen) is an analgesic drug that is used worldwide in the manufacture of many millions of tablets and other forms every year. The crystal structures of two known polymorphs are monoclinic (form I) and orthorhombic (form II). Monoclinic paracetamol, which is commercially used, is not suitable for the direct compression into tablets. So the ability to produce form II in quantity has attracted much interest because of the potential commercial benefits to be gained by not using binders during the manufacture of tablets[6].

Two well-known examples of polymorphism in inorganic materials are carbon and calcium carbonate. Carbon has two polymorphs, diamond and graphite. The crystal structure and morphology of diamond and graphite are shown in figure 1.1. Another example is calcium carbonate. Calcium carbonate has three different polymorphs, calcite, aragonite and vaterite. These three crystals belong to different crystal systems and have very different physical properties as shown in table 1.2 [14].

Table 1.2 Crystallography and Physical Properties of Calcium Carbonate

Polymorphs	Calcite	Vaterite	Aragonite
Crystallo-graphy	Trigonal-Hexagonal Scalenohedral R3-c	Hexagonal-Dihexagonal Dipyramidal, P63/mmc	Othorhombic-Dipyramidal Pmcn
Cell Dimension	A=4.986 C=8.5	A= 7.135 C=16.98	A=4.95 B=7.97,C=5.74
Density	2.71	2.54	2.93
Hardness:	3 - Calcite	3 - Calcite	3.5-4 - Copper Penny-Flourite
Cleavage:	[1011] Perfect.	—	[010] Distinct
Optical Properties	Uniaxial (-), e=1.486, w=1.64-1.66, bire=0.1540-0.1740	Uniaxial (+), w=1.55, e=1.65, bire=0.1000.	Biaxial (-), a=1.529-1.53, b=1.68-1.682, g=1.685-1.686, bire=0.1560
Stability	Most stable	Least stable	unstable

At room temperature, calcite is the most thermodynamically favored form and vaterite is the least thermodynamically favored form. Because of their well-known crystal structures and morphologies (figure 2.2), polymorphs of calcium carbonate are chosen as model crystals in this research.

In this research, we have shown how the polymorphs of the crystalline materials can be controlled by template directed nucleation using functional surfaces. By choosing a proper functional group of template, thermodynamically unfavored form of vaterite, instead of calcite, will be nucleated.

1.3 Thermodynamics of crystallization

From the previous section we saw that different polymorphs of a substance have very different physical properties and this is very important in many industrial applications. The difference in properties among polymorphs is due to the different ways the atoms or molecules arrange inside the crystal lattice. So understanding how to control the arrangement of atom/molecules inside crystal is a very important subject but remains a mystery for most crystals. It is impossible for us to put atom/molecules into crystalline lattice one by one, but we can control the arrangement of atom/molecules by some other approaches. So it is important for us to understand the thermodynamics during the crystallization process.

There are two steps during the crystallization process. Firstly, the atoms/molecules aggregate to form nuclei. Secondly, the growth of the nuclei forms the larger crystalline particles. Compared to the crystal growth, nucleation is more crucial to the process. It usually will decide which crystalline form we will get during the crystallization process. Based on whether there are foreign agents or not, nucleation is considered to be

homogenous nucleation and heterogeneous nucleation. Figure1.3 shows the heterogeneous nucleation of a solid on a nucleation substrate.

In the nucleation process, two kinds of energy changes must be considered:

The volume free energy released by the phase transition and the interfacial energy required to form the new solid surface of the nucleus.

$\Delta G_t = \Delta G_v + \Delta G_s = -nkT \ln (S) + \gamma A$

Where S is the supersaturation and γ is the interfacial free energy of nuclei. For the homogenous nucleation (hm), only the nucleus/liquid (nl) interface is involved:

$\gamma_{hm} = \gamma_{nl}$

However, for the heterogeneous nucleation (ht), the interfacial energy term is given by the sum of interfacial energies of the nucleus-liquid (nl) and nucleus-substrate (ns) interfaces minus that for the liquid-substrate interface that is displaced. This is given by: 15,16

$\gamma_{ht} A_{ht} = \gamma_{nl} A_{nl} + (\gamma_{ns} - \gamma_{ls}) A_{ns}$.

Figure 1.4 show the free energy changing during the nucleation process. From the figure we can see that the important parameter during nucleation process is the free energy change for the critical nucleus formation, which in turn can be directly related to the interfacial energy of all interfaces involved. By choosing the right surface, we should be able to reduce the total interfacial energy form dashed curve to solid curve (Figure

1.4). So the total free energy is reduced and the critical radius of nuclei is decreased. By this way the rate of nucleation is increased and the desired polymorph can now continue to grow.

If we have two different polymorphs A and B, It is possible for us to design such a template that the interfacial energy between template and polymorph A (γ_{nsA}) is much smaller than that of B (γ_{nsB}) because of their different interaction with the substrate. Thus polymorph A will be induced due to the reduced interfacial energy. This is the theoretical basis for the templated selective polymorph crystallization. However, The details of selection mechanism remain unclear, such as how the ions in the crystalline lattice interact with the template and reduce the interfacial free energy between them. There are still a lot of difficulties relating experiments that measure parameters such as interfacial free energy with those are designed to probe the surface structure and chemical moieties.

1.4 Template crystallization in nature—Biomineralization and biomimetic synthesis

Biomineralization is one of the most complicated and exquisite processes in the nature. Organisms have been producing mineralized skeletons and shells for the past 550 million years. More than 60 different minerals, such as diatom frustules, coccoliths, shells and bones, are known to be formed biologically. These include the three polymorphs of calcium carbonate: calcite, aragonite and vaterite. Organisms have evolved many

strategies for improving these materials at almost all-hierarchical levels from Angstroms to millimeters [17]. Figures 1.5, Figure 1.6 and Figure 1.7 are some examples of biominerals from literatures [18,19].

A lot of efforts have been put into understanding the biomineralization process. The study of biomineralization will offer valuable insight into the scope and nature of material chemistry at inorganic-organic interface. The interest of biomineralization is how this organic architecture can associate with inorganic solids to give unique and exquisite biominerals in which the structure, size shape, orientation, texture and assembly of the mineral constituents are precisely controlled. Although we still have a long way to go in understanding this process, the following steps are commonly believed during the biomineralization: [19-21]

- Supramolecular pre-organization
- Interfacial molecular recognition (templating)
- Cellular processing

The first step of biomineralization is the construction of an organized reaction environment for mineral deposition. Two kinds of macromolecules are involved in this process. One of them is referred as 'framework macromolecules'. These molecules will provide a three dimensions matrix or frame in which the mineral will form. They are usually insoluble and hydrophobic. Common examples of framework molecules are Gly-

and Ala- rich proteins (structurally similar to silk-fibroin) in mollusc shell, type I collagen in bone and tooth dentin, amelogenin in tooth enamel, α-chitin in crustaceans and β-chitin in mollusc shells. The second type is referred as 'controlled macromolecules'. These are usually acid proteins rich in aspartic acid, glutamic acid, and often in association with sulphated polysaccharides. They are usually the quantitatively minor components and are assembled on the framework macromolecules. The crystallization then take place at the interface between the control protein and aqueous environment. [20,21]

The second step of biomineralization is interfacial molecular recognition (templating). It involves the controlled nucleation of inorganic clusters from aqueous solution. The pre-organized architecture consisting of functional surface in the first step served as templates for inorganic nucleation. Heterogeneous nucleation at the appropriate 'functional site' is initiated. The interaction includes electrostatic, structural and stereochemical complementarity. The morphology, location, orientation, and crystalline phase depend on the structure and chemistry of the interfaces between organic template, mineral and medium [22-24].

The final step of biomineralization is cellular processing which is associated with a variety of constructional processes involving larger-scale cellular activity. In this stage,

biominerals are endowed with unusual texture and shapes, giving rise to elaborate ultra- and micro-structural assemblies.

By the above strategies, organisms are able to synthesis the ordered structure scaling from Angstroms to millimeters.

Although the details of biomineralization are still a puzzle, a lot of efforts have been put into mimicking this exquisite process — biomimetic material synthesis [25-30]. The basic constructional processes of biomineralization can provide useful archetype for molecule-scale building in inorganic materials chemistry. Mann calls this as 'molecular tectonics' in his review paper [17,20]. The connections between molecular tectonics, biomineralization and biomimetic synthesis are shown as Figure1.8.

1.5 Langmuir, Langmuir-Blodgett and Self-Assembled Monolayers

Langmuir monolayers are monomolecular films that form when amphiphilic molecules spread at the air/water interface. They can be described as two-dimensional systems that can exist in several different surface phases such as gaseous state (G), 'liquid expanded' state (LE), 'liquid-condensed' (LC) and solid state (S) [31-33]. At different states, the intermolecular spacing is different. The interaction between monolayer and aqueous solution under monolayer depends on the headgroup (hydrophilic part) of monolayer, the pH and ion in the subphase[34-37]. By choosing a proper

headgroup, Langmuir monolayers can serve as templates for crystallization from the subphase [38,39].

Self-assembled monolayers (SAMs) are ordered molecular assemblies formed by the adsorption of an active surfactant on a solid surface. Self-assembling surfactants, the building blocks of SAMs, consist of a head group, which attach to the solid surface, an intermediate chain, and a terminal functional group (Figure 1.9). The ability to tailor both head and tail groups of the constituent molecule have made SAMs suitable for numerous applications in the fields of electrochemical processes, adhesion, wetting, lubrication, corrosion, template crystallization, and modeling complex interfaces of membranes and polymers. Based on the different interactions between the head group of the self-assembling surfactants and the substrate, SAMs have been divided to three most common types [40,41]:

- Carboxylic acids on native oxidized silver and aluminum oxide surface.
- Organosilicon compound on hydroxylated surfaces [42,43]
- Organosulfur adsorbates on metal and semiconductor surfaces.[44,45]

For all three types of SAMs the self-assembling surfactants chemisorbs at the solid-monolayer interface. More specifically, for carboxylic acid on oxide surfaces system the interaction is an acid-base reaction, and the driving force is the formation of a surface salt between the carboxylate anion and a surface mental cation. The formation of SAMs of

oganosilicon requires hydroxylated surfaces as substrates. The driving force for this self-assembly is the formation of polysiloxane, which is connected to surface silanol groups (-SiOH) via Si-O-Si bonds. For the organosulfur SAMs, the driving force is that sulfur compounds have a strong affinity to the transition mental surfaces, such as gold and silver. The energy associated with these chemisorptions is of the order of tens of kcal/mol. So the monolayers of SAMs are much stronger than that of Langmuir-Blodgett films. By choosing different intermediate chain and terminal functional group, we are able to obtain a variety of functional surfaces with different properties and conformation. SAMs are good candidates as templates for selective crystallization because they allow us to tailor surface properties of the templating surface at will and with ease.

1.6 Templated crystallization using Langmuir monolayers

In nature, organisms use macromolecules, (e.g. acidic proteins) as templates for nucleation and crystal growth and have successfully fabricated various biominerals over the span of millions of years. Scientists and engineers from a variety of disciplines are striving to understand this complicated biochemical process and mimic it. Although some progress has been made in this area recently, it is almost impossible for researchers to understand this process completely in the recent future. Until now, most of the work has been done is *in vitro*, It is still unknown what happens *in vivo* at the early stage of the nucleation process[24,26,46-49].

Even though, at this point it is very difficult to understand and control biomineralization processes, a number of researchers have tempted to mimic this process to control the morphology and direction of crystal by using a simpler but promising method, such as Langmuir, Langmuir-Blodgett monolayers and SAMs as template for nucleation. Several inorganic and organic crystals have been templated under Langmuir monolayer at air/liquid interface as summarized in Table1.3. Two most typical systems include polymorph control for calcium carbonate and the control of crystal habit for α-glycine.

1.6.1 Controlling polymorphs of $CaCO_3$

Calcium carbonate has three different polymorphs, calcite, aragonite and vaterite. These three crystals belong to different crystal systems and have very different physical properties. At room temperature, only calcite is stable form and vaterite is the thermodynamically most unfavorable form. Mann and his coworker [38,50-52] have shown that the polymorphs of calcium carbonate can be controlled by using Langmuir monolayer as templates. Several different monolayers, such as stearic acid, octadecylamine, octadecanol and cholesterol have been investigated in their research. $CaCO_3$ crystallization under octadecanol monolayer was inhibited and crystal growth in the presence of cholesterol films was similar to the control experiment. However, nucleation under octadecylamine monolayers gave vaterite aligned either along the [00.1]

or [11.0] crystallographic axes. For stearic acid monolayers, the polymorphs obtained depend on the concentration of calcium ion. At total $[Ca^{2+}]$=9mM, calcite with the [1$\underline{1}$.0] axis perpendicular to the organic surface is induced, while at $[Ca^{2+}]$=4.5 mM, oriented vaterite with the [00.1] axis normal to the monolayer is templated.

The inter-headgroup space of stearate is about 5Å when compressed on an aqueous subphases. The Ca^{2+}—Ca^{2+} distances between coplanar atoms in the (1$\underline{1}$.0) face of calcite are 4.96 Å and 8.6 Å in the two co-planar directions. So there seems to be a geometric matching between calcite lattice face and stearate monolayer. Based on their results and analysis, these authors believed that the following three factors are important for the templating crystallization: (1) positively charged calcium ion accumulation under the negatively charged stearate head group, (2) geometric matching of lattice distances (for calcite) and (3)stereochemical correspondence between carboxylate and carbonate groups at monolayer/crystal interface. Mann and coworkers also pointed out the reason of the change from calcite to vaterite nucleation on stearate films at low $[Ca^{2+}]$ is that the extent of Ca^{2+} binding is important for the oriented calcite nucleation because of the lattice geometric matching. However, this argument seems to be contradicted to the recent work by Lochhead and coworker [53]. In their work, monolayer electrostatic parameters and ion distributions in the interfacial aqueous solution have been calculated using a Gouy-Chapman-Stern electric double-layer model that incorporates the multiple, multivalent

cation and anions. Their results show that the calcium binding concentration is quite similar for 4.5 and 9.0 mM Ca^{2+} solutions in the Stern layer, Γ_{Ca}=0.22 and 0.26 respectively. Furthermore, due to their calculation, Γ_{Ca} is ≤0.5 for all experiment conditions. So Ca^{2+}—Ca^{2+} spacing in the bound layer is larger than the headgroup COO^-—COO^- Spacing. This means that the geometric matching of lattice distance between (1$\underline{1}$.0) faces of calcite crystal and stearate monolayers can not account for the calcite nucleation even at high Ca^{2+} concentration either. These authors believed that cation-to–anion ratio near the carboxylic acid monolayer is more important factor for calcium carbonate crystallization. The departure from lattice ion stoichiometry is significantly larger for low [Ca^{2+}] solutions, which may favor vaterite because of its more disordered structure.

Other monolayers have been used as templates for $CaCO_3$ crystallization include superamolecule 5-hexadecyloxyisophthalic acid (C_{16}ISA). In this case, 75%—95% of crystals templated under monolayer are aragonite, with their [010] axis aligning perpendicular to the monolayer surfaces [54].

1.6.2 Oriented growth of α-glycine crystals

Another successful example for the templated crystallization is the oriented growth of crystal of the α-glycine under chiral Langmuir monolayers comprising amphiphilic α-

amino acids. Landau and coworker [39,55,56] have reported that the orientation of the crystal of the α-glycine depends on the R or S configuration of the monolayers. Monolayers of α-amino acid of R configuration, containing long hydrocarbon chains, induce glycine to crystallize with its (010) face attached to the monolayer, while the corresponding S amino-acid monolayers induce attachment of the ($0\underline{1}0$) face of glycine. Twelve different resolved α-amino acids have been used as template for crystallization by these authors[56]. Two of these monolayers did not lead to crystallization at the interface, while others yielded a fast crystallization with partially or complete orientation. They believe that the packing of polar head groups determines the nucleation rate and the degree of orientation of the α-glycine crystal attached to the monolayers. The results of synchrotron grazing incidence X-ray diffraction and reflectivity measurement also support their conclusion. The recent results showed there exists two-dimensional (2-D) crystalline packing arrangement of enantiomerically pure α amino acid monolayer on the water and the glycine aqueous solution [57].

1.6.3 Other examples of templated crystallization under Langmuir monolayers.

Other crystals also have been templated under Langmuir monolayers at air/liquid interface, such as $BaSO_4$ under eicosanoic acid and n-eicosyl sulfate monolayers [58], Hydroxyapatite under dihexadecylphosphate [59] or stearic acid [60] monolayers,

Benzenesulfonic acid under GUAN-ODS monolayer [61,62]. Several phospholipid monolayers, such as dipalmitoylphosphatidylcholine (DPPC), Dimyristoylphosphatidylserine (DMPS), Dimyristoylphosphatidylethanolamine (DMPE), Dimyristoylphosphatidic Acid (DMPA), have been used by Letellier and coworkers [63] to investigate the template crystallization of calcium oxalate monohydrate.

1.7 Templated crystallization using SAMs

SAMs are molecular assemblies covalently attached to the rigid substrate. So the interfaces formed by SAMs are chemically and structurally more stable than Langmuir or Langmuir-Blodgett monolayers. Therefore SAMs are more practical for templated crystallization than Langmuir monolayers. Some researches have been carried out using SAMs as template for crystallization as summarized in table 1.4.

The crystallization of $CaCO_3$ was investigated on surfaces of alkanethiolate SAMs on gold [64-67], and recently it was reported that the crystal orientation of calcite can be partially controlled by SAMs of functionalized alkanetiols [68,69]. SAMs of Organosilane also have been used to promote the heterogeneous nucleation and growth of ion hydroxide films [70] and to study the effect of surface chemistry on calcite nucleation and growth [71]. SAMs and mixed SAMs of alkanetiol also have been used to control the nucleation and growth of α-glycine [72] and malonic acid [73].

As we can see, although some research has been carried out using SAMs as template for crystallization, only few of these have successfully controlled the polymorphs of crystals.

1.8 Outline of research

Although some work has been tried to mimic the biomineralization process by using Langmuir monolayers or SAMs as templates for crystallization, only few studies has very successfully controlled crystal polymorphism, which is very important in a lot of industrial applications. The reason may lie in that only a narrow range of functional groups has been tried and the structure and arrangement of functional molecules on the surfaces have not been constructed properly.

1.8.1 Objective

The overall objective of our research is to develop a method for the crystallization of a desired form of a crystalline material, which can exist in several different forms (or polymorphs). The approach is based on using Langmuir monolayers and functionalized solid surfaces as nanotemplates for heterogeneous and selective nucleation and growth of three-dimensional seed crystals of the desired polymorph. We have focused on the development of the templating surfaces. The template development involves the selection of chemical moieties to be attached to a surface, and the determination of their density

and arrangement, such that, when the constituents of the crystal are exposed to the surface, a particular face of the desired polymorph assembles from solution. Once this nucleating face forms, growth of the three-dimensional seed crystal follows. The templates are developed through a rational, molecular design approach. Calcium carbonate was investigated as a model crystal system to show how polymorphs can be controlled by a templating surface developed as described above.

1.8.2 Templated crystallization under Langmuir monolayers

At the first part of this project, we used Langmuir monolayers at air/liquid interfaces as templates for polymorph selective crystallization. Several kinds of monolayers with different functional groups have been investigated. Monolayers with negatively charged (stearic acid and perfluorododecanoic acid), positively charged (octadecylamine) and without charge (octadecanol) were used as template for polymorph selective crystallization of $CaCO_3$. The aim of this part of the research is to template vaterite, which is the thermodynamically most unfavorable form of $CaCO_3$ and usually is very difficult to obtain, by choosing a proper Langmuir monolayer as template. The effects of the headgroup of monolayers, the pH of the supersaturated solution and also the hydrophobic part of the amphiphilic molecule on the crystalline phases induced under the monolayer have been investigated.

1.8.3 Templated crystallization using SAMs

Compared to the Langmuir monolayers at air/liquid interface, SAMs on the solid surfaces are more robust and suitable for industrial applications. At this part of the research, we utilized the specific interaction between the incipient nuclei and the functional groups of SAMs to control the polymorphs of $CaCO_3$ crystals. Several SAMs with different functional groups have been investigated to show how the different polymorphs of $CaCO_3$ can be selectively induced on the functionalized solid surfaces. The effects of terminal groups of the SAMs, substrate used (Au or Si) and the properties of intermediate chains on the templated crystallization have been investigated. Both SAMs of organosilicon on silicon surfaces and organosulfur on gold surfaces were used as templates for crystallization.

1.8.4 Interactions potentially responsible for the templating process

In this part of research, we investigated the interactions between incipient nuclei and organized organic assemblies, which decide the polymorph types of crystals induced by templates. Infrared reflection experiments (FTIR) were used to determine the binding mode and extent of binding of the crystal constituents on the templates. In addition, Atomic force microscopy (AFM) images during the early stages of nucleation on the functional surface was investigated to show how the templating occurs within the first few layers of the developing crystals.

Table 1.3 Template directed nucleation using Langmuir monolayers

System	Monolayer	Conc. (mM)	Mineral	Nucleated face	Refs
$CaCO_3$	Stearic Acid	9	Calcite	(1$\underline{1}$.0)	38,50-52
		4.5	Vaterite	(00.1)	
	Octadecylamine	4.5-9.0	Vaterite	(00.1),(11.0)	
	Octadecanol	4.5-9.0	Calcite	Nonoriented	
	Cholesterol	4.5-9.0	Calcite	Nonoriented	
$CaCO_3$	C_{16}ISA	9-9.5	Aragonite	(01.0)	54
$CaCO_3$	Stearic Acid	8	Calcite	(01.0)	74,75
	Octadecylsulfate			(00.1)	
	m-PDA			(01.2)	
$CaCO_3$	Porphyrin	8.5	Calcite	(00.1)	76,77
$BaSO_4$	n-eicosyl sulfate	0.16	Barytes	(100)	58
	Eicosanoic acid	0.16	Barytes	(010)	
Hydroxyapatite	Stearic Acid	5.0	HAp	(00*l*)	60
	$(CH_3(CH_2)_{15})_2PO_4H$	3.8	HAp	(*h*00)	59
CaC_2O_4	DPPC, Eicosanol	0.22	COM(type I)	(1$\underline{0}$1)	63
	DMPS, DMPA, Eicosanoic acid		COM(type II)	Unknown	
	DMPE,		COM(type I)	Nonoriented	
BSA	GUAN-ODS	—	Diphenyl sulfone	(100)	61,62
Glycine	(R)-9	4.66M	α-Glycine	(010)	39,55, 56
	(S)-9			(0$\underline{1}$0)	
	(R)-10			(010)	
	(S)-10			(0$\underline{1}$0)	
Glycine	(R) or (S) leucine	S=1.05	Triangular prism (α)	(010) or (0$\underline{1}$0)	78,79
	(R,S)- α-AOA		Thin plate		
	Triton X-405		Bitriangular prism (α)		
	(R,S)-α-AOA+ triton X-405		Thin plate + Bitriangular prism		

***Amphiphilic surfactant used for template crystallization:**

Stearic Acid: $CH_3(CH_2)_{16}COOH$, Octadecylamine:$CH_3(CH_2)_{17}NH_2$

Octadecanol: $CH_3(CH_2)_{17}OH$, Cholesterol: C27H45OH

C_{16}ISA: 5,hexadecyloxyisophthalic

m-PDA: Monomeirc 10,12-pentacosadiynoic acid

n-eicosyl sulfate: $CH_3(CH_2)_{19}OSO_3^-$, Eicosanoic acid: $CH_3(CH_2)_{19}COOH$

DPPC: Dipalmitoylphosphatidylcholine, DMPS:Dimyristoylphosphatidylserine,

DMPE: Dimyristoylphosphatidylethanolamine, DMPA: Dimyristoylphosphatidic Acid,

GUAN-ODS: Guanidine hydrochloride+Sodium 1-octadecanesulfonae

DHP: Dihexadecylphosphate $(CH_3(CH_2)_{15})_2PO_4H$

(S)-1: 5-α-cholestan-3-β-$OCOCH_2CH(NH3^+)CO_2^-$

(R)-2: $(X)_2NCOCH_2CH(CO_2H)SCH_2CH(NH_3^+)CO_2^-$, ($X=CH_3(CH_2)_{14}COOCH_2CH_2^-$)

(S)-3: $CF_3(CF_2)_9(CH_2)_2OCOCH_2CH(NH_3^+)CO_2$-

(S)-4: $CH_3(CH_2)_{14}CONH(CH_2)_3CH(NH_3^+)CO_2$-

(R)-5: $CH_3(CH_2)_{17}OCO(CH_2)_2CH(NH_3^+)CO_2$-

(S)-5: $CH_3(CH_2)_{17}OCO(CH_2)_2CH(NH_3^+)CO_2$-

(R)-6: $CH_3(CH_2)_1CH(NH_3^+)CO_2$-

(S)-6: $CH_3(CH_2)_1CH(NH_3^+)CO_2$-

(R,S)-6: $CH_3(CH_2)_1CH(NH_3^+)CO_2$-

(S)-7: $CH_3(CH_2)_{17}NHCOCH_2CH(NH_3^+)CO_2$-

(S)-8: $CH_3(CH_2)_{17}NHCO(CH_2)_2CH(NH_3^+)CO_2$-

(R)-9: $CH_3(CH_2)_{14}CONH\ (CH_2)_4CH(NH_3^+)CO_2$-

(S)-9: $CH_3(CH_2)_{14}CONH\ (CH_2)_4CH(NH_3^+)CO_2$-

(R)-10: $CH_3(CH_2)_{14}CONH\ (CH_2)_2CH(NH_3^+)CO_2$-

(S)-10: $CH_3(CH_2)_{14}CONH\ (CH_2)_2CH(NH_3^+)CO_2$-

(R)-11: $CH_3(CH_2)_{17}OCO\ CH_2CH(NH_3^+)CO_2$-

(S)-11: $CH_3(CH_2)_{17}OCO\ CH_2CH(NH_3^+)CO_2$-

(S)-12: $CH_3(CH_2)_{11}OCO\ CH_2CH(NH_3^+)CO_2$-

*Note:

COM: Calcium Oxalate monohydrate

BSA: Benzenesulfonic acid

HAp: Hydroxyapatite, $Ca_{10}(PO_4)_6(OH)_2$

Table 1.4 Template directed nucleation using SAMs

System	Monolayer	Conc. (mM)	Mineral	Nucleated face	Refs
$CaCO_3$ (thiol) (22 °C)	C11PO3H,C11OH ,C16SH,C16COO H,C12SH, C16H	10	Calcite + vaterite	V (00.1) +(01.0)	64-67
	C11COOH, C10SO4Na		Calcite	C (00.1) +(11.0)	
	C3SO3Na		C+V+A		
$CaCO_3$ (thiol on Au)	$HS(CH_2)_{15}CO_2^-$	10	Calcite	(01.5)	68,69
	$HS(CH_2)_{11})OH$		Calcite	(10.4)	
	$HS(CH_2)_{11}SO_3^-$		Calcite	(00.1)	
	$HS(CH_2)_{11}PO_3^{2-}$		C+V(99:1)	—	
	$HS(CH_2)_{15}CH_3$		C+V(2:1)	—	
	$HS(CH_2)_{11}(CH_3)_3^+$		NO Cryst	—	
$CaCO_3$ (Siloxane)	APS	2.5	Calcite	(10.4)	80
	APS-DCDA			(00.1),(11.0)	
	APS-NTA			(11.0),(11.3),(11.6)	
	$APS-POCl_3$			(00.1)	
Iron hydroxide	Sulfonated polysterene sulfonated SAMs	0.1~100	goethite films	(020)	70
CaC_2O_4 (Siloxane)	Imidazole, (Si) Thiazolidine-carboxylic Acid	0.4	COM (induced)	Not Available	71
	Methy l, Bromo		inhibited		
Malonic acid(thiol) (HOOCC H_2COOH)	$-(CH_2)_{11}COOH$	Sublimation	—	(001)	73
	$-(CH_2)_{15}COOH$		—	—	
	$-(CH_2)_{11}CH_3$ $-(CH_2)_{11}COO\ CH_3$		—	random	
Glycine	I (-OH)	S=1.25	α-Glycine	(011)	72
	I+III (1:1)			(*h0l*), (101)	
	II			(105)	
	II+III(3:1)			(121)	
	II+III(1:3)			(010)	

*Note
APS: (3-aminopropyl)triethoxysilane,
NTA: Nitrilotriacetic Acid, DCDA: Docosanedioc Acid,
A: aragonite, C: calcite, V: vaterite
I: 4'-hydroxyl-4-mercaptobiphenyl
II: 4-4-(mercaptophenyl)-pyridine
III: 4'-methyl-4-mercaptobiphenyl

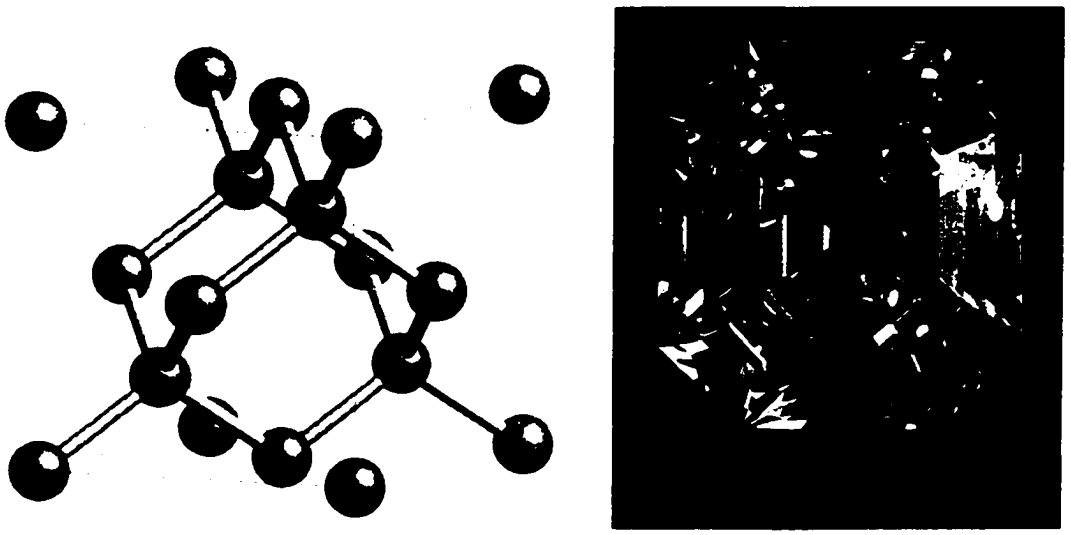

(a) diamond

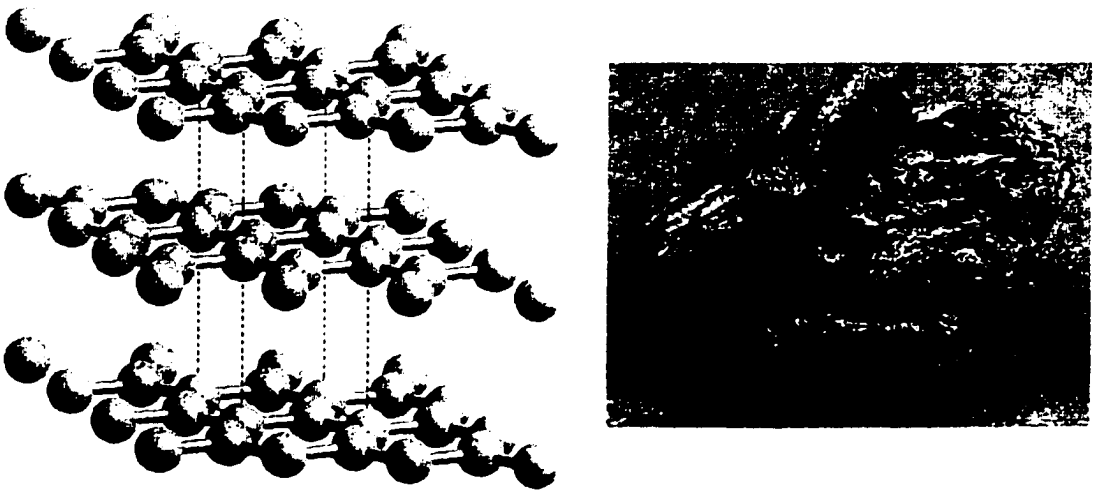

(b)graphite

Figure 1.1 Morphology and crystal structure of diamond and graphite

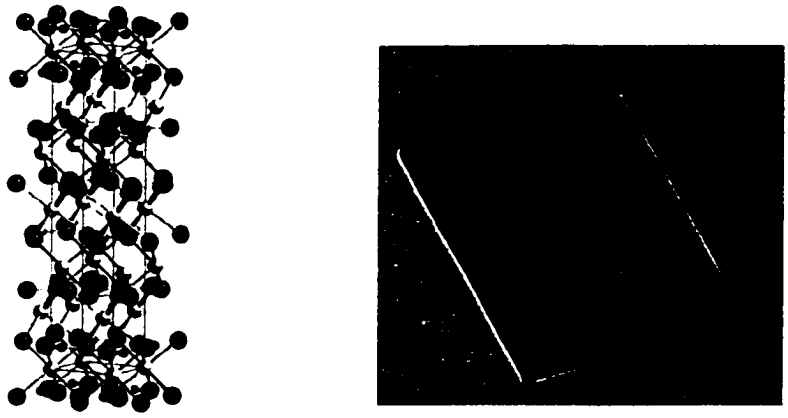

(a) calcite

(b) vaterite

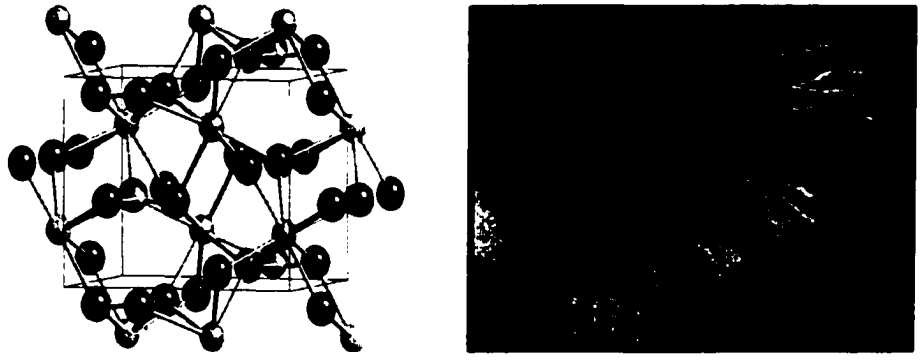

(c) aragonite

Figure 1.2 Morphology and crystal structure of calcite, vaterite and aragonite

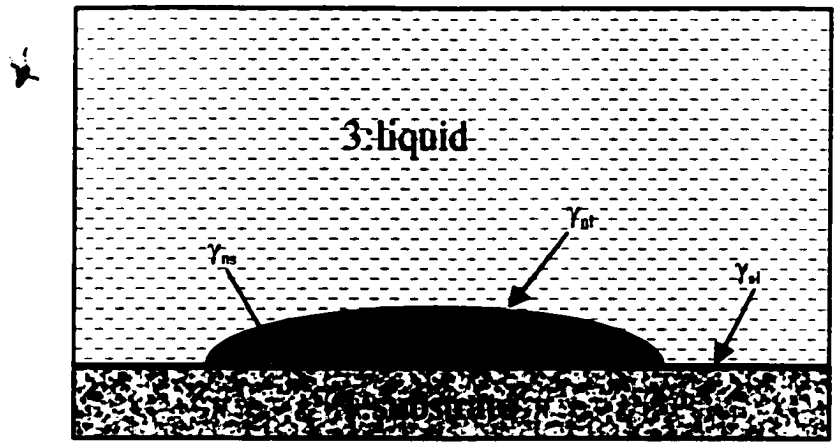

Figure 1.3 Heterogeneous nucleation process

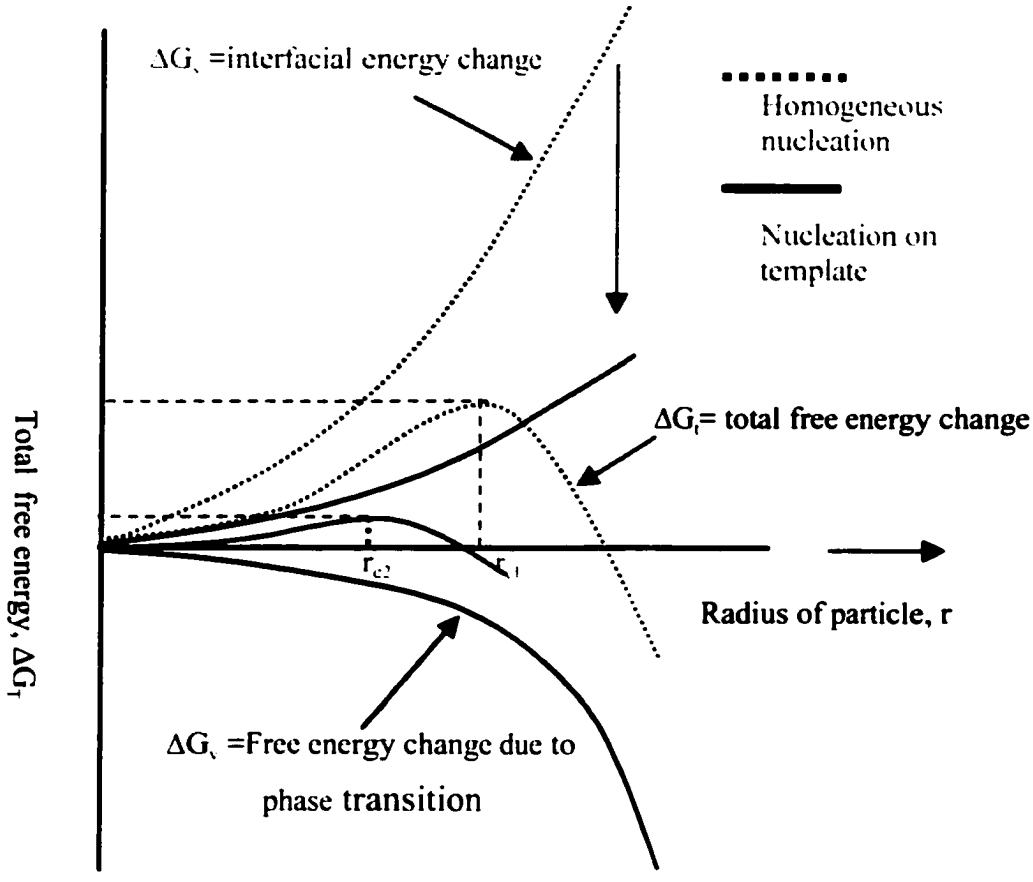

Figure 1.4 Free energy change ΔG vs. radius of embryo

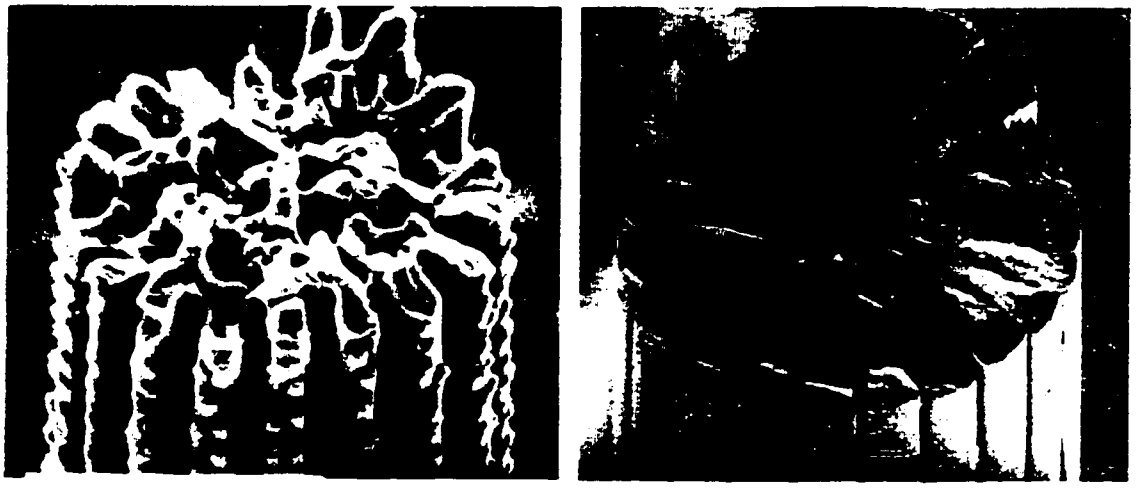

Figure 1.5 Fracture surfaces of immature (left) and mature (right) spines of the sea urchin Paracentrotus lividus. *Source:* [19]

Figure 1.6 Fracture surface of the prismatic calcite layer of the shell of the mollusc Atrina serrata showing the polygonal crystals (left) and Tooth enamel of the incisor of a rat. Each elongated rod is composed of hundreds of spaghetti-shaped crystals of carbonated apatite(right). *Source:* [19]

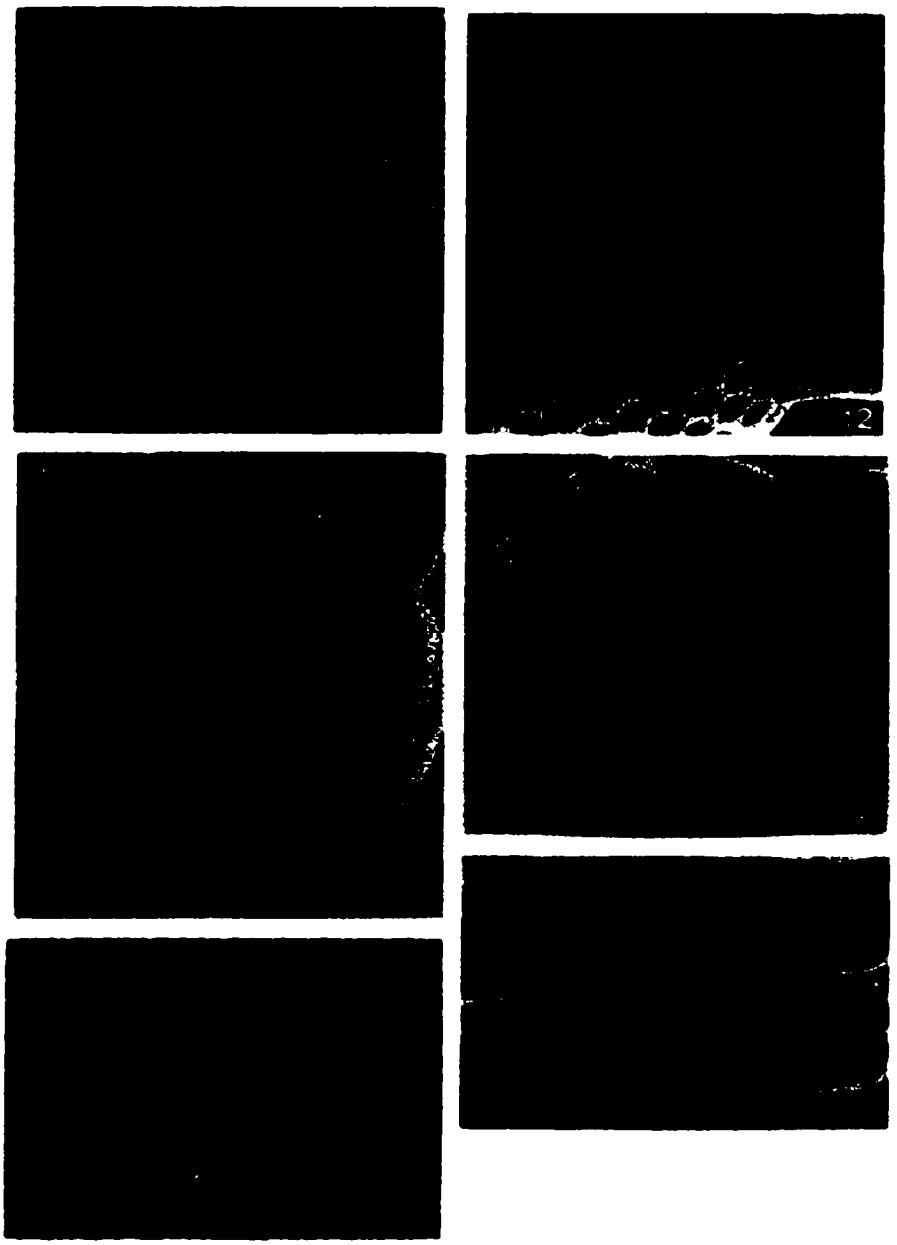

Figure 1.7 Natural microskeletons: (A, top left) radiolaria concentric mesh, (B,top right) radiolaria honeycomb, (C, middle left) disk-shaped diatom, (D,middle right) disk-shaped diatom, (E, bottom left) radiolaria extended mesh,(F, bottom right) radiolaria surface bowls. Source: [18]

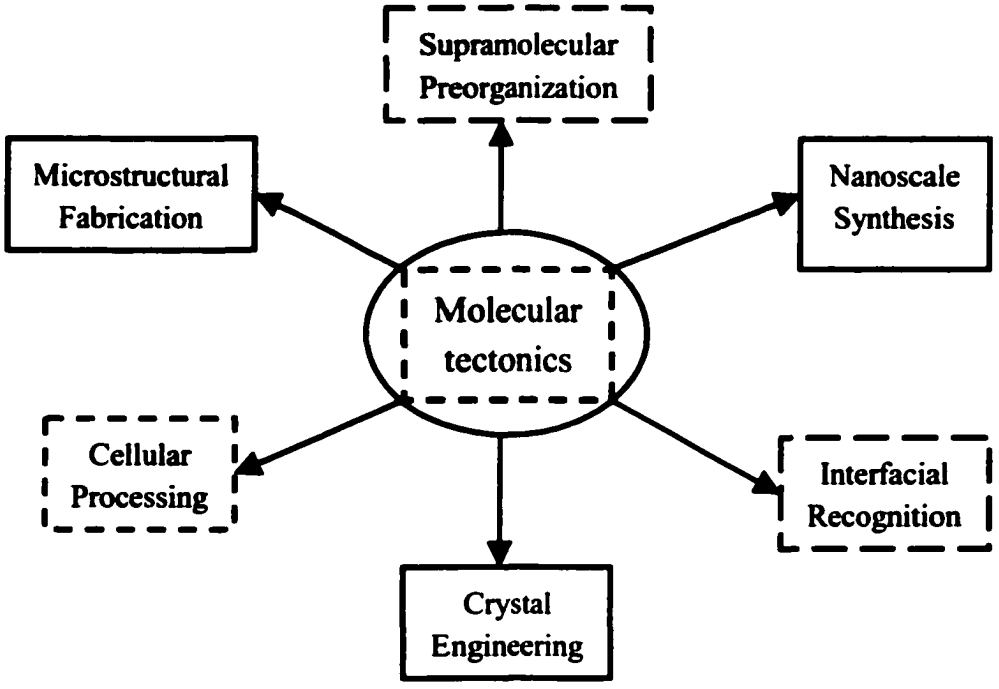

Figure 1.8 The connections between molecular tectonics, biomineralization (dashed boxes) and biomimetic material synthesis (solid boxes). Biomimetic strategies for nanoscale synthesis are based on supramolecular reorganization and interfacial recognition. Crystal engineering is based on the integration of processing and recognition, and microstructural fabrication on the combination of reorganization and processing. Source: Ref.[20]

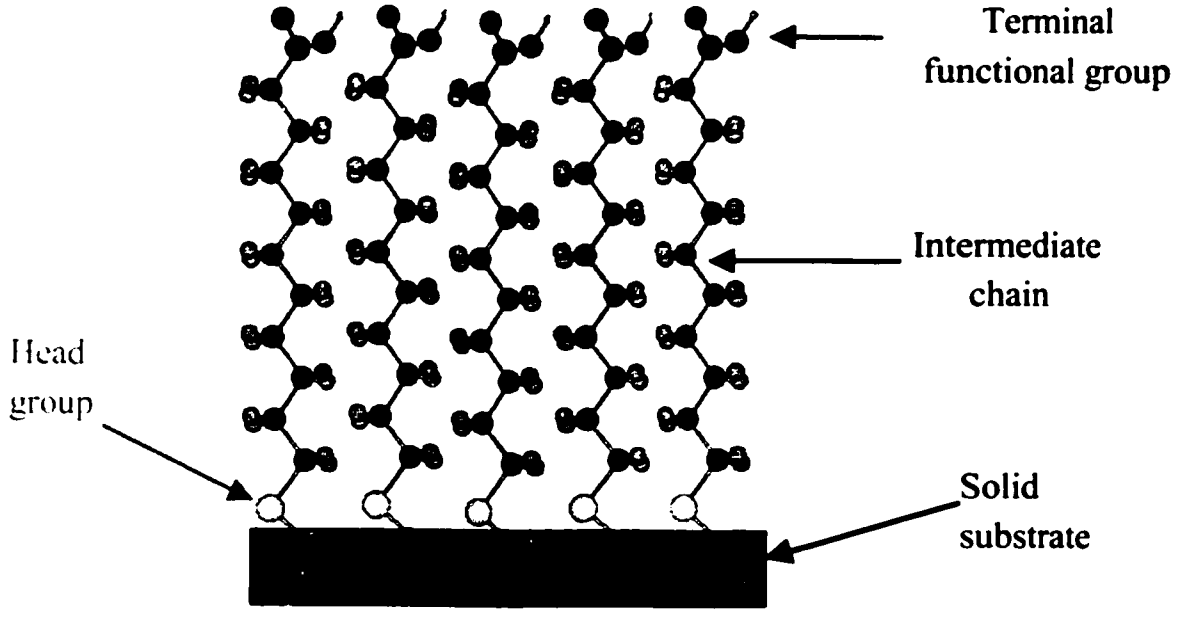

Figure 1.9 Structure of Self-Assembled Monolayers

Chapter 2

Template directed polymorph selective crystallization of $CaCO_3$ using Langmuir/LB monolayers: the role of electrostatic interaction and geometric matching

Several Langmuir monolayers with various properties have been investigated as templates for polymorph selective crystallization of $CaCO_3$ to understand the molecular interaction between the functional groups of the monolayers and the ionic components in the supersaturated solution during the template heterogeneous nucleation. The crystalline phases of polymorphs of $CaCO_3$ observed under monolayers mainly depend on the dissociation of the headgroup of monolayers instead of the molecular packing density and the properties of the hydrophobic chains. Our experimental results clearly showed that the electrostatic interactions between the functional groups of templates and the ionic components of the crystals in the supersaturated solution play a crucial role in the templating crystallization of $CaCO_3$, while exact geometric matching is not necessary. Templating happens only when the functional groups are completely dissociated and ions of the crystalline component from solution bind to the ionized functional group. When the structure of this binding layer mimics one of the lattice planes in the desired

crystalline phase, the interfacial energy between template and the crystalline phase is very small and the growth of 3-dimensional nuclei will follow.

2.1 Introduction

Langmuir monolayer is the monomolecular film that forms when amphiphilic molecules spread at air/liquid interface. The hydrophilic part of the monolayer will interact with the ions from the aqueous solution at air/liquid interfaces. The interactions between the headgroups of the monolayer and the ions from the subphase have been extensively studied.[34-37,81-86]. For example, the interactions between metal ions and fatty acid depend on not only the kind of metal ion been used, the temperature, but also the pH and the concentration of the ions in subphase. This ion-monolayer interaction makes Langmuir monolayer a good candidate for template directed nucleation because the reduced interfacial energy between monolayer and crystalline phase due to the strong interaction. The interactions between the monolayers and the crystals nucleated underneath can be adjusted by the functional groups and the hydrophobic parts of the amphiphilic molecules. Substantial work has been done by using Langmuir monolayers as templates for crystallization (see review article by Rapapot etc[87]). However few have successfully controlled the polymorphism of crystals grown underneath the Langmuir monolayers.[38,50,51] How the interactions between the functional groups of monolayers

and the ions in the subphase affect the crystalline phase nucleated underneath remain unclear.

In this research, we have used calcium carbonate as a model crystal system to investigate the templating process. Calcium carbonate has three polymorphs: calcite, aragonite and vaterite. These three crystals belong to different crystal systems and have very different physical properties. At room temperature, only calcite is stable and vaterite is very unstable. In this research, we will show that by choosing a right terminal functional group of surfactants, the thermodynamically unfavorable vaterite, instead of calcite, can be nucleated under the monolayer. Several amphiphilic surfactants with different functional groups have been used as templates. It was found that the electrostatic interaction between the headgroup of the monolayer and the ion component in the subphase is the most important factor for the successful templating of vaterite nucleation.

2.2 Experimental Section

2.2.1 Materials.

Stearic acid (99.5%, Standard for GC), octadecylamine (99%, GC), didecylamine, and 1-octadecanol (99.5, GC) were purchased from Fluka. $CaCO_3$ (99%) was also purchased from Fluka. Perfluorododecanoic acid was purchased from Aldrich Chemicals.

Chloroform (HPLC, Aldrich Chemicals) was used as the spreading solvent. All chemicals were used as received without further purification. The water was purified with a Millipore water purifier and the resistivity was 18.0 MΩ.

2.2.3 Measurement of Langmuir monolayer isotherm and formation of LB film.

Langmuir monolayer π-A isotherms were produced in a thermostated Teflon-coated trough (Nima Mini-Langmuir trough). The pH of the subphase was adjusted by addition of hydrochloric acid, ammonium hydroxide or sodium hydroxide solution. The surface of the subphase was cleaned by aspiration until zero surface pressure was reached through out expansion and contraction of the barriers. Surfactants were dissolved in chloroform (1.0~1.5 mg/ml) and spread at the air-water interface (Figure 2.1). After the chloroform was allowed to evaporate for 2 min, the monolayer film was compressed at a speed of 10 cm^2/min. For every experiment, at least three isotherms were recorded for comparison. After each measurement the subphase was completely sucked off and rinsed by de-ionized water for three times and then replaced by a fresh solution.

The LB film deposition was carried out on a KSV2000 Langmuir-Blodgett trough (KSV Instruments). After spreading, the chloroform was allowed to evaporate for 5 min, the monolayer film was compressed at a speed of 2mN/m/min. After the target pressure was reached, the film was stabilized for 5 min before the transfer. The condensed monolayer on the water surface was transferred onto a hydrophobic silicon wafer at a

constant surface pressure with a dipping speed of 5 mm/min. The wafers, on which LB monolayers were deposited, were cleaned by our cleaning protocol and then made hydrophobic with OTS. This protocol consisted of first sonicating the silicon wafers in a solution of sulfuric acid and Nochromix® for 30 minutes followed by rinsing and further sonication in Millipore® water.

2.2.2 Preparation of supersaturated solution.

Supersaturated solutions of calcium carbonate were prepared according to the procedure of Kitano[88]. Carbon dioxide gas was bubbled through a stirred aqueous suspension of $CaCO_3$ (2g calcite per liter) for approximate 3 h to give the supersaturated solution according to the following reaction:

$$CaCO_3(s) + CO_2(g) + H_2O(l) \Leftrightarrow Ca^{2+}(aq) + 2HCO_3^-(aq)$$

The suspension was then filtered (0.22μm, Millipore membrane). The procedure is shown in figure 2.2. The pH of resulting solution was 5.8-6.0. The concentration of calcium ion in the solution was determined by ethylenediaminetetraacetic(EDTA) substitution titration at pH >10, with Eriochrome black T as indicator[89]. The supersaturated solution was stocked in a flask and diluted to the desired concentration before the crystallization experiment. All concentrations of Ca^{2+} in the diluted solutions are 4.5 mM, except otherwise specified.

2.2.4 Template crystallization under Langmuir monolayers.

The above solution was used as subphase in a Langmuir trough (Nima Mini-Langmuir trough) and crystallization dishes or beakers. As CO_2 is lost from the supersaturated solution according to the following reactions:

$$Ca^{2+}(aq) + 2HCO_3^-(aq) \rightarrow CaCO_3(s)\downarrow + CO_2(g)\uparrow + H_2O(l)$$

Solution becomes supersaturated with respect to $CaCO_3$ and precipitation begins.

Langmuir monolayer films were formed at the air/liquid interface by carefully spreading surfactant (dissolved in chloroform as solvent) on the surface of the $CaCO_3$ solution subphase. For experiments done in the Langmuir trough, the surface of the subphase was first cleaned by aspiration until zero surface pressure was reached through out expansion and contraction of the barriers. Compression of the barrier began 2 minutes after spreading to allow complete evaporation of the chloroform. After the target surface pressure was reached, the barrier was held and the monolayer was left undisturbed during the crystallization period from the subphase. For experiments done in crystallization dishes and beakers, the surface of the subphase was also first cleaned. The amount of the amphiphilic surfactant solution to be added was calculated based on the known isotherm before spreading (single shot spreading). After spreading the surfactant on the surface, the dishes or beakers were left undisturbed while crystallization occurred. After 16~18 hours, crystals were collected from both the monolayer interface and control experiments

by dipping a glass slide into the subphase. Crystals formed at air/solution interface were therefore captured for structural and morphological analysis. The temperature of the Langmuir Trough is controlled at 17 °C. All other experiments are carried out at room temperature (22°C). A Nikon microscope with video capture capability was used to study the crystalline morphology in situ and on the glass slide dipped through the films.

2.3 Results and Discussion

2.3.1 Control experiments.

Control experiments were carried out in crystallization dishes without spreading any amphiphilic monolayer at the air/liquid interfaces. Crystals were collected after 16~18 hr by dipping the glass slide into the solution and examined by optical microscopy. Over the pH range of 5.8-7.8, the crystals observed were calcite with an average size of 40 μm. The typical morphology of crystals are shown in Figure 2.3. All the crystals observed in these control experiments (without any surfactants) do not exhibit any preferential orientation with respect to the air/liquid interface.

2.3.2 Negatively Charged Monolayers

Stearic acid. The crystalline phase and morphology of the crystals templated under the stearic acid monolayers was affected by the pH of the subphase solution. The results

were shown in Figure 2.4. At the low pH of 5.8~6.0, only rhombohedral calcite was nucleated under the monolayers. The results were very similar to the control experiments. The presence of stearic acid film doesn't affect the crystallization behavior at low pH. But when the pH of the saturated solution in the subphase was increased to 7.5, the results were totally different. About 80% of crystals nucleated under the monolayers are vaterite, with their [00.1] axis perpendicular to the monolayers. The different results are apparently caused by the different states of the carboxylic acid headgroups, i.e. the degree of ionization of the stearic acid monolayer at different pH. The pKa of stearic acid is 5.6. If the pH of the saturated solution is 5.8, only about half of the stearic acid is dissociated as stearate anion according to the following reaction:

$$CH_3(CH_2)_{16}COOH \leftrightarrow CH_3(CH_2)_{16}COO^- + H^+$$

At low solution pH (pH=5.8), the dissociation of stearic acid is incomplete. The interaction between the head group of the monolayer and the Ca^{2+} in the subphase is not strong enough to induce the nucleation of the metastable phase of $CaCO_3$. When the solution pH is increased to 7.5, the dissociation of the head is complete. At high pH, Ca^{2+} ions from the subphase evidently bind to COO^- groups in the monolayer and form a layer of Ca^{2+}, initiating the growth of the 3-dimentional vaterite structure (figure 2.5), which is characterized by alternating positive (Ca^{2+}) and negatively (CO_3^{2-}) charged layers.

The calcium ion binding to the carboxylate headgroup was evidenced by the dramatically change of π-A isotherm when the calcium ion was introduced in the subphase. Figure 2.6 shows the isotherms of stearic acid with pure water as subphase and 4.5 mM stocked $Ca(HCO_3)_2$ solution as subphase. The difference of phase behavior was obvious. With water as subphase, the monolayer transforms from G(gaseous) phase to L(liquid) Phase, then from L phase to S(solid) phase when compressed. However, with $Ca(HCO_3)_2$ solution as subphase, the monolayer didn't go through the L phase. It transformed from the G phase directly to S phase. The presence of Ca^{2+} in the subphase condensed the monolayer. The calcium-carboxylate reaction can produce a solid-condensed film, which is rigid and has no measurable surface viscosity. By this, Deamer etc[90] suggested that a polymeric film was formed by the binding of Calcium ion from the subphase. Enever and Pilpel used surface viscometry to study the reaction kinetics between stearic acid and calcium ion at air/water interface.[37,81,82] They suggested the interaction probably comprises four stages: (i) Diffusion of calcium ions into the interfacial region; (ii) reaction at the interface between calcium ions and ionized carboxyl groups; (iii) subsequent structural reorientation in the mixed calcium stearate + fatty acid film leading possibly to (iv) further reaction between calcium ions and stearate ions due to the removal of steric hindrance. Their result also showed that at pH 5.2, stearic acid monolayer was only partial ionized, which agrees with our conclusion.

The calcium ion binding lowers the interfacial energy of incipient nuclei's surfaces and increases the rate of nucleation. The presence of a binding calcium ion layer favors the oriented nucleation of crystal faces consisting of only calcium atoms. The (00.1) face of vaterite (figure 2.7) fits this criterion. The stereochemical similarities between the (00.1) face of vaterite and the orientation of carboxylate group at monolayer surfaces may be also important for the selective nucleation of vaterite.[51] The (00.1) face of calcite crystal (figure 2.8) also has a layer consisting of only calcium ion. However, the trigonal planar carbonate anions in calcite are oriented parallel to the (00.1) face. In vaterite, they are perpendicular to (00.1) face. The orientation of carbonate in vaterite is similar to the orientation of carboxylate headgroup. This may also favor the nucleation of vaterite over calcite with (00.1) face parallel to the monolayers.

Perfluorododecanoic acid. The results of templated crystallization under stearic acid monolayers depend on the pH of the supersaturated solution because the degree of dissociation of the –COOH group of stearic acid is very sensitive to the pH at the range of 5.8~7.8. We suspected that the electrostatic interaction and counter ion binding between the head groups of the monolayers and the moieties from the supersaturated solution, which depends on the dissociation of the headgroup, is very important for the templating process. To verify that the vaterite selection observed under stearic acid monolayers is the result of complete or nearly complete ionization of the monolayer,

experiments were performed with perfluorododecanoic acid monolayers. These acids are –COOH terminated surfactants whose pKa is much lower than the pH range of our experiments. If our ion interaction hypothesis is correct, template directed crystallization under such a surfactant should not depend on pH (within our experimental range) and vaterite should always be templated.

Perfluoroalkanecarboxylic acids are good choice for such experiments, being very strong acids compared to alkanecarboxylic acids. The dissociation constant, pKa, of perfluorododecanoic acids is about 2.8[91]. So they will be completely dissociated under our experimental conditions.

Crystals observed under perfluorododecanoic acid are mostly floret vaterite (85%). These vaterite crystals nucleated with their [00.1] crystallographic axis perpendicular to the monolayer (Figure 2.9), which is similar to the results under stearic acid at high pH. But with perfluorododecanoic acid monolayers, the result doesn't depend on pH of our supersaturated solution because the solution pH is always significantly above the pKa of the acid. The head group of perfluorododecanoic acid is therefore always nearly completely dissociated and negatively charged.

So the Ca^{2+} ion in the subphase will bind to the headgroup of the monolayer. This Ca^{2+} binding process is crucial for the nucleation of vaterite because it leads to the reduction of the interfacial energy between the crystal and monolayer.

Here also the hypothesized Ca^{2+} binding to the head group is supported by the isotherm of perfluorododecanoic acid on supersaturated solution. Figure 2.10 shows isotherms of perfluorododecanoic acid using different solutions as subphase or different waiting time between spreading and compressing. At pH of 6 pure water as subphase, different waiting time results in different isotherms (curve a and b) and the limiting area is much smaller than the reasonable value. This mean, at pH of 6, the monolayer of perfluorododecanoic acid is very unstable and partially dissolved into the bulk solution because the head group is totally ionized and highly hydrophilic. If we use 0.1 M HCl acid solution as subphase, the isotherm is totally different from that of pH 6 water. Now the head group doesn't dissociate and the dissolution of surfactant has been reduced (curve c). If the supersaturated calcium bicarbonate solution is used as subphase, the phase behavior of perfluorododecanoic acid was totally different from that of pure water as subphase. The monolayers have been stabilized by the presence of Ca^{2+} in the subphase. Even at pH of 6, monolayer didn't dissolve into the bulk solution. The surface pressure was increased by the presence of Ca^{2+} in the subphase. The Ca^{2+} binding to the headgroup of the monolayer is obviously. But why has the dissolution of the monolayer been reduced by the Ca^{2+} binding? One possibility is that each Ca^{2+} ion interacts with several cation of the headgroup of the monolayers (not necessarily two) as it does in the crystalline lattice. By this electrostatic binding, every perfluorododecanoic acid molecule has been connected to its several nearest neighbors, and thus the monolayers have been

stabilized. Some binding mechanisms also have been reported [36,37], but usually only a stoichiometric reaction between head group and the ion in the subphase has been suggested.

On the other hand, this multi-ion binding will also help the monolayer to organize into an ordered two-dimensional structure, such as hexagonal packing. When this self-arrangement process to such a point that packing structure of the Ca^{2+} ion in the stern layer becomes similar to one of the crystallographic face, such as (00.1) face of vaterite crystal, nucleation will be initiated under the monolayer.

2.3.3 Neutrally Charge Monolayers

Octadecanol. To test the requirement for ionization, crystallization experiments under uncharged octadecanol monolayers were performed. The crystals observed under the monolayer were rhombohedral calcite (figure 2.11). The crystal density at the surface is less than that of control experiment. This inhibition of nucleation under the inert monolayer is probably the result of the reduction in the diffusion rate of CO_2 from the supersaturated solution to air caused by the presence of a monolayer as a barrier at the air/liquid interface.

2.3.4 Positively Charged Monolayers

Amine termination. Two types of amine-terminated monolayers have been investigated as crystallization templates: single chain octadecylamine Langmuir

monolayer and double chain didecylamine Langmuir-Blodgett (LB) films (figure 2.12). The isotherms of octadecylamine and didecylamine were shown in figure 2.13 and 2.14. The reason we use LB films for didecylamine instead of Langmuir monolayers is that Langmuir monolayers of didecylamine at air/liquid interface are very unstable.

Similar to the stearic acid monolayer, the stability of didecylamine can be increased by either changing the pH or adding the counter ion in the subphase. Instead of decreasing, here we need to increase the pH of subphase to stabilize the monolayer (figure 2.14). The monolayer can also be stabilized by the presence of HCO_3^- or CO_3^{2-} in the subphase. By a simple calculation, the amount of HCO_3^- is much larger than the amount of CO_3^{2-} in the subphase:

$HCO_3^- \Leftrightarrow CO_3^{2-} + H^+$, $K=4.8 \times 10^{-11}$, So at pH 7:

$$\frac{[CO_3^{2-}]}{[HCO_3^-]} = \frac{K}{[H^+]} = 4.8 \times 10^{-4}$$

So most probably, the amine headgroup was bound by HCO_3^-, not by CO_3^{2-}. The result is similar to the calcium ion binding to the carbonyl headgroup as discussed in the previous section.

Unlike the results under stearic acid monolayers, the templated crystallization of $CaCO_3$ under amine-terminated monolayer is independent of the pH of the supersaturated solution. This is apparently because octadecylamine monolayers are always ionized when

the pH of solution is in our experimental range of 5.8~8.0 according to the following reaction.

$CH_3(CH_2)_{17}NH_3^+ \Leftrightarrow CH_3(CH_2)_{17}NH_2 + H^+$, pKa=10.6

The positively charged monolayers will interact with the anion, HCO_3^- or CO_3^{2-} from the supersaturated solution. The metastable form of $CaCO_3$, vaterite, is induced under the monolayers.

Vaterite crystals were also obtained on the didecylamine LB film. The molecular packing area of didecylamine (52.5 $Å^2$) is much larger than that of octadecylamine (18 $Å^2$). The average area of calcium or carbonate ion in (00.1) plane of vaterite crystal is only 14.8 $Å^2$ (figure 2.7). This further confirms our previous conclusion that the geometric matching between template and crystal lattice is not necessary for template directed nucleation of vaterite.

2.3.5 Electrostatic interaction and structure matching between the template and the lattice plane inside the crystalline phase.

From our experimental results under different monolayers (table 1), we find that the electrostatic interaction between the headgroup of the template and the solute ions, either Ca^{2+} or CO_3^{2-} or HCO_3^- from supersaturated solutions of $CaCO_3$ is crucial to the templating crystal nucleation.

For negatively charged monolayers, the Ca^{2+} ion in the subphase binds to the headgroup of the monolayer. This Ca^{2+} binding is believed to be crucial for the nucleation of vaterite. If we examine the vaterite crystal structure along the [00.1] direction, there are planes which are composed of Ca^{2+} alternating with planes of CO_3^{2-} ions (Figure 2.7, a). The binding of Ca^{2+} to the monolayer creates a plane of Ca^{2+}. Evidently, the nucleation of vaterite is initiated because interfacial energy between the monolayer and vaterite crystalline phase is dramatically lowered by this Ca^{2+} binding process. From our experiments, it is clearly shown that the counter ion binding to headgroup of monolayer from the supersaturated solution is very important to the templating process. Correspondingly, the binding of HCO_3^- or CO_3^{2-} to positively charged monolayers serves the same purpose.

However, exact geometric matching between the template and the crystal lattice plane is not necessary for polymorph selective templating. As shown in figure 2.7, the average area per Ca^{2+} or CO_3^{2-} ion at the templated (00.1) lattice plane in the vaterite crystal is 14.76 $Å^2$. The limiting molecular areas of the surfactants used in this study, stearic acid, octadecylamine, perfluorododecanoic acid, didecylamine are about 18 $Å^2$, 18 $Å^2$, 22 $Å^2$ and 52.5 $Å^2$ respectively - much larger than the area/ion templated. Obviously exact geometric matching between crystalline phase and template monolayer is not necessary for selective nucleation of the unstable polymorph. However, if the counter ions from supersaturate solution bind to the template, this ion binding is not necessary

stoichiometric binding. The structure of this binding layer of Ca^{2+} or $CaCO_3^{2-}$ ion may rearrange into two-dimension and become similar to the crystalline structure.

Table 2.1. Effects of dissociation of functional groups and molecular limiting packing area on templated crystallization

Surfactant	Packing limiting area ($Å^2$/molecule)	pKa	Solution pH	Templating of Vaterite
Stearic acid	18	5.6	5.8-6.0	No
		5.6	7.5-8.0	Yes
Perfluorododecanoic acid	22	2.8	5.8-6.0	Yes
Octadecanol	18	—	5.8-6.0	No
Octadecylamine	18	10.6	5.8-6.0	Yes
Didecylamine (LB film)	52.5	10.7	5.8-6.0	Yes

2.4 Conclusions

In this chapter, we demonstrated that crystalline polymorphs of calcium carbonate can be selectively nucleated by using Langmuir monolayers as templates. The crystalline phases of polymorphs nucleated under monolayers depended on the dissociation of the headgroups of the monolayers. By using ionized monolayer templates, vaterite, the

metastable form of $CaCO_3$, has been nucleated under Langmuir monolayer at the air/liquid interface.

Crystallization under stearic acid monolayers (pKa=5.6) depended on the pH of the supersaturated solution. Templating happens only at pH significantly above the pKa, when the COOH group is ionized to COO^-. In contrast, crystallization using amine-terminated monolayers didn't depend on the pH of the supersaturated solution over the range studied, $5.5 < pH < 8.0$. Over this range, amine terminated monolayers (pKa ~10.6) are completely protonated and were found to template vaterite over calcite. For perfluorododecanoic acid monolayers, the results were similar to those of stearic acid at high pH, except that pH had no effect on the templating process over the range studied because of its low pKa, meaning that the headgroup is always negatively charged. Template directed crystallization of $CaCO_3$ under uncharged octadecanol monolayers was inhibited and no vaterite was observed.

Based on our experimental results and analysis, the electrostatic interaction between the headgroup of the monolayer and the counter ion in the supersaturated solution is crucial to the templating process. However, exact geometric matching between functional group and the crystal lattice is not necessary for template directed nucleation.

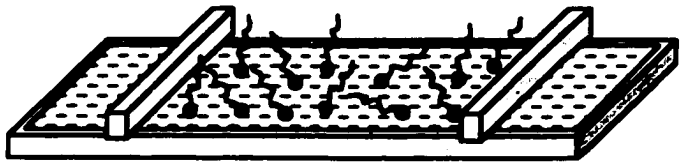

Figure 2.1 Langmuir film formed at air/liquid interface in a trough

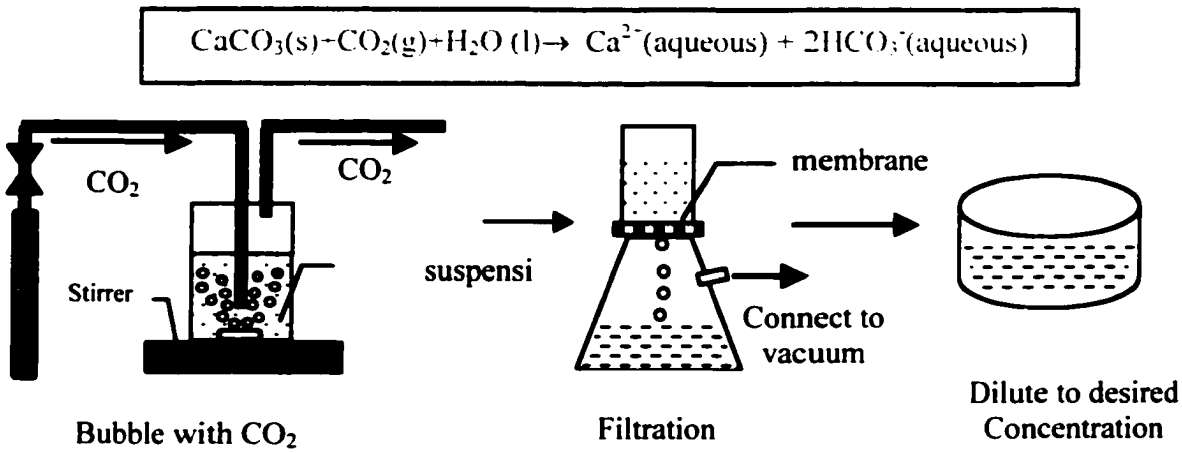

Figure 2.2 Preparation of supersaturated solution

Figure 2.3. Crystallization without monolayers at air/Liquid interface, ($[Ca^{2+}]$=4.5 mM). Only calcite crystals are observed. These crystals are randomly oriented.

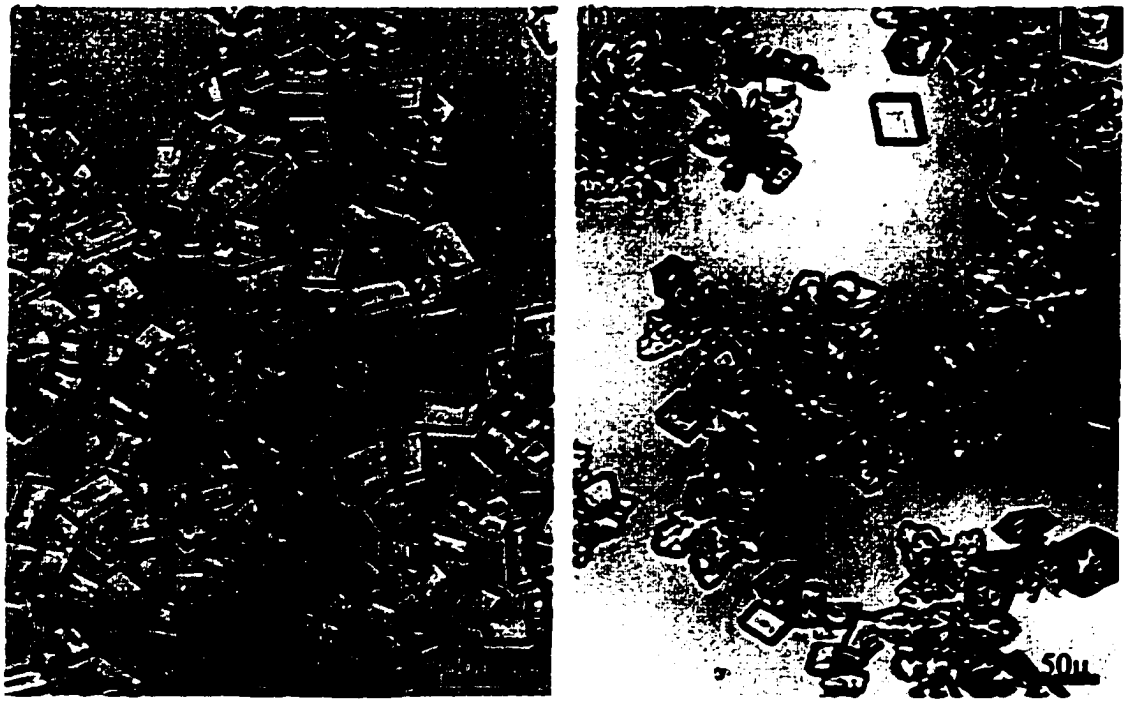

Figure 2.4 Crystallization under stearic acid monolayer at air/liquid interface at different pH. (a) pH=5.8, only calcite;(b) pH=7.5, Mostly Vaterite.

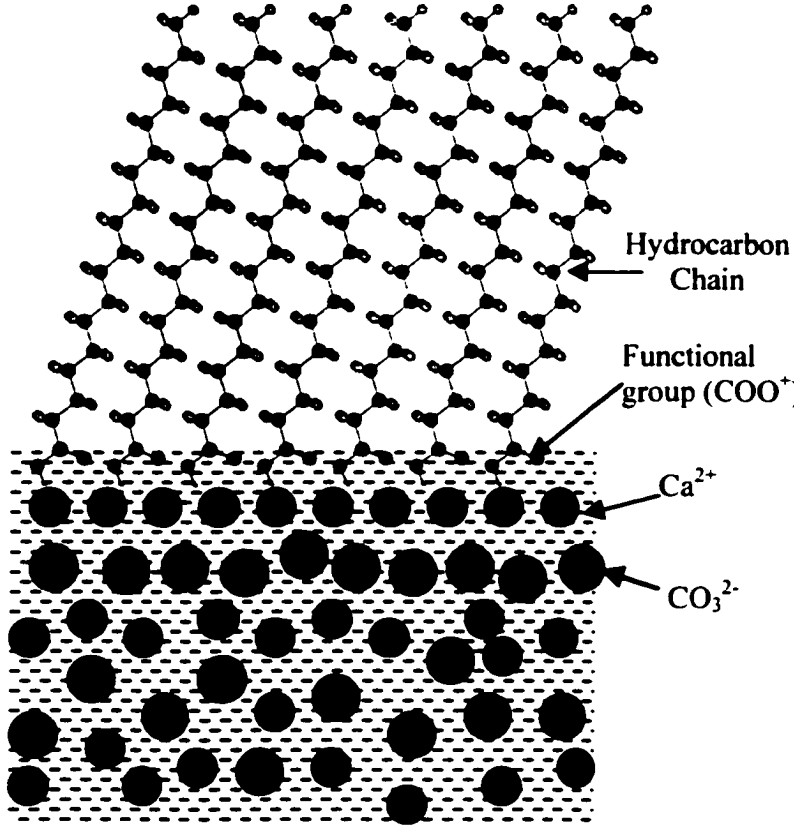

Figure 2.5 Ca^{2+} ions from the subphase bind to the COO^- group and form a layer of Ca^{2+}, which follows the growth of a 3-dimentional vaterite structure

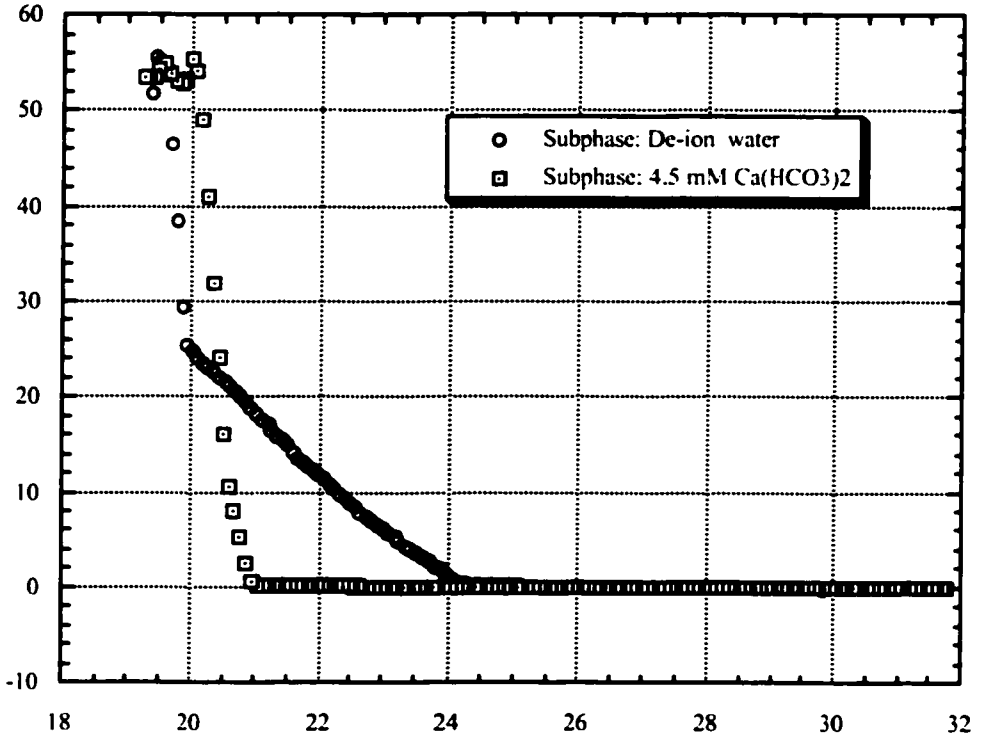

Figure 2.6 Effects of ionic carboxylate-Ca^{2+} interactions on isotherm of stearic acid

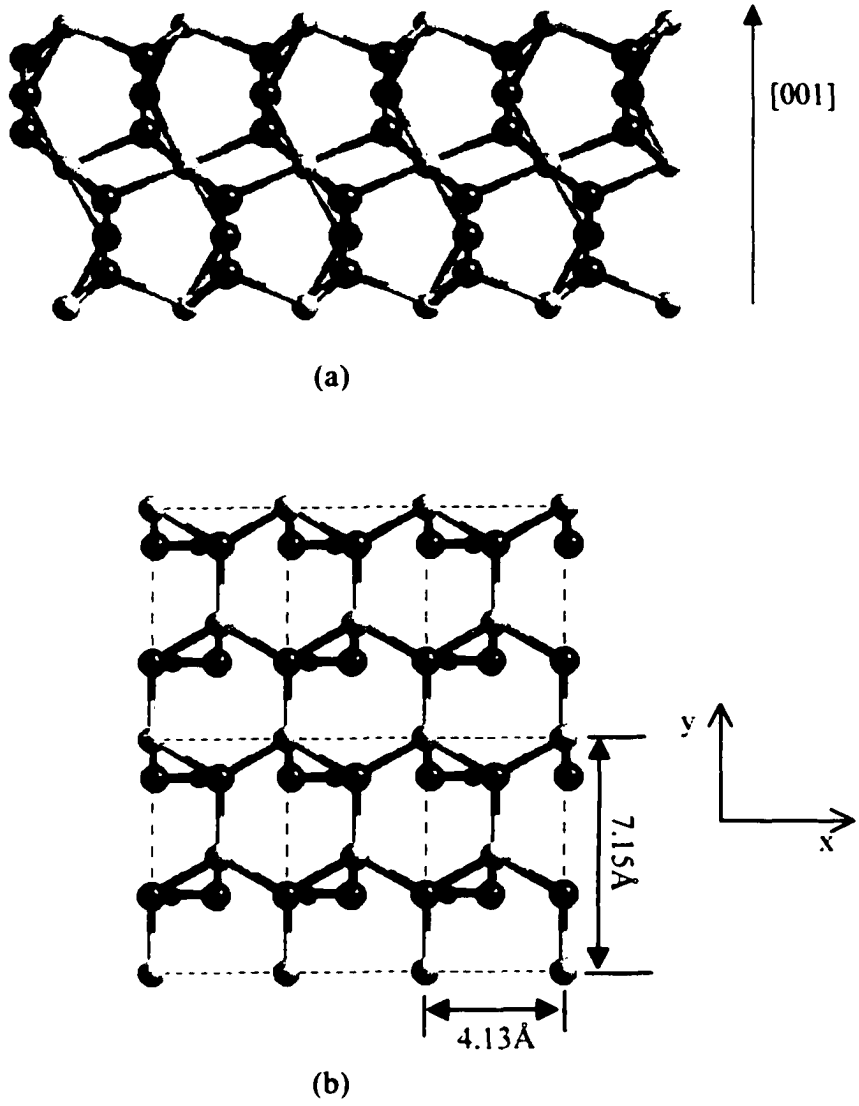

Figure 2.7 Vaterite crystal structure. (a)along [00.1] direction; (b) (00.1) face.

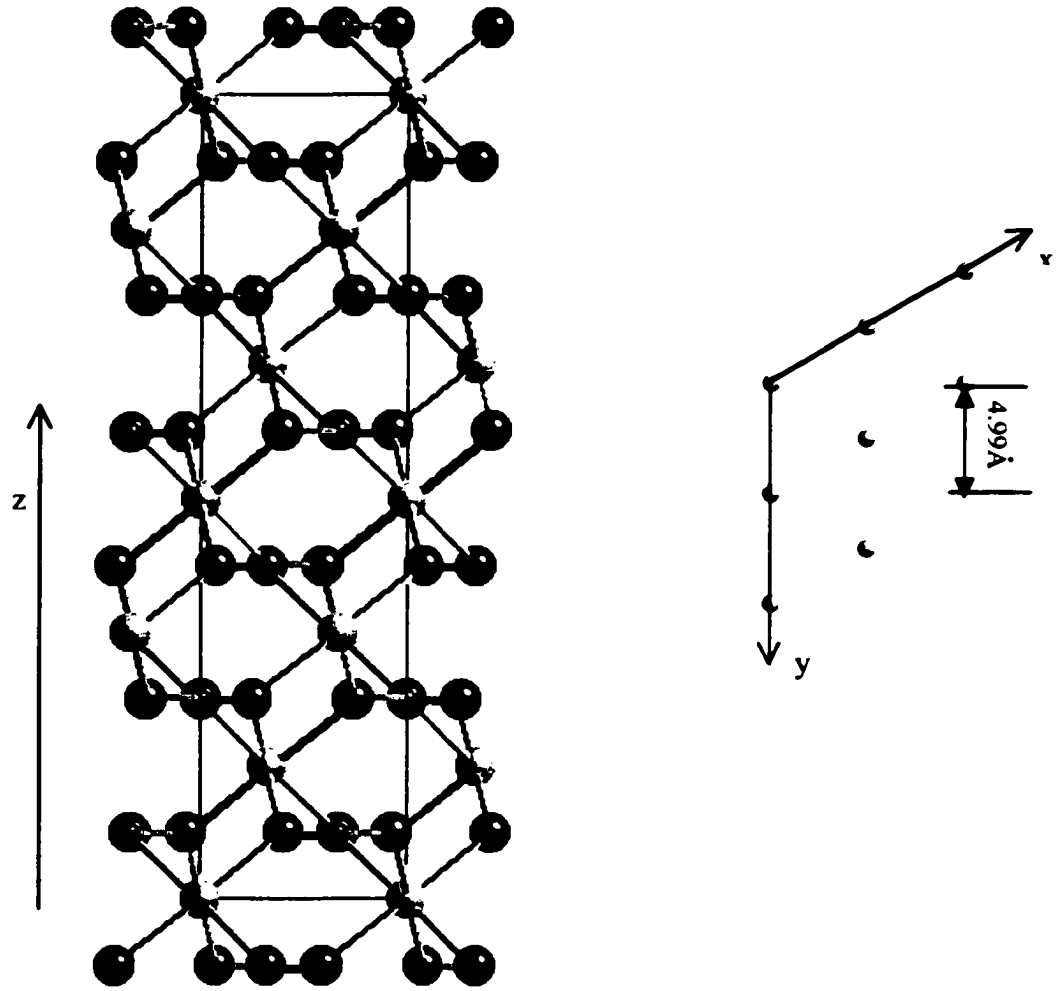

Figure 2.8 Calcite crystal structure view along [10.0] direction (left); and (00.1) face with only one layer of calcium ion (right).

Figure 2.9 Crystallization under perfluorododecanoic acid monolayer, Solution pH=5.8.

More than 80% crystals are vaterite crystals

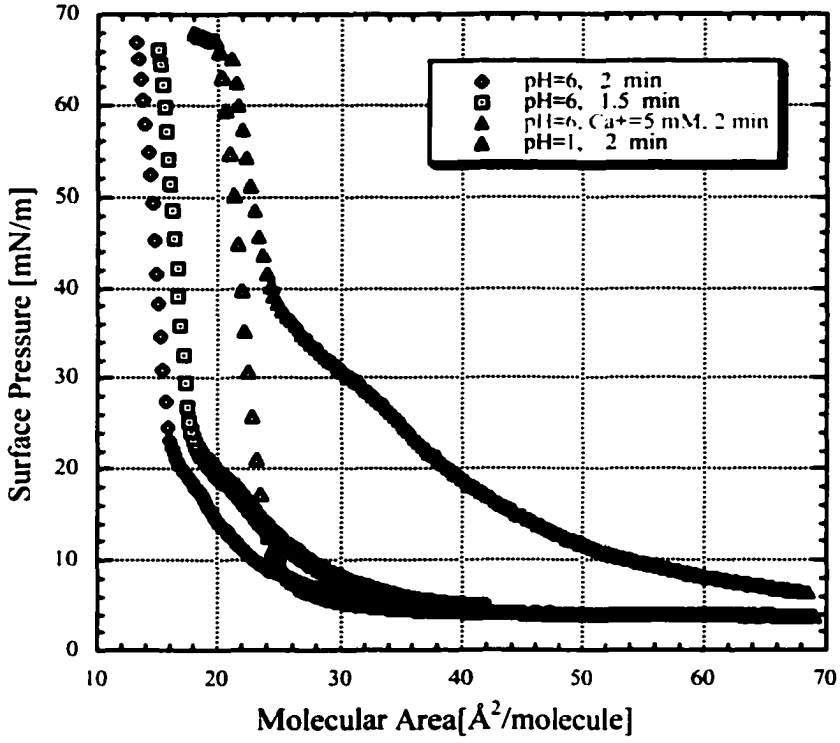

Figure 2.10 Isotherm of perfluorododecanoic acid (Effects of Subphase)

(curves from left to right: a, b, c, d)

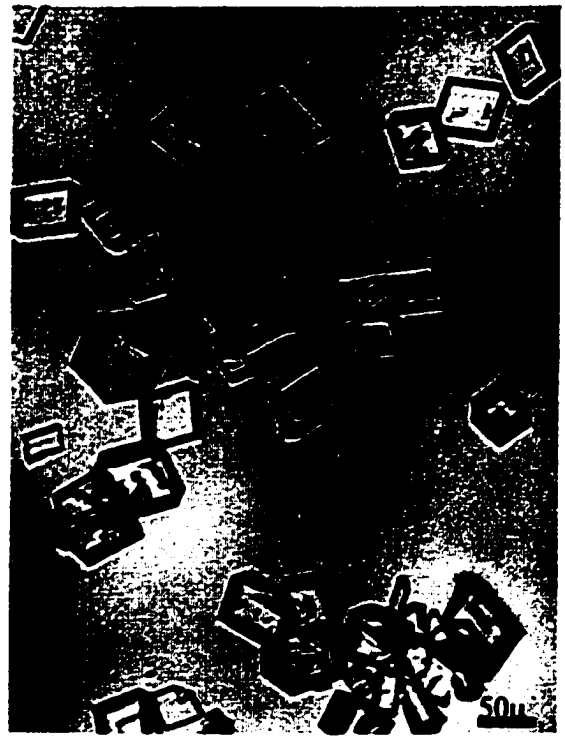

Figure 2.11 Crystallization under octadecanol monolayers at air/liquid interface

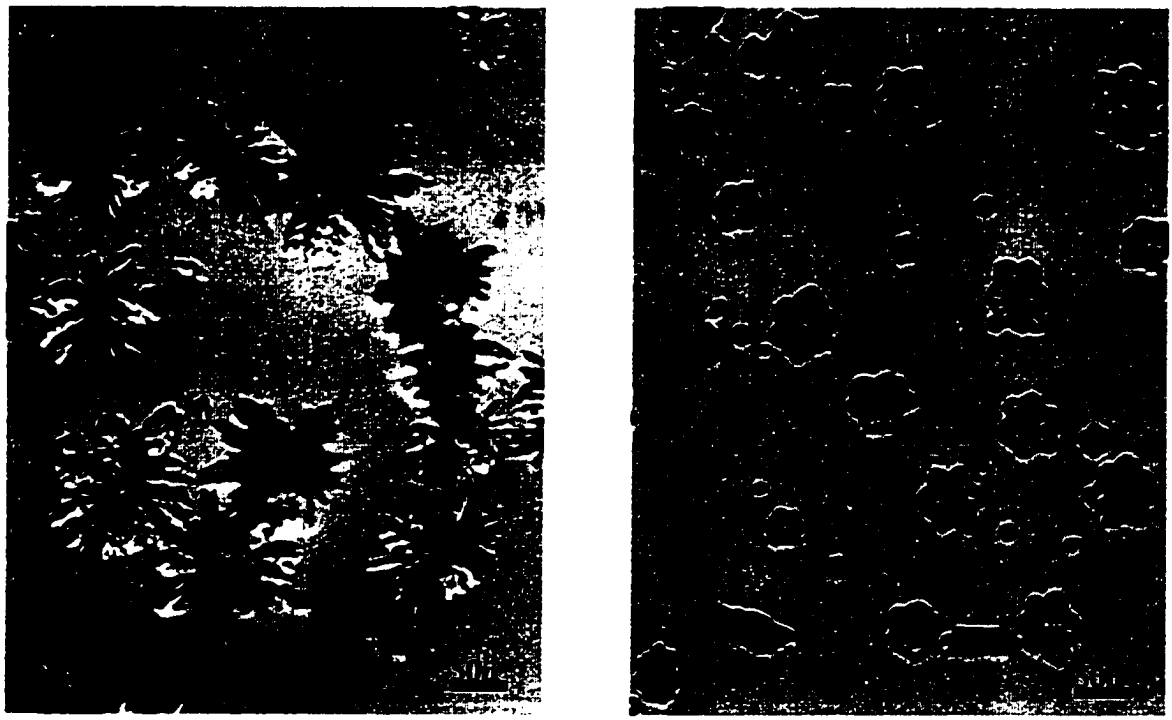

Figure 2.12 Crystallization using amine-terminated monolayers. (a) under octadecylamine monolayer at air/liquid interface; (b) on didecylamine LB Film, Solution pH=5.8, $[Ca^{2+}]$=4.5mM

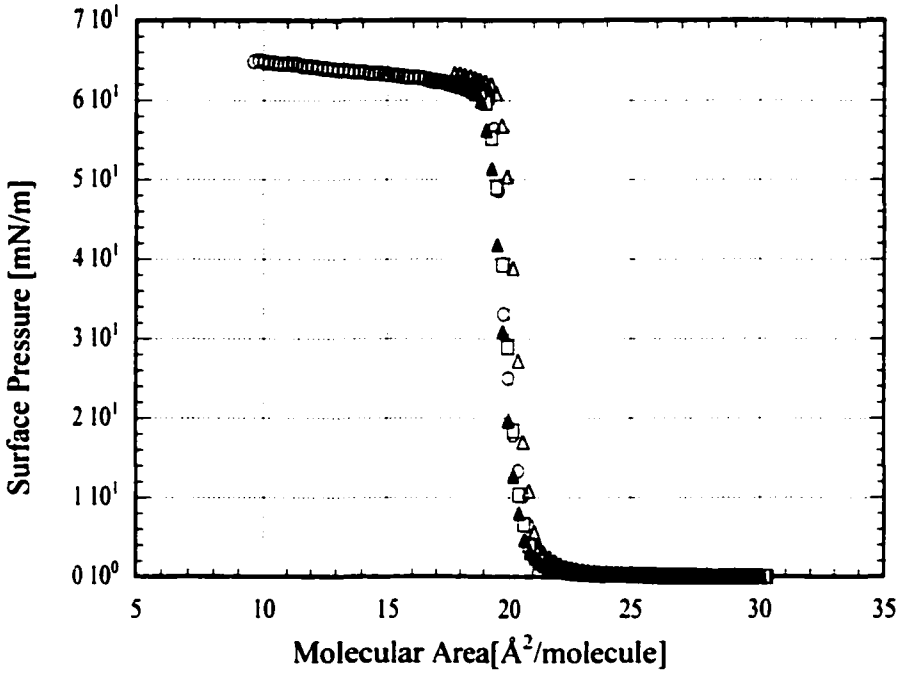

Figure 2.13 Isotherm of octadecylamine

(Subphase: 4.5 mM $Ca(HCO_3)_2$ solution, temperature.=17° C)

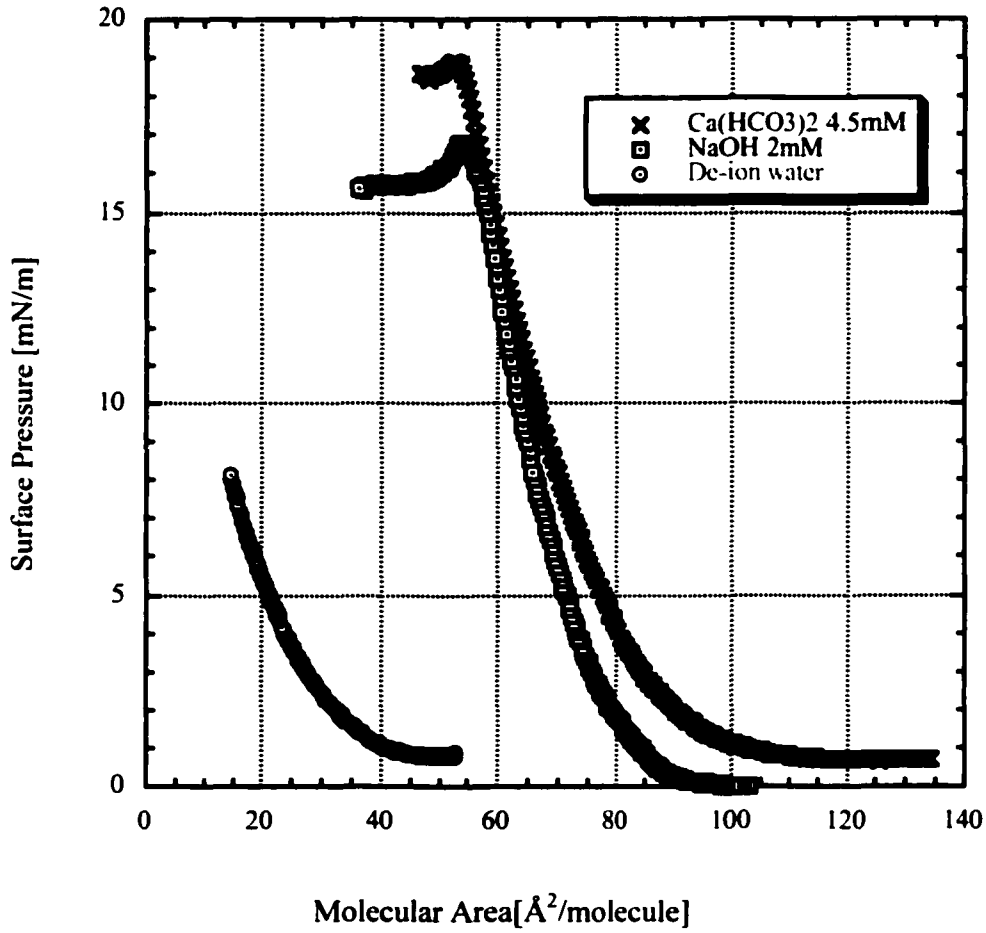

Figure 2.14 The effect of subphase on the isotherm of didecylamine. The monolayer of didecylamine can be stabilized either by the high pH or by the binding of HCO_3^- or CO_3^{2-} to the amine headgroup

Chapter 3

Polymorph selective template directed nucleation of calcium carbonate using SAMs

In the previous chapter, we have shown that polymorphism of calcium carbonate can be controlled by using Langmuir monolayer at air/liquid interface as template. Compared to the Langmuir monolayers at air/liquid interface, Self-Assembled Monolayers (SAMs) on the solid surfaces are more robust and suitable for industrial applications. At this part of the research, we used SAMs for template directed nucleation to control the polymorphism of calcium carbonate. Several SAMs with different functional groups were investigated to show how the different polymorphs of $CaCO_3$ can be selectively induced on the functionalized solid surfaces. The effects of terminal groups of the SAMs, substrate used (Au or Si) and the properties of intermediate chains on the templated crystallization have been investigated.

3.1 Introduction

Template directed nucleation utilize the potential of controlling the molecular recognition event, which may exists between the incipient nuclei and organized organic

assemblies. In the previous chapter, we have already shown that polymorphism of $CaCO_3$ can be controlled by using Langmuir monolayers at air/liquid interface as templates.

However, templated crystallization at air/liquid interface is not very suitable for industrial application, which is our original motivation for this project. This is not only because the large-scale applications require large surface areas, but also the fragile and un-reusable nature of the monolayers at air/liquid interfaces. So, more robust and reusable functional surfaces are in demand for the templated crystallization technology to be applicable in the industry. Self-Assembled Monolayers (SAMs) will be very good candidates for this industrial application. Self-assembled surfactants consist of a head group, which attaches to the solid surface via a specific interaction, an intermediate hydrocarbon chain and a functional group attached to the opposite end of the chain (see figure 1.9). The properties of SAMs can be very different by attaching different functional groups to hydrocarbon chain, so it will provide us with many types of functional surface with various properties.

In recent years, using silane SAMs on silicon surfaces and thiol SAMs on gold surfaces as template for crystallization has received great attention as a promising alternative to control the nucleation and crystal growth, polymorphic selectivity, parttening of crystal, crystal orientation and morphology. Compared to Langmuir monolayers at air/liquid interface, SAMs have the advantages of stability. The surfaces of alkanethiolate SAMs on gold have been used to control the polymorphs and orientation

of calcium carbonate [64-67], to facilitate the nucleation and growth of semiconductor particles,[92] and to investigate the effects of functional groups of SAMs on the nucleation rate and orientation of malonic acid.[73] SAMs and patterned SAMs of functionalized alkanetiols have also been used to control the orientation and growth pattern of calcite crystals[68,69]. SAMs of Organosilane have been used to promote the heterogeneous nucleation and growth of ceramic films, [70,93] calcium oxalate monohydrate crystals,[71], and to study the effect of surface chemistry on calcite nucleation and growth [80]. More recently, SAMs and mixed SAMs of alkanetiol have been used to control the nucleation and growth of α-glycine [72] and malonic acid [73].

Although considerable work has been carried out using SAMs as template for crystallization, none of these have successfully controlled the polymorphs of crystals, which is very important in pharmaceutical and agrochemical application. In this research, both silane SAMs on silicon surfaces and thiol SAMs on gold surfaces were used for template directed nucleation to control the polymorphic selection of $CaCO_3$ crystals. Several SAMs with different functional groups were investigated to show how the different polymorphs of $CaCO_3$ can be selectively nucleated on the functionalized solid surfaces.

3.2 Experimental Section

3.2.1 Materials

Octadecyltrichlorosilane, OTS (95%), ethyl alcohol (HPLC grade), 11-mercapto-1-undecanol (97%), 11-mercaptoundecanoic acid (95%), 16-mercaptohexadecanoic acid and 1-dodecanethiol (97%, GC grade) were purchased from Aldrich Chemicals. (3-aminopropyl) trimethoxysilane, APS (97%) and 4-aminothiophenol (90-95%) were purchased from Fluka. Toluene, sulfuric acid (95-98%) and Nochromix® crystals were purchased from Fisher. Silicon wafers were obtained from WaferNet Inc., California. HPLC grade hexadecane, chloroform, and carbon tetrachloride were obtained from Aldrich. All chemicals were used as received without any further purification. Deionized water with a resistively of 18MΩ cm from a Millipore® system was used.

3.2.2 Preparation of OTS SAMs on silicon surfaces

It is very important to make sure that the substrates we used are clean. The silicon wafers were cleaned by the following procedure. The silicon wafers were sonicated in a freshly prepared Nochromix® solution for 30 minutes. The Nochromix® solution was prepared by dissolving the Nochromix® crystals in sulfuric acid. Then the wafers were rinsed and further sonicated in Millipore® water. The substrates were then dried in a stream of N_2 just before use.

OTS monolayers were deposited by dipping the freshly cleaned substrates in a 2 mM OTS solution with a mixed solvent of n-hexadecane, carbon tetrachloride, and chloroform (80:12:8 by volume) for 30 min. Then the wafer were rinsed with chloroform for two minutes and dried by a stream of N_2.

3.2.3 Preparation of APS SAMs on silicon surfaces

APS SAMs were prepared by using the method described by Petri[94]. Firstly, the silicon wafers, which were covered with a SiO_2 layer, were cleaned with the following procedure. The wafer were kept in dichloromethane for 15 min, and then were immersed in a mixture of NH_3 (25% in volume), H_2O_2 (30% in volume), and water (By Millipore filter, 18MΩ) in the volume ratio of 1:1:5 at the temperature of 70°C. After 20min, the wafers were rinsed with water for several times and dried by a stream of N_2

The APS monolayers were prepared by dipping freshly clean silicon wafers into a 1wt% solution of APS in toluene for 10 min at 60 °C. Then the wafer were washed several times with toluene to remove the physically absorbed molecules and dried by a stream of N_2.

3.2.4 Preparation of alkylthiol SAMs on gold surfaces

Evaporation of gold onto clean silicon wafer substrate was done in thermal evaporator at pressure of 5×10^{-6} Pa. The thickness of the coating gold layer is about 60

nm. The alkylthiol monolayers were deposited by putting the substrates into 1 mM alkylthiol solution with ethanol as solvent. After 24 hr, they were removed from solution and rinsed vigorously with ethanol and blown dry with N_2. The SAM preparation process was shown as Figure 3.1.

SAMs on gold or silicon substrate were characterized by contact angle measurement, ellipsometry and atomic force microscopy (AFM). Contact angle of SAMs with water was determined using contact angle goniometer. A Rudolph Eillipsometry (Rudolph Instrument, Model 444A12) was used to determine the thickness of the monolayers. AFM images of the SAMs were obtained by using Digital Instruments Nanoscope III multimode atomic force microscope. Triangular silicon nitride cantilevers (model NPST, Digital Instruments) with a force constant of ~ 0.58 N/m were used.

3.2.5 Crystallization experiment

The crystallization experiment was done by putting the substrate (with SAMs on the surfaces) into a beaker containing the supersaturated calcium bicarbonate solution. The supersaturated solution was prepared by the bubbling method described in Section 2.2.2. The whole system was put in a desiccator to prevent any contamination and disturbance from environment. By losing the CO_2 from the solution, supersaturation was obtained and $CaCO_3$ crystals will be templated on the functionalized solid surfaces. After 16~18hr, the samples were taken out and examined by Optical Microscopy, X-Ray diffraction and

electron diffraction. All the experiments done for solid surface were in room temperature (about 20~23 ºC). The Ca^{2+} concentration in the supersaturated solution was 4.5 mM.

3.3 Result and discussion

When the supersaturated solution contacted with the SAMs, the components of the crystals will attached to the monolayers by the specific interaction between the ions in the supersaturated solution and the headgroups of the SAMs (Figure 3.2). By using different types of SAMs with different functional groups, we are able to adjust the interaction between the incipient nuclei and organized organic assemblies, and thus control the polymorphs of the crystals induced by the monolayers. The following will discuss the different polymorphs of $CaCO_3$ induced by different SAMs in our experiments.

3.3.1 Formation and properties of SAMs of OTS and APS on silicon surfaces

Two kinds of alkylsilanes, 3-aminopropyl trimethoxysilane (APS) and octadecyltrichlorosilane (OTS) have been used in our experiments as templates for $CaCO_3$ crystallization. The properties of these two monolayers are quite different. OTS forms densely packed, well-ordered with the monolayer height of ~25 Å (See Kurmar etc [95] and references within). It is a highly hydrophobic monolayer. The contact angle of OTS monolayers with water in our experiments is about 103º~106º. However, the monolayers of APS are quite disordered as shown by the AFM images (Figure 3.3). This

is because the chain of APS is much shorter than that of OTS and chain-chain interaction is much weaker. The amine-terminated APS SAMs are very active and can interact with many different functional groups. The water contact angle of freshly prepared APS monolayer is in the range of 25º~30º. However the contact angle of APS monolayer increases as a function of time because of the adsorption of dust from the atmosphere.[94] Amine termination is very active and APS will easily form multi-layer structure. Some time APS layer also contains defects such as clumps and holes such as shown in figure 3.4. The thickness of APS film in figure 3.4 is about 2.31 nm. So it's almost a three layer structure, considering the height of a single layer is about 8~9 Å. Fortunately, these defects and multi-layer formation doesn't affect its function as crystallization template, as long as the surface is amine-terminated.

Because the chain-chain interaction between APS molecules is weak, the film of APS is not as strong as OTS monolayers. As shown in figure 3.5, APS film can be easily removed by AFM tip. The patch in figure 3.5 was produced by repeatedly scanning 10 times in that area.

3.3.2 Template directed nucleation of $CaCO_3$ using SAMs of organosilicon on silicon surfaces

Crystallization on clean bare silicon substrate was used as a control experiment for comparing. As expected, most crystals grown on bare silicon surface are calcite. Only

very few of vaterite crystals were observed, as shown in the left image of Figure 3.6. The presence of OTS monolayers on the Si surface inhibits the crystal growth on surfaces. The crystal morphology on OTS monolayers (Figure 3.7) is very similar to that on bare Si surface. Only calcite crystals were observed on OTS surfaces. Calcite crystals on the OTS surface are randomly oriented. The average number of crystals grown on OTS surface is less than that on bare silicon surface. This is not a surprise, since the surface of OTS is highly hydrophobic, while the surface of silicon is highly hydrophilic. There is no sign of any templating between the crystalline phase and OTS monolayer. This is because the alkyl-terminated group does not interact with any components of crystals in the supersaturated solution.

In contrast, the crystals nucleated on the APS surfaces are almost exclusively vaterite (Figure 3.8, a). The shape of these vaterite crystals is hexagonal with a circle (probably also a hexagon) in the center. The early stage images show that the hexagonal structure was developed from a single spot from the center (Figure 3.8,c). This single spot is identified by electron diffraction as a single crystal of vaterite with its [00.1] direction perpendicular to the surface. So our experiments have strongly demonstrated that (00.1) face of vaterite crystal was templated by the APS monolayers.

The XRD experiments were performed to identify the phase and direction of crystals on the substrate. The sample was analyzed by θ-2θ mode with Cu-Kα_1 radiation (λ=1.540

Å). In this mode, only diffraction planes (templating planes) parallel to the plane of substrate produce diffraction peaks. The X-ray diffraction pattern of calcium carbonate crystal templated on APS surface was shown in Figure 3.9. The peak with $2\theta=21°$ is the diffraction from 002 plane of vaterite with inter-plane d=20.933 Å.[96,97] However, the peak from (10.0) with $2\theta=24.87°$ was not observed in the diffraction pattern (The intensity of this peak will be the strongest if the vaterite crystals are randomly oriented). This confirms the observation by optical microscopy that vaterite crystals were templated with (00.1) plane parallel to the surfaces

This templating process happens because of the interaction between the monolayer and the ions in the supersaturated solution. The pKa of APS is about 10.6, so at the solution pH of 6, the functional group of APS ($-NH_2$) will be protonated as NH_3^+ and the surface will be positively charged. The anion (HCO_3^- or CO_3^{2-}) will accumulate and binding onto the solid surface because of the electrostatic interaction. When the conformation of the accumulated CO_3^{2-} ions on the surfaces become similar to the lattice structure of a crystalline face (such as (00.1) in vaterite crystal), the interfacial energy between the solid surface and crystalline phase is dramatically reduced. And the nuclei of the corresponding crystalline phase are induced on the template. The situation here is very similar to the octadecylamine monolayers at the air/liquid interfaces as described in chapter 2.

3.3.3 Templated crystallization of $CaCO_3$ on SAMs of organosulfur

Five different types of organosulfur SAMs with different termination and chain length have been investigated as the templates for selective crystallization of $CaCO_3$ in our experiments. They are SAMs terminated with amine (4-aminothiolphenol), acid (11-mercaptoundecanoic acid and 16-mercaptohexadecanoic acid), alcohol (11-mercapto-1-undecanol) and alkyl (1-dodecanethiol). Because of different terminal functional groups, the surface properties of these SAMs are very different. Their contact angles with water have been listed in Table 3.1.

Table 3.1 Contact angle (advancing) of SAMs with water

SAMs	H_2O Contact angle
Amine terminated (4-aminothiolphenol)	21º~24º
Acid terminated (11-mercaptoundecanoic acid)	18º~20º
OH-terminated (11-mercapto-1-undecanol)	24º
Alkyl-terminated (1-dodecanethiol)	94º
gold	75º
OTS	103º~106º

The results of the polymorphic selective templating crystallization are shown in figure 3.9 to figure 3.13 and are summarized in table 3.2. As expected, crystallization on SAMs with uncharged terminal groups, such as 1-dodecanethiol (Figure 3.10, a) and 11-mercapto-1-undecanol (Figure 3.10, b), was inhibited. Only rhombohedral non-oriented calcite crystals were observed. Also the crystal density for these two uncharged surfaces

is very low, 59 crystals/mm^2 for OH-terminated surfaces and 55 crystals/mm^2 for CH_3-terminated surfaces.

Table 3.2 Template directed nucleation of $CaCO_3$ on SAMs of organosulfur with different functional groups on gold surfaces.

Thiols	Functional group	Polymorphs nucleated	Crystal frequency (App. number/mm^2)
1-dodecanethiol	-CH_3	calcite	55
11-mercapto-1-undecanol	-OH	calcite	59
4-aminothiolphenol	-NH_2	vaterite	263
11-mercaptoundecanoic acid	-COOH	calcite (pH5.8~6.0)	63
		vaterite (pH 7.5)	68
16-mercaptohexadecanoic acid	-COOH	calcite (pH5.8~6.0)	58
		vaterite (pH 7.5)	127

In contrast, crystals templated on the amine-terminated SAMs (4-aminothiolphenol) are almost exclusively vaterite (Figure 3.11). These vaterite crystals nucleated with their [00.1] axis perpendicular to the monolayers. The crystallization density is also much higher than that of methyl or alcohol terminated surfaces as shown in Table 3. 2. So it is very obviously that nucleation of vaterite crystals on the solid surfaces is induced by the terminal functional groups of the SAMs. From figure 3.11-b, we can see very clearly the circle spot of single vaterite crystal nucleated on the surfaces. These vaterite crystals on gold surfaces are characterized by electron diffraction technique (Figure 3.12). The

results of electron diffraction confirmed our observation that the [00.1] crystallographic axis of vaterite crystal is perpendicular to the substrate, which means vaterite crystals were templated by SAMs on (00.1) face. The situation of induced nucleation here is very similar to that at air/liquid interface as we discussed at chapter 2. The interfacial energy between the templates and the crystalline phases was reduced by the interaction between the functional groups of SAMs and the chemical moieties of the crystals. Although electrostatic interaction is much loner range and dominates, the interaction may also include stereochemical correspondence.

The chemical states of $-NH_2$ for aminothiophenol film on gold substrate and APS film on silicon substrate were studied by Hooper using x-ray photoelectron spectroscopy (XPS). [98] It was found that the chemical states of $-NH_2$ in both cases are similar. This indicates aminothiolphenol SAMs on gold surface is positive charged when contacted with supersaturate solution. So there exists direct electrostatic interaction between amine groups and the ionic components from the solution. In addition, the stereochemical correspondence between the phenol groups on the surface and the carbonate groups in the vaterite crystal may also contribute to the nucleation of vaterite on the surfaces. Obviously, the planes of phenol groups in the monolayer lie perpendicular to the surface of the substrate. The direction of carbonate planes inside vaterite crystal is perpendicular to the (00.1) face. So it is possible that the stereochemical correspondence between the

phenol groups and the carbonate groups also contributes to the vaterite nucleates with (00.1) plane on the substrate.

The results of template directed nucleation using acid terminated SAMs are similar to the results of crystallization under stearic acid monolayers at air/liquid interface. Template directed nucleation of calcium carbonate have been performed by using 11-mercaptoundecanoic acid and 16-mercaptohexadecanoic acid on the gold surfaces (see figure 3.13 and 3.14). In both cases, when the supersaturated solution pH is low (5.8~6.0), most of crystals (more than 90%) on the substrate are calcite. Also the nucleation frequency is low, 63 crystals/ mm^2 for SAMs of 11-mercaptoundecanoic acid and 58 crystals/ mm^2 for SAMs of 16-mercaptohexadecanoic acid. Obviously, at pH of 5.8~6.0, the acid terminated SAMs do not have the capability to template the nucleation of calcium carbonate, because the dissociation of COOH group is incomplete at this pH value. However, when the pH of supersaturate solution increases to 7.5, vaterite crystals with [00.1] axis perpendicular to the surfaces were observed. The important factors influence the template directed nucleation of vaterite crystals on the acid-terminated surfaces may include the electrostatic interaction and stereochemical correspondence between the template and the vaterite crystals as we discussed in chapter 2.

Figure 3.14-d is an interesting optical microscopic picture with focusing on the central spot of vaterite crystal. It clearly shows the shape of central spot of vaterite crystal is hexagonal. This agrees with the hexagonal crystal structure of vaterite and confirms

our conclusion that the central spot is a single crystal with (00.1) face (templating face) parallel to the substrate.

3.4 Conclusion

In this chapter we have shown that polymorph selective crystallization can be achieved by using Self-Assembled Monolayers (SAMs) as templates. The specific interactions between the functional groups of SAMs and the chemical moieties of the crystals in the supersaturated solution will decide the polymorphs of the crystals induced on the solid surfaces.

Calcium carbonate has been chosen as a model crystal system in this research. The crystalline phases of $CaCO_3$ nucleated on the functionalized solid surfaces are controlled by the terminal groups of the SAMs, while the substrate used (Au or Si) and the properties of intermediate chain are not very important to the templating process. SAMs of organosilicon on silica surfaces and organosulfur on gold surfaces have been used as template for crystallization. In both cases, vaterite crystals with [00.1] axis perpendicular to the monolayers were induced by the amine-terminated SAMs. With uncharged alkyl-terminated or alcohol-terminated SAMs, Most of crystals are randomly oriented calcite. For acid terminated SAMs, the results depend on the pH of supersaturate solution because the dissociation of acid headgroup is different at different pH. At the solution pH

of 5.8, most of crystals obtained on acid-terminated SAMs are calcite, while at pH of 7.5, vaterite crystals with [00.1] axis perpendicular to the substrate were templated.

From our experimental results, it is obviously that the electrostatic interaction and stereochemical correspondence between SAMs and crystals are the most important factors for the templating process. The mechanism of the templating process on the functionalized solid surface is similar to that under the Langmuir monolayers at the air/liquid interfaces.

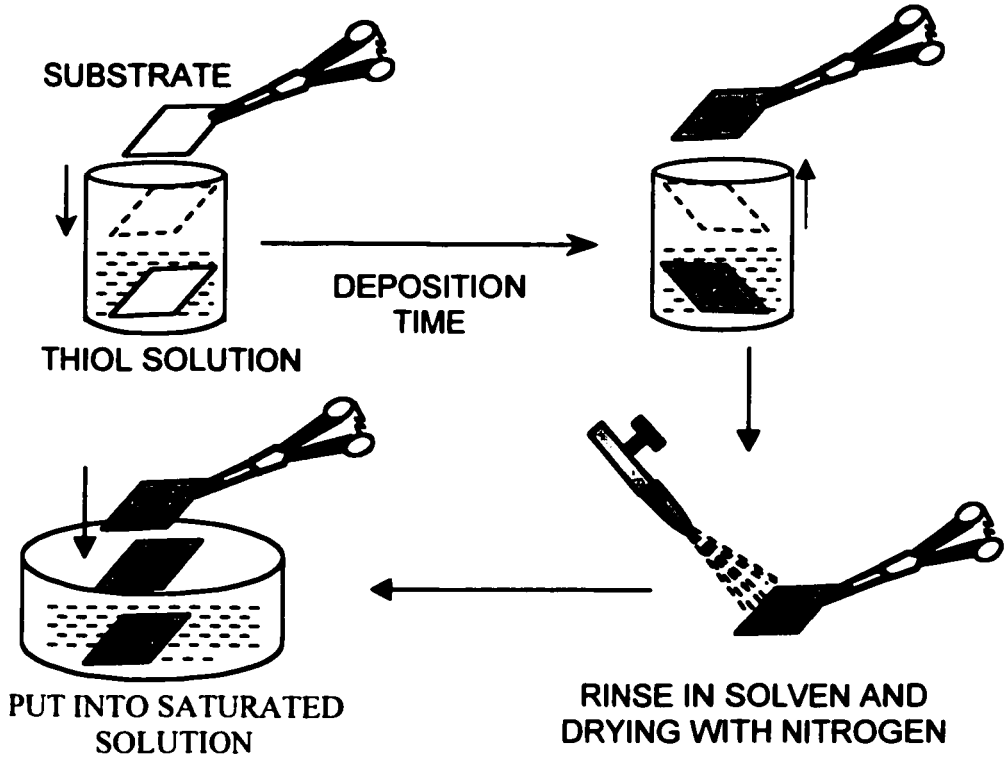

Figure 3.1 The procedure of alkylthiol SAMs preparation and crystallization

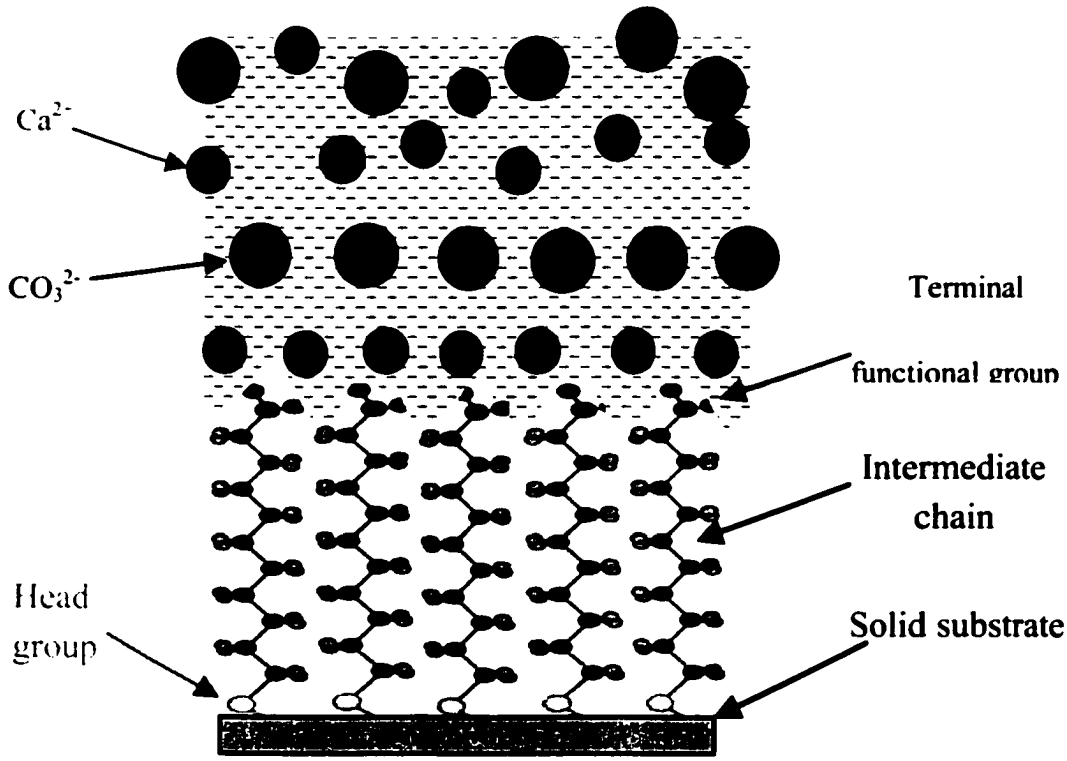

Figure 3.2 Template directed nucleation of crystals on SAMs (Thiol SAMs with Acid Termination)

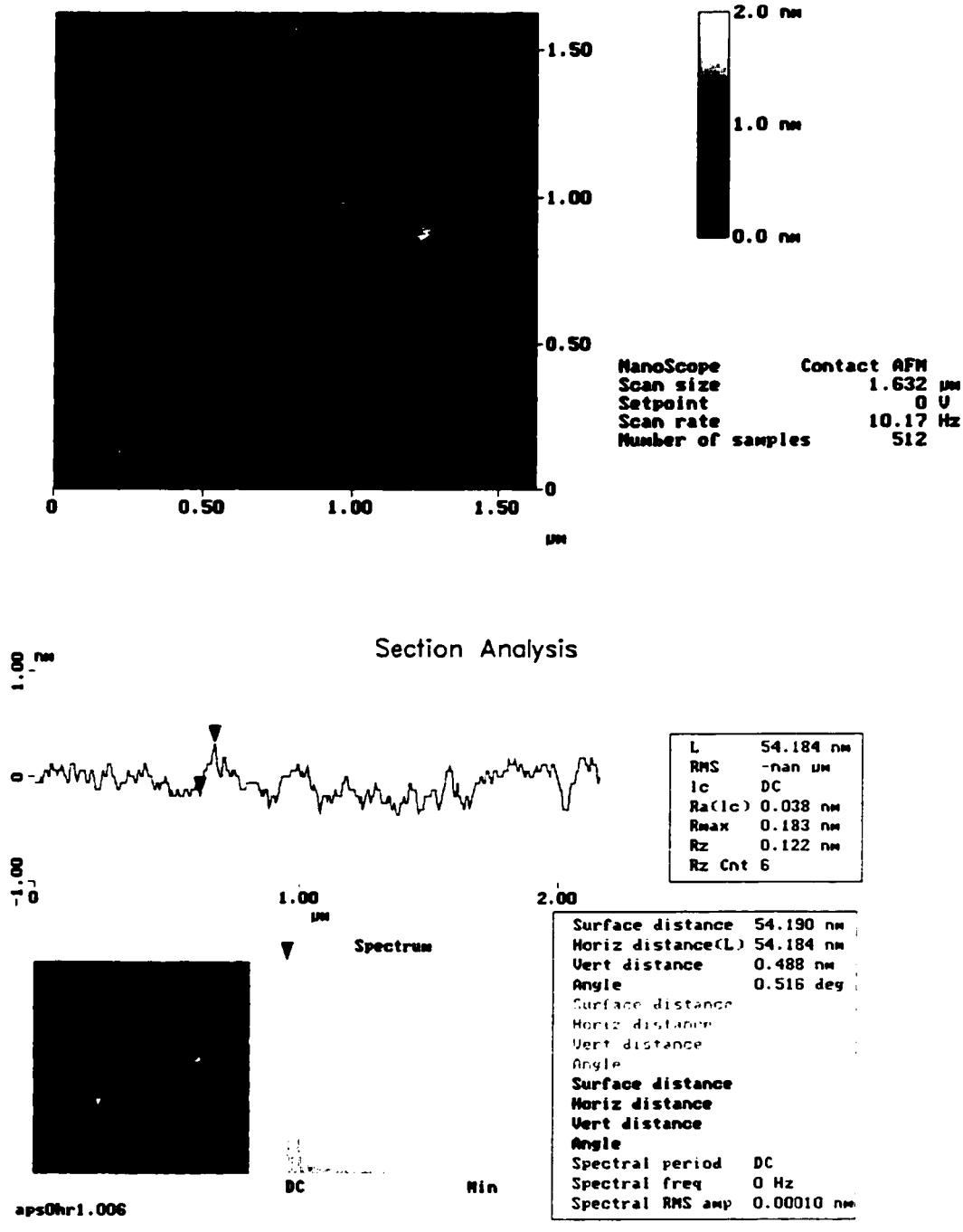

Figure 3.3 AFM image of APS monolayer on silicon wafer

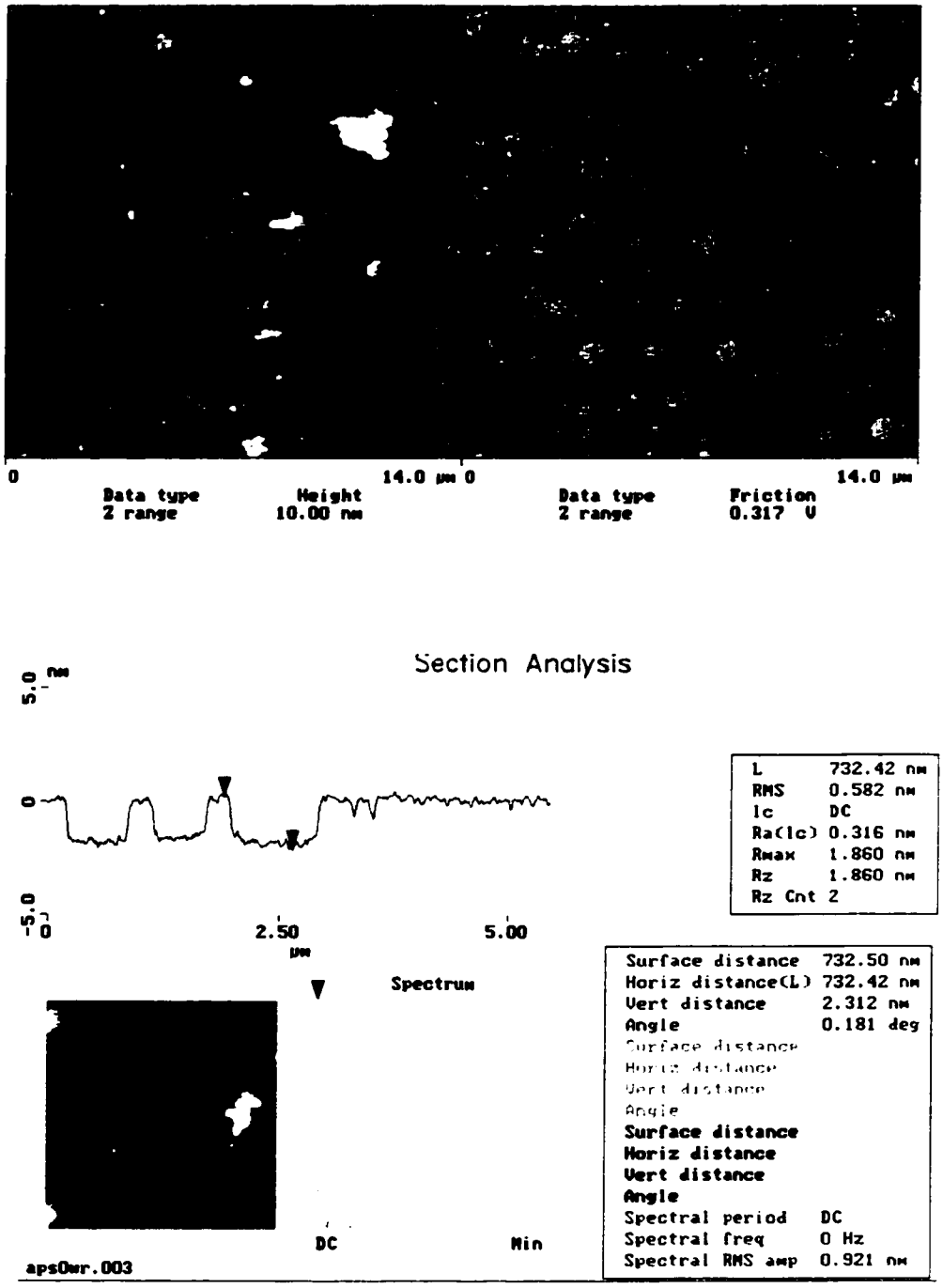

Figure 3.4 AFM images of APS layers on the silicon surface. The defects such as clumps and holes were observed (Top image). The film is composed of multi-layer (3 layers) APS molecules based on section analysis (Bottom image),

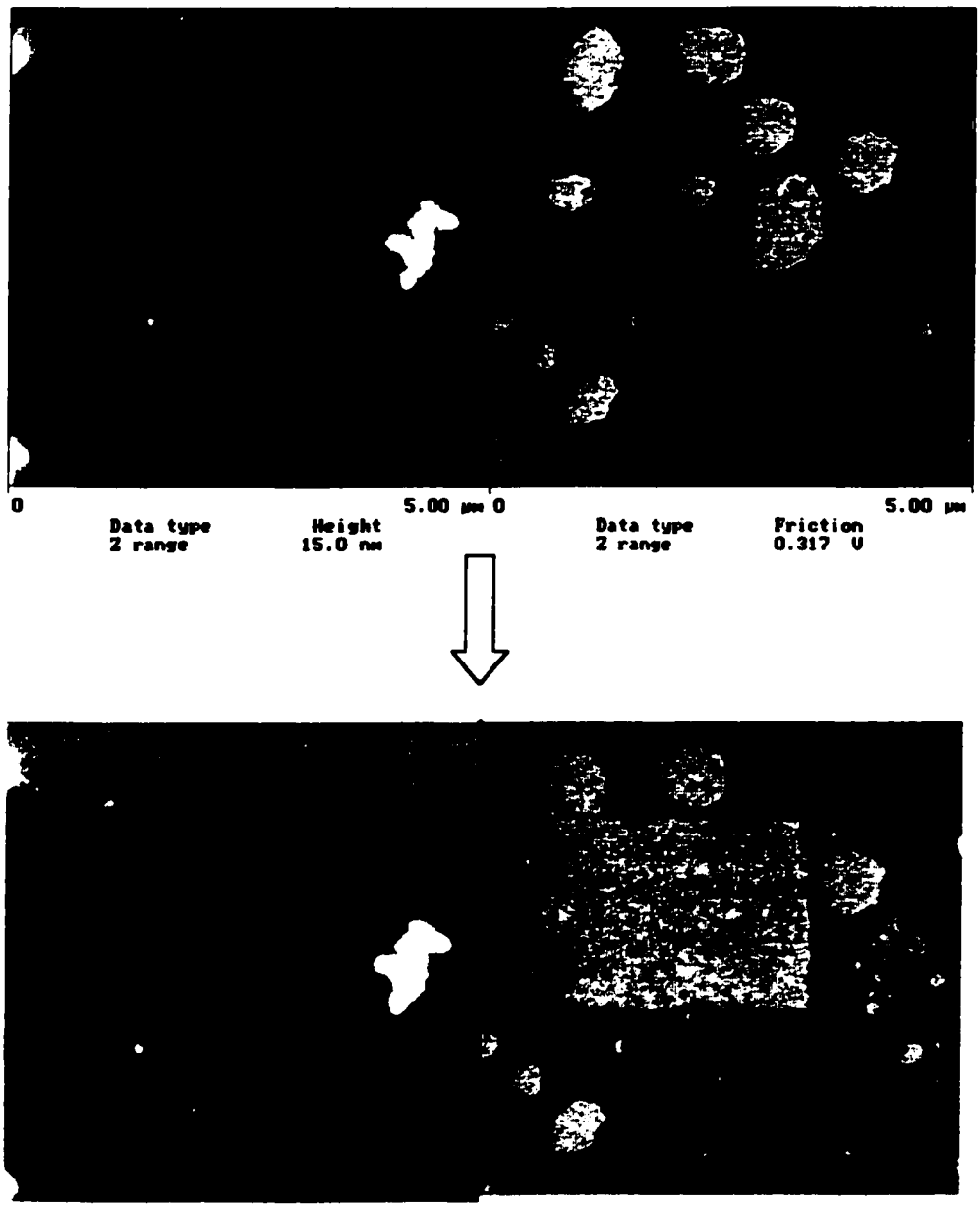

Figure 3.5 APS film was removed by AFM tip (repeatedly scanning for 10 times)

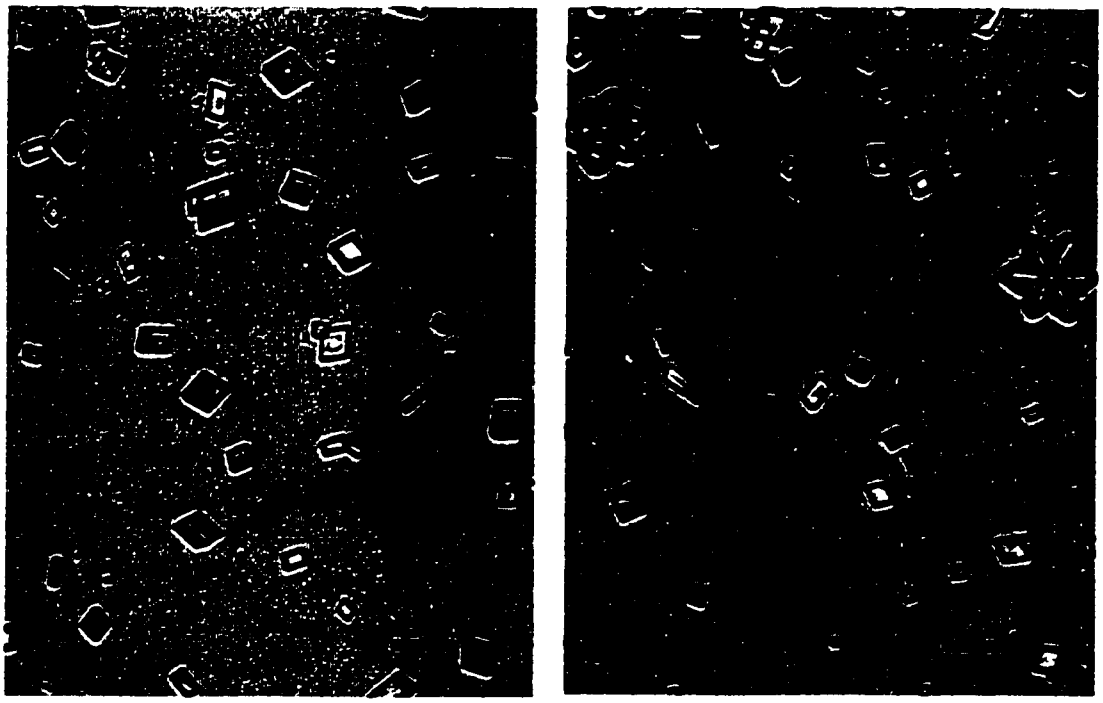

Figure 3.6 Calcium carbonate crystal grown on the on (111) bare silicon wafer surface. Most of crystals are calcite.

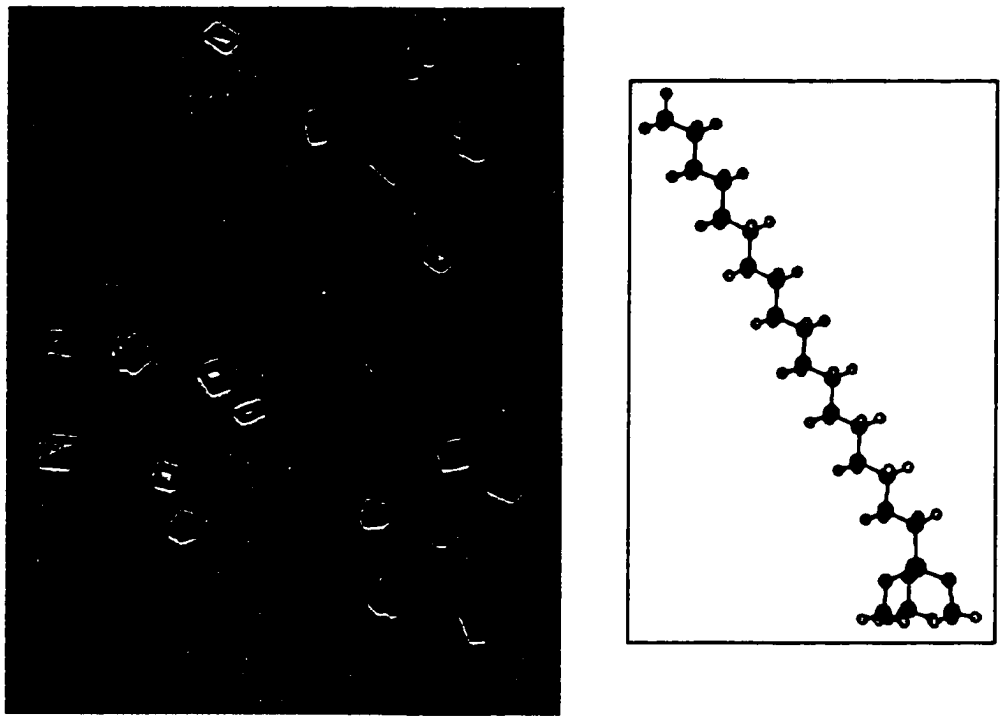

Figure 3.7 Calcite crystals grown on the surafce of octadecyltrichlorosilane(OTS) SAMs on silicon.

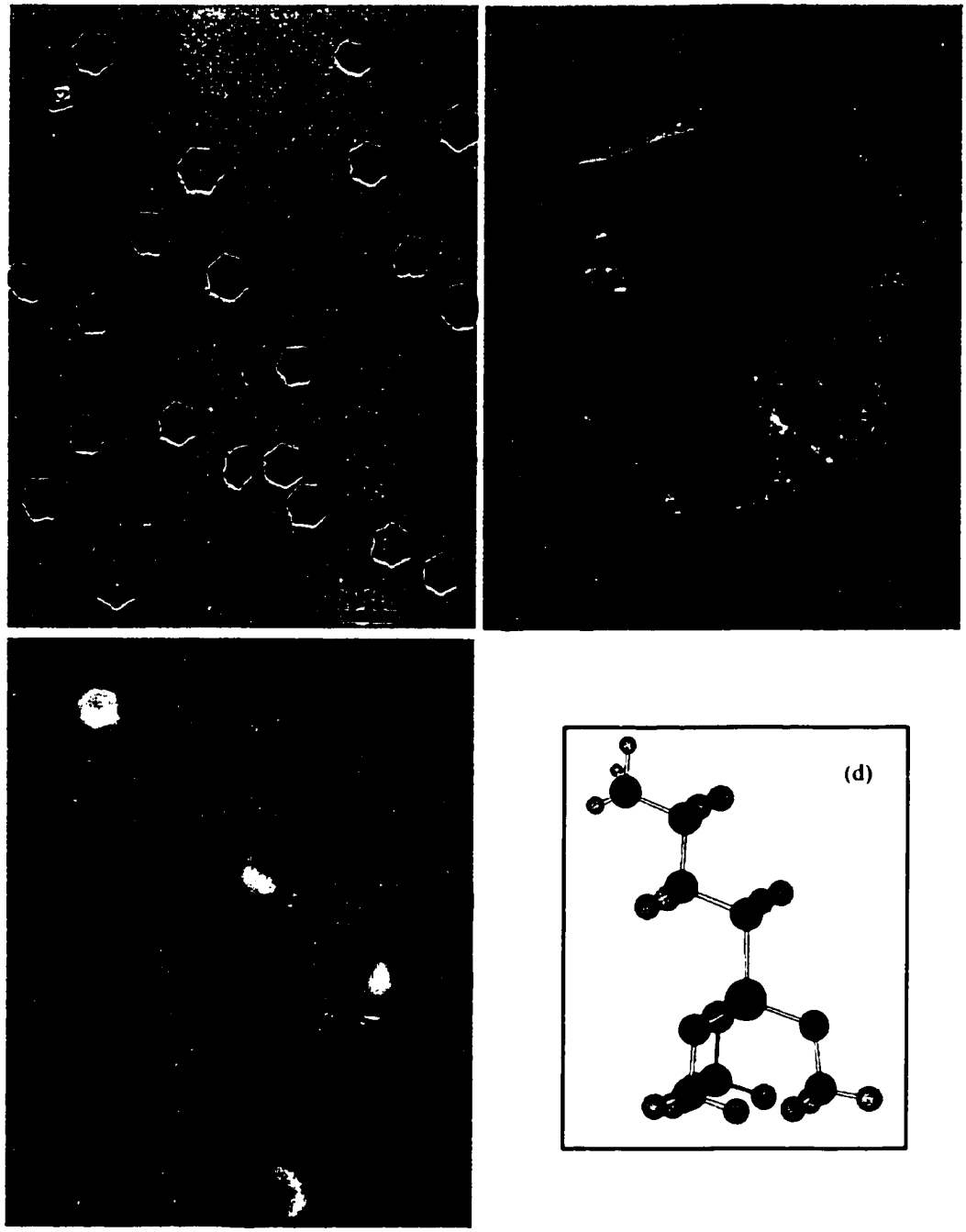

Figure 3.8 Template directed nucleation of calcium crystallization on SAMs of (3-aminopropyl) trimethoxysilane (APS) on silicon surfaces. (a)Most of the crystals observed are vaterite; (b) high magnification; (c) early stage of nucleation; (d) the molecular structure of pronated APS

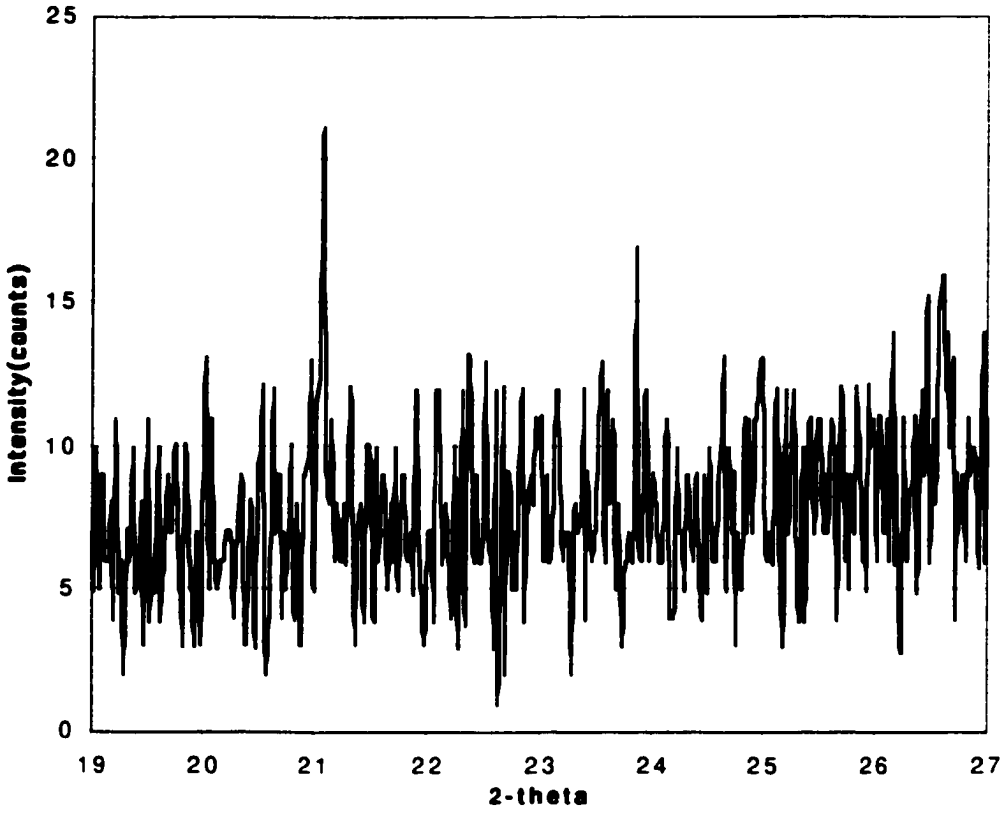

Figure 3.9 X-ray diffraction pattern of calcium carbonate crystal templated on APS surface. The sample was analyzed by θ-2θ mode. Only diffraction planes parallel to the plane of substrate produce diffraction peaks. The peak at 2θ=21 °C is the diffraction from 002 plane of vaterite. This indicates vaterite crystals were templated with (00.1) plane parallel to the surfaces.

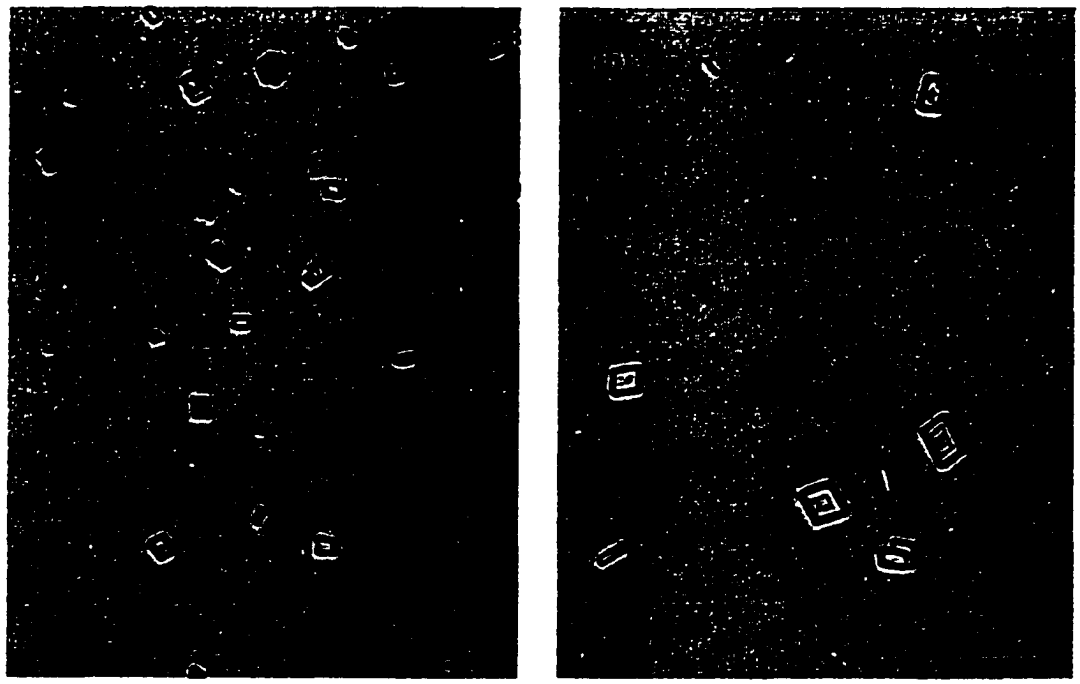

Figure 3.10 (a) Calcite crystals on Alkyl-terminated SAMs surfaces (1-dodecanethiol); (b) calcite crystals on OH-terminated SAMs surface(11-mercapto-1-undecanol)

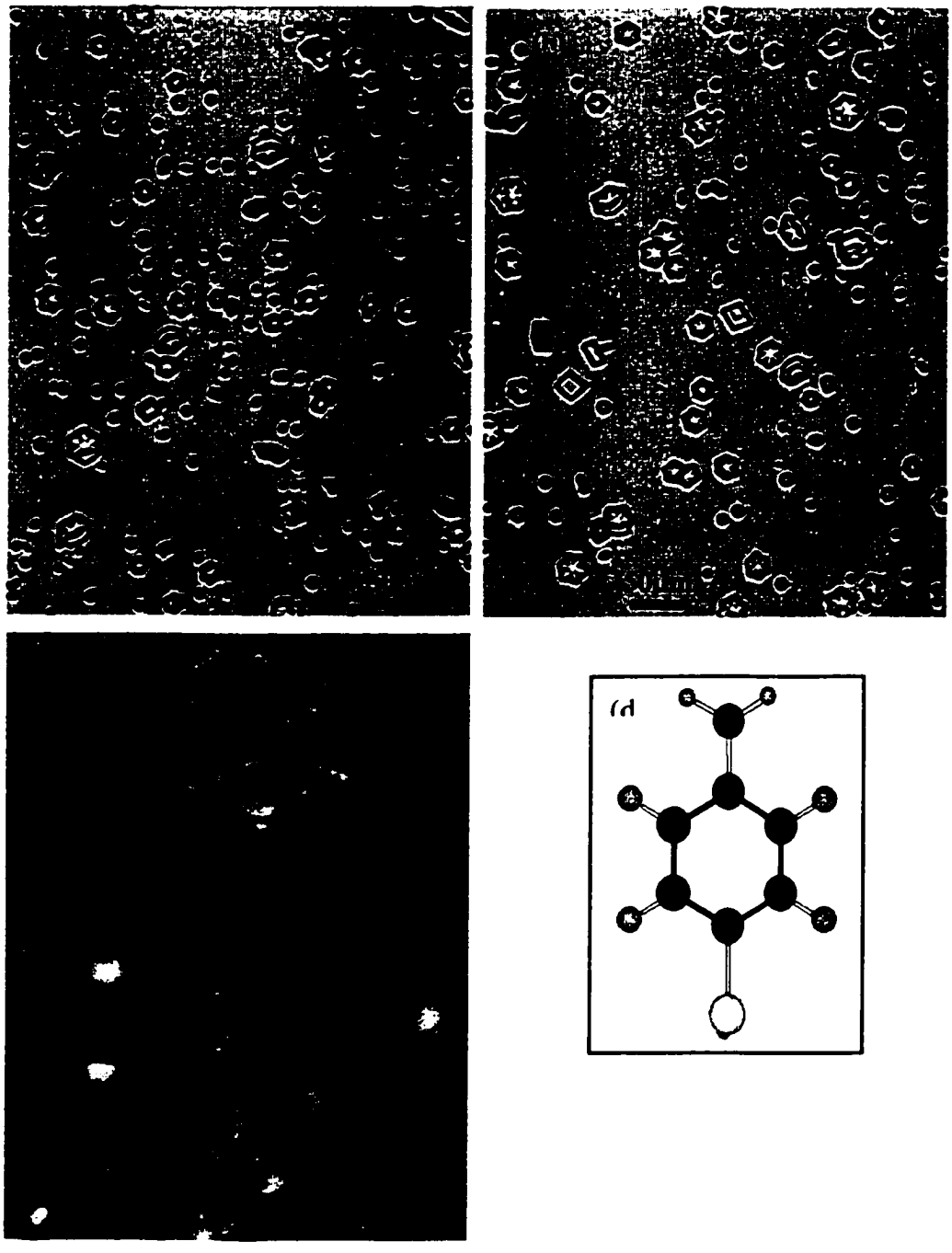

Figure 3.11 Template directed nucleation of calcium carbonate on SAMs of 4-aminothiolphenol on gold surfaces. (a, b) most of crystals formed on SAMs are vaterite; (c) high magnification of (a); (d) molecular structure of 4-aminothiolphenol

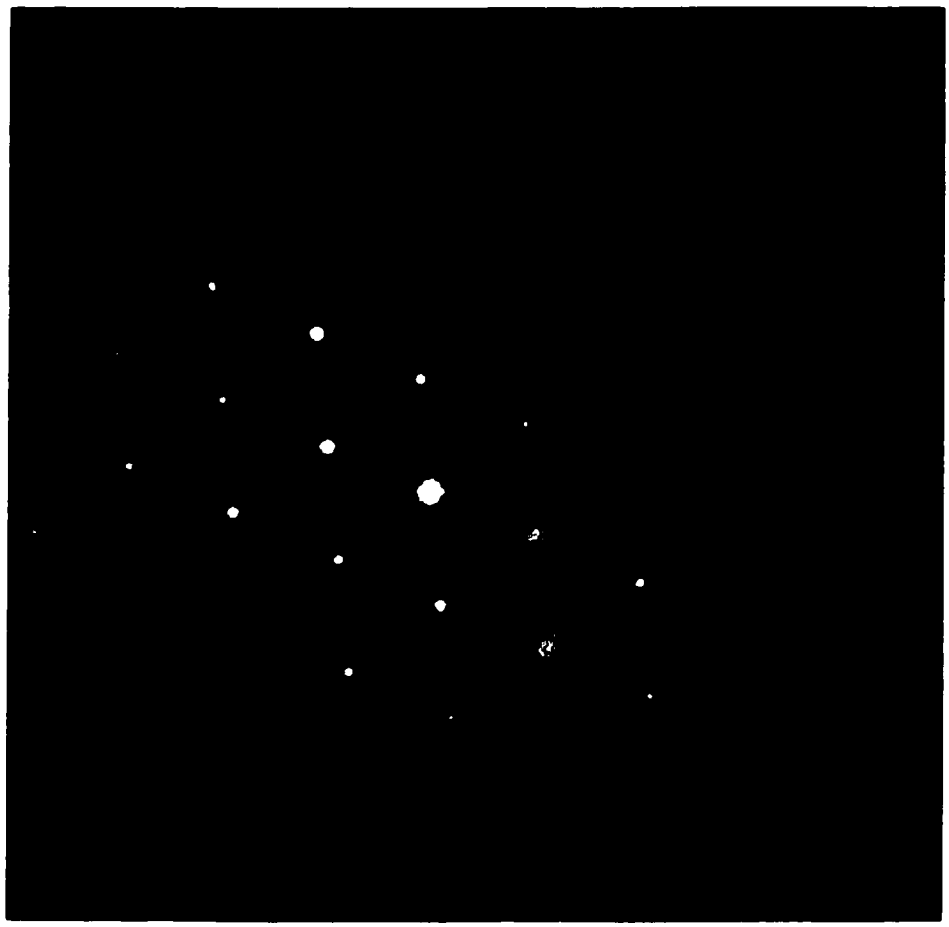

Figure 3.12 Electron diffraction pattern of calcium carbonate crystals grown on the SAMs of aminothiolphenol on gold surface. The crystal is identified as vaterite with their [00.1] perpendicular to the substrate surface.

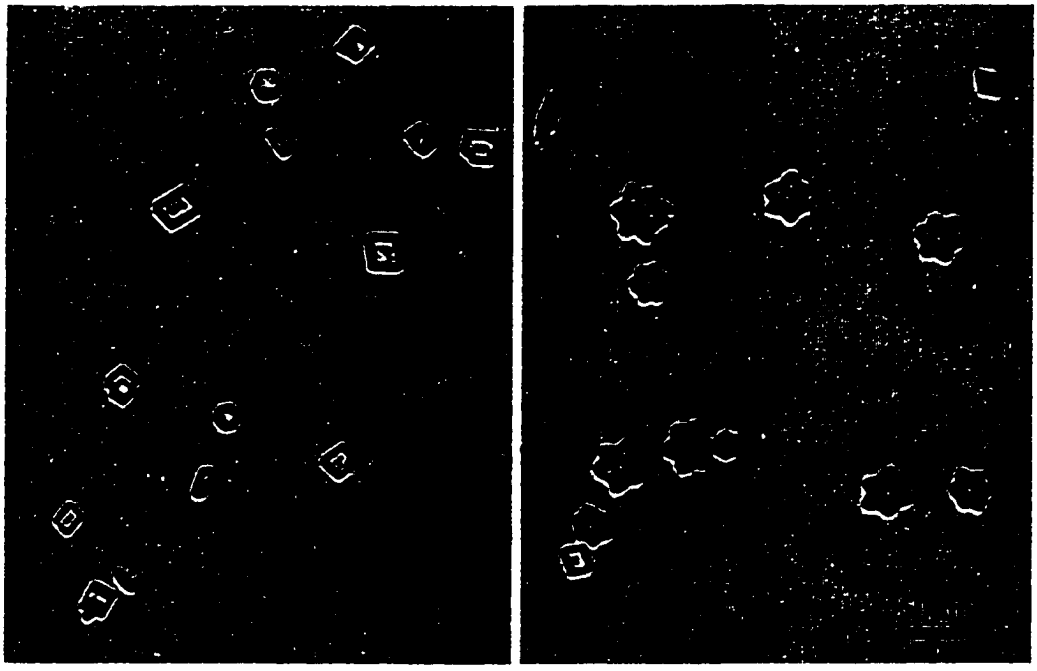

(a) (b)

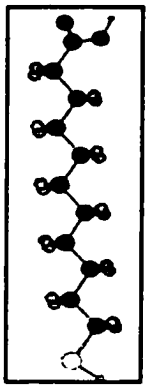

Figure 3.13 Template directed nucleation of calcium carbonate using SAMs of 11-mercaptoundecanoic acid on gold surface. (a) calcite crystals formed on SAMs at pH=5.8-6.0, [Ca2+]=4.5mM; (b)vaterite crystals were templated at pH=7.5, [Ca2+]=4.5mM; (c) the structure of 11-mercaptoundecanoic acid.

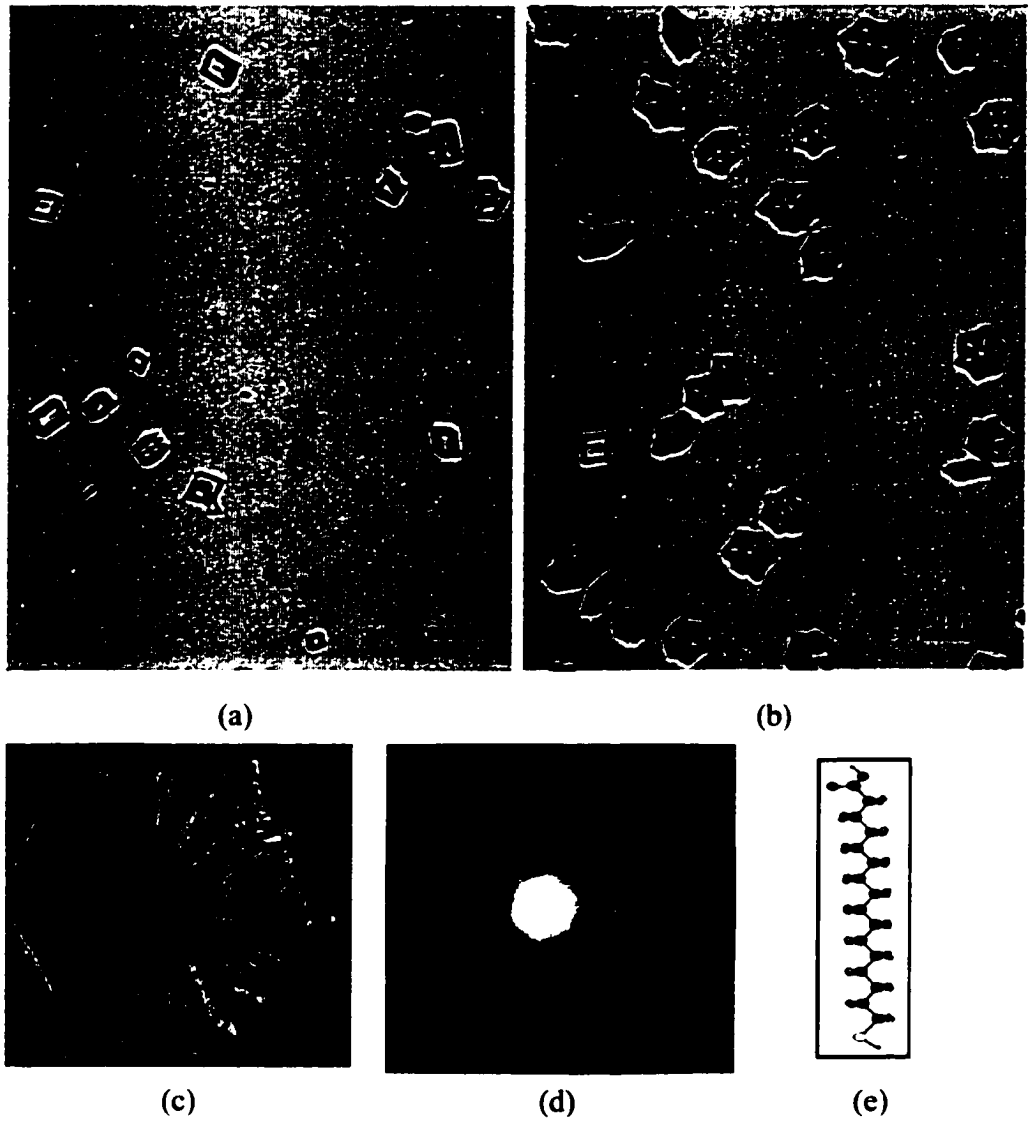

Figure 3.14 Template directed nucleation of calcium carbonate using SAMs of 16-mercaptohexadecanoic acid on gold surface. (a) calcite crystals were formed on SAMs at pH=5.8-6.0, [Ca2+]=4.5mM; (b)vaterite crystals were templated on SAMs at pH=7.5, [Ca2+]=4.5mM; (c) vaterite crystal from (b) with higher magnification; (d) the same crystal as (c) with different focus to show hexagonal shape of the central spot; (e) the structure of 16-mercaptohexadecanoic acid.

Chapter 4

Detecting the kinetics and interacting dynamics of template directed nucleation with ATR-FTIR and AFM

In the previous two chapters we have demonstrated that polymorphs of $CaCO_3$ crystals can be controlled by using Langmuir monolayers at air/liquid interfaces or SAMs at solid/liquid interfaces as templates. Our results showed that the electrostatic interaction and stereochemical correspondence between incipient nuclei and organized organic assemblies are the predominant factors in determining the specific nucleation face and the polymorphic types of the crystals. However, we still do not have direct evidence for these interactions at early stage of aggregations and interactions. Also the kinetics of template directed nucleation at early stage remains unclear. In this chapter, we will use in situ attenuated total reflectance Fourier transform infrared spectroscopy (ATR-FTIR) to detect the dynamics of interactions between the templates and the moieties of crystals. Also atomic force microscopy (AFM) will be used to detect the development of nuclei morphology and the kinetics of the template directed nucleation at early stage

4.1 Introduction

The polymorphism and the orientation of crystals can be affected by the presence of organic thin film as we demonstrated in the chapter 2 and chapter 3 and also by others (see table 1.3 and table 1.4). The organic thin films serve as templates for selective nucleation of crystalline materials at the interfaces. The formation of crystals is affected by physical, chemical and molecular interactions between the organic templates and the moieties of nuclei. These interactions could include geometric matching,[55,56,75,87,99] stereochemical correspondence and electrostatic interactions[38,50,51,80]. For geometric matching, the functional group of template is matched to the nucleating species, so that the 2-D structure of headgroup at interface mimics a crystal plane in the bulk crystal and hence leads to the nucleation of the bulk crystal face. For electrostatic interactions, the headgroup of thin film is charged and this leads the accumulating and binding of opposite charged ions from the solution. The charge and structure of this binding layer could be very similar to the crystal face in bulk crystals and induce the nucleation.

For different templates and crystalline materials, the main interaction, which leads to induce the nucleation, could be different. As we pointed out in chapter2 and chapter 3, the electrostatic interaction between the functional group of organized organic assemblies and the ionic components from the solution is the major factor for the nucleation of

vaterite crystals, while geometric matching between template and crystal faces is not necessary.

Although a lot of mechanisms have been proposed for the template directed nucleation process, most of them are postulations based on the morphology of crystals and the properties of thin films, such as molecular structure and molecular area of monolayer. There are only few studies that have directly detected the interaction between the template and the crystalline component during the nucleation.[74] In addition, how the morphology and the number of nuclei change with time remains unclear.

Fourier Transform Infrared (FTIR) spectroscopy is a very powerful tool for probing the structure and molecular dynamics of organic monolayer. It has been widely used to study the surfactant orientation and structure of Langmuir monolayers and LB films.[100-103] [104] Attenuated total reflectance Fourier transform infrared spectroscopy (ATR-FTIR) have been extensively used to study the thin film on the single crystal substrate because of it unique advantage of detecting the molecular events at interface. The ATR-FTIR method has been applied successfully for the study of surfactant adsorption onto solid surfaces,[105] surface chemistry of siloxane SAMs,[106] and water transportation in LB films,[107] etc. In our lab, ATR-FTIR has been used to investigate the kinetics of octadecyltrichlorosilane self-assembly on silicon oxide surfaces[43] and the adsorption of trisiloxane and alkyl poly-ethoxylate surfactants on hydrophobic silane monolayers. [108]

The binding of cation to the fatty acid and phospholipid monolayers has also been investigated by external reflection FTIR spectroscopy at the air-water-interface.[109,110] Also Ahn and coworker[74] have used external reflection FTIR to study the dynamics of template directed calcite crystallization at air/liquid interface by fitting a mini-trough into the FTIR sample chamber.

In this research, we investigated the interactions between incipient nuclei and organized organic assemblies, which decide the polymorph types of crystals induced by templates. Due to its powerful capability of detecting the interactions between molecules, ATR-FTIR was used to determine the binding mode and extent of binding of the crystal constituents on the templates. Stearic acid LB film deposit on hydrophobic germanium crystals was used as template for FTIR study.

Atomic force microscopy (AFM) is a scanning probe microscopy (SPM) technique, which is able to study surface properties of materials from atomic to micron level. In this chapter, we will also discuss the results of using AFM to detect the development of nuclei's morphology and the kinetics of the template directed nucleation at early stage.

4.2 Experimental section

4.2.1 Materials

Octadecyltrichlorosilane, OTS (95%), chloroform (>99.9%, HPLC), carbon tetrachloride (>99.9%, HPLC grade) and hexadecane (HPLC grade) were purchased from Aldrich Chemicals. Stearic acid (99.5%, Standard for GC) and (3-aminopropyl) trimethoxysilane, APS (97%) were purchased from Fluka. Acetone (AR grade), toluene, sulfuric acid (95-98%) and Nochromix® crystals were purchased from Fisher Scientific. Silicon wafers were obtained from WaferNet Inc. All chemicals were used as received without any further purification. De-ionized water with a resistively of 18MΩ cm from a Millipore® system was used. The Germanium ATR element IRE, (50 x 10 x 3 mm, SPP 45°) were obtained from Harrick Scientific Corporation, NJ.

4.2.2 Preparation of Hydrophobic Surface and LB film on Ge ATR element

The germanium ATR element was cleaned just before used. The procedure includes sonication in acetone for 10 min and rinse with the de-ionized water and again sonication in water for 10 min. The surface of germanium ATR element was made hydrophobic by the deposition of OTS monolayer. The procedure is similar to the deposition of OTS monolayers on the silicon wafer. The freshly cleaned ATR element was dipped into a 2 mM OTS solution with a mixed solvent of n-hexadecane, carbon

tetrachloride, and chloroform (80:12:8 by volume) for 30 min. Then the ATR was rinsed with chloroform for 3-5 times to remove the physically adsorbed OTS. The ATR was dried by a stream of N_2 gas.

The stearic acid LB monolayer was deposited on the top of OTS layer with the carbonyl groups on the top of surfaces. The LB film deposition was carried out on a KSV5000 Langmuir-Blodgett trough (KSV Instruments). The de-ionized water was used as subphase. The pH of subphase was adjusted to 2 by adding concentrate HCl solution. The surface of the subphase was cleaned by aspiration until zero surface pressure was reached throughout expansion and contraction of the barriers. After spreading, the chloroform was allowed to evaporate for 5 min, the monolayer film was compressed at a speed of 2mN/m/min. After the target pressure (30mN/m) was reached, the film was stabilized for 20 min before the transfer. The condensed monolayer on the water surface was transferred onto a hydrophobic Germanium ATR element at a constant surface pressure with a dipping speed of 5 mm/min. The deposition occurred during the first pass of the substrate through the air-water interface so that the hydrocarbon chain came against the surface of the substrate and thus the "tail" was deposited first.

4.2.3 Procedure of in situ ATR-FTIR experiment

The ATR-FTIR cell consists of two Teflon plate with rectangular cavity in the center of plate and orifice on the side for inlet and outlet for solution.[108] The silicon rubber

gaskets were used to seal the gap between ATR optical element and the Teflon plates. The Teflon ATR-FTIR cell, the connector and the silicon rubber gaskets are cleaned thoroughly before used. The Teflon plates were cleaned by the following procedure. The plates were sonicated in a freshly prepared Nochromix® sulfuric acid solution for 30 minutes. Then the plates were rinsed with water for 3-5 times and further sonicated in Millipore® water for 30 min. The Teflon plates were then dried in a stream of N_2 just before used. The silicon rubber gaskets and the connector were sonicated in ethanol and water for 10 min respectively and rinsed with water for several times. After everything is cleaned, the ATR-FTIR cell was assembled inside a clean hood. The cell was connected by tubing to the solution reservoir. ALKB Micropeppex ® peristaltic pump was used to recycle the solution. The experimental setup is shown in figure 4.1. The middle part of the figure shows the ATR-FTIR flow cell construction. The bottom part of figure 4.1 shows stearic acid LB film deposit on the OTS treated Germanium ATR element. The crystal was nucleated on the top of LB film.

The IR spectra are collected using Bio-Rad FTS 175 spectrometer. A highly sensitive, liquid nitrogen cooled Mercury-Cadmium-Telluride (MCT) detector is used to detect the IR beam. The spectra were collected as interferograms with a resolution of 2 cm^{-1} and Fourier transformed with triangular apodization. Each spectrum was averaged over 200 scans. The assembled ATR cell is kept inside the chamber of spectrometer and

purged with nitrogen to remove water and CO_2 vapors. IR spectra are collected in situ at regular intervals during the template directed nucleation. The spectra of OTS monolayer contacted with water were used as background for the *in-situ* experiment.

4.2.4 Crystal morphology development at early stage studied by AFM

The APS SAMs on silicon surfaces were chosen as template for this study. The APS monolayers were prepared by dipping freshly clean silicon wafers into a 1wt% solution of APS in toluene for 10 min at 60 °C. Then the wafer were washed several times with toluene to remove the physically absorbed molecules and dried by a stream of N_2.

The silicon substrates coated with APS SAMs were dipped into beakers containing the supersaturated calcium bicarbonate solution. The Ca^{2+} concentration in the supersaturated solution was 4.5 mM. After 1hr, 3hr, 6hr, the samples were taken out from the solution respectively, quickly rinsed once with water. Most of water remained on surfaces was removed by using Kimwip tissues. The samples were then blown dried with nitrogen. The size and morphology of nucleus on the surfaces were examined by AFM.

Atomic force microscopy images were obtained using Nanoscope III (Digital instruments, Inc,). Silicon nitride sharpened tips with a force constants of 0.58N/m, (purchased from Digital Instruments, Inc.) were used for height and friction images in contact mode. Images were obtained from at least three macroscopically separated areas on each sample. All images were processed using procedures for plane-fit and flatten in

Nanoscope III software without any filtering. Dimensions of the domains were measured directly from the AFM height images and height of nuclei were estimated from section analysis of the topographic images.

4.3 Result and discussion

4.3.1 FTIR spectra of OTS SAMs and the stearic acid LB film

The ATR-FTIR absorption spectra of OTS SAMs and the stearic acid LB film are shown in figure 4.2 and figure 4.3. These spectra are measured in air. The clean germanium surface was used as background for the absorption spectrum of OTS SAMs. OTS SAMs on germanium surface was used as background for the spectrum of stearic acid LB film. The stretching and bending bands for hydrocarbon alkyl chain are clearly shown in the spectra. Also a high signal-to-noise ratio of carbonyl head group's peak from stearic acid LB film spectrum is also shown in the figures. The characteristic bands of OTS SAMs and stearic acid LB film have been summarized as table 4.1.

From figure 4.2 and figure 4.3, we are able to get some useful information about the molecular packing and conformation of alkyl chain in monolayer films. The characteristic bands of OTS monolayer on germanium surface agreed well with those of OTS monolayer on silicon surfaces (see Krishnan[43] and references inside). However, the stretching bands from alkyl chain of stearic acid LB films shift to lower wavenumber

compared to those of OTS SAMs. This means that stearic acid LB monolayer has higher ordering than OTS SAMs. The methylene asymmetric and symmetric stretching frequencies are very sensitive to the structure and conformation of the hydrocarbon chain. According to Fujimoto etc., [100], the stretching bands of CH_2 appear near 2918 and 2848 cm^{-1} when the hydrocarbon chain takes trans-zigzag confirmation. These two bands can shift towards near 2928 and 2858 cm^{-1} depending the content of gauche confirmation. This indicates that stearic acid LB monolayer in our experiment is highly ordered and takes trans-zigzag confirmation. The OTS monolayer is a mixture of trans-zigzag and gauche conformation.

Table 4.1 Characteristic bands of OTS SAMs and stearic acid LB film

Wavenumber (cm^{-1})		Band assignment
OTS SAMs	Stearic acid LB film	
2959.5	2954	asymmetric methyl(CH_3) stretching
2920.9	2917	asymmetric methylene (CH_2) stretching
2851.4	2849.5	symmetric methyl(CH_2) stretching
1468.1	1472, 1464.3	methylene bending
N/A	1705.4, 1691.9	carbonyl stretching

In figure 4.3, in addition to the shift of the stretching peaks of alkylchain, we also observe that the characteristic peak of the methylene bending mode at ~1470 cm^{-1}

undergoes a split in stearic acid LB film. The CH_2 bending band is very sensitive to the intermolecular interaction. This split in the bending mode peak is indicative of an orthorhombic subcell packing with the restriction of hydrocarbon rotation around its long axis. [100,111,112]

The bands near 1700 cm^{-1} in the spectra of stearic acid LB film are assigned to the carbonyl stretching.[74,100,101,106] Careful observation (figure 4.3) reveals peak splitting into two components near 1700 cm^{-1}: one at 1705 cm^{-1} and another at 1692 cm^{-1}. Fujimoto etc observed similar peak splitting of carbonyl stretching band of arachidic acid monolayer.[100] The peak splitting of carbonyl stretching band indicates the carboxylic groups form hydrogen bonding or a ring dimer between the neighboring molecules.

4.3.2 The calcium ions binding to the carbonyl groups of stearic acid LB film.

The interactions between the headgroup of stearic acid Langmuir monolayer and the calcium ions from the subphase have been discussed in Chapter 2. The calcium ion binding to the carboxylate headgroup was indirectly evidenced by the dramatically change of π-A isotherm when the calcium ions were introduced into the subphase. (see figure 2.6). Here we used FTIR to directly detect the binding of calcium ions to the carboxylate headgroups.

Figure 4.4 shows spectra series of stearic acid LB film with contact of 10 mM $CaCl_2$ solution. The carboxylate asymmetric stretching bands at 1580 cm^{-1} and 1547.2 cm^{-1}

indicate the calcium ion binding to the carbonyl headgroup.[74,101,107] These two peaks appeared as soon as the $CaCl_2$ solution was introduced into the flow cell and reached the maximum after half an hour. Besides the increase of carboxylate peaks at 1580 cm^{-1} and 1547.2 cm^{-1}, we also observed that the carbonyl stretching peak at 1710 cm^{-1} decreased with time. This strongly indicates the carbonyl converses to carboxylate by the calcium binding from the solution. For the free carboxylate without calcium ion binding, The asymmetric stretching band appears as a single peak centered at ~1550 cm^{-1}, instead of doublet as we observed in our experiment.[106]

4.3.3Dynamic interaction between nuclei and template studied by FTIR

In situ FTIR spectra in the course of template directed nucleation of calcium carbonate on stearic acid LB film were shown in the figure 4.5. The pH of supersaturation solution used in this experiment is 7.5. At this pH value, the headgroups of stearic acid are mostly ionized to COO^-. When supersaturate solution was introduced into the flow cell, the calcium ions were immediately binding to the headgroups and the peaks of calcium-carboxylate at 1580 cm^{-1} and 1547.2 cm^{-1} reached maximum within two minutes as shown in figure 4.5. This fast calcium-carboxylate complex formation is very different from the much slower calcium-complex formation from the calcium chloride solution, in which it took half an hour for the calcium binding process to complete. Obviously this difference is not because of the difference of calcium ion

concentration. The calcium concentration in supersaturate solution is 4.5 mM and that in the calcium chloride solution is 10 mM. One reason for the fast calcium binding during the template crystallization could be that the pH of supersaturated solution is higher than that of the calcium chloride solution, The higher the pH, the better the ionization of the headgroups and also the easier the calcium ions binding will be. Another reason could be the synergic effect between the calcium binding and the template directed nucleation. The calcium binding to the surface helps the nucleation of crystals of calcium carbonate. Also the nucleation of crystals on the surface reduces the accumulation of positive charge near the surface and helps more calcium ions transfer to the interfacial region.

In figure 4.5, a broad peak centered 1450.8 cm^{-1} and a sharp peak at 874 cm^{-1} are also observed. These two peaks are from the carbonate vibration, which indicates the formation of calcium carbonate crystals on the ATR surfaces. The peak at 1450.8 cm^{-1} is assigned to the in-plane asymmetric carbonate stretching and the peak at 874 cm^{-1} is assigned to the out-of-plane carbonate bending.[14,74,113]. Unfortunately from the spectra of carbonate, we are unable to tell which polymorph we obtained on the ATR surfaces because the spectra of vaterite, aragonite and calcite crystals are not very different.[113]. After the in-situ experiment was finished, the flow cell was dissembled and ATR crystal was examined under optical microscopy. The crystals observed on the ATR surfaces are

mostly vaterite with [00.1] perpendicular to the ATR surface (figure 4.6). The results agree with that in the chapter 2 and chapter 3.

In contrast, very different spectra behavior was observed when the pH of supersaturate solution was low (5.6~5.8). The time series of IR spectra for template directed nucleation with lower solution pH were shown in the figure 4.7. Except the solution pH, the experimental conditions are the same as those performed for figure 4.5. The comparison of *in situ* FTIR spectra of template directed nucleation of calcium carbonate on stearic acid LB film at different pH was shown in figure 4.8. One direct observation is that the increases of carbonate in-plane asymmetric stretching at 1450.8 cm^{-1} and out-of-plane bending at 874 cm^{-1} at low solution pH (pH=5.6~5.8) are much slower than that at higher solution pH (pH=7.5), which indicates the slower formation of crystals on the surfaces at lower pH. Another observation is that at low solution pH, the calcium binding peaks at 1543.4 cm^{-1} and 1580 at 2 min is much smaller than that at 120 min. This indicates the calcium binding to the carbonyl headgroup is slow at low pH value (5.6~5.8), which is very different from the fast calcium binding at solution pH of 7.5. At the beginning of nucleation, the headgroups of stearic acid only partially bound with calcium ion at low pH. This verifies our hypothesis of incomplete calcium ion binding to the carbonyl headgroup at low solution pH as we discussed in previous chapters. This incomplete Ca^{2+} binding didn't induce the nucleation of calcium carbonate

on the surfaces. This is also the reason for the slower formation of crystals on the surfaces at lower pH.

4.3.4 The nucleation and crystal growth during template crystallization on solid surface

Crystallization from the solution is a two-step process: nucleation and crystal growth. The crystals we showed in chapter 2 and chapter 3 are the final products of these two steps. The crystalline phase of nuclei will decide the polymorphism of crystals we obtained. So usually the crystal structures of nuclei at early stage are the same as that of final products. However, the morphology of nuclei at early stage of template directed nucleation and how these nanometer-sized nuclei developed into micro-sized crystals remain unclear. Here we used atomic force microscopy (AFM), for the first time, to investigate the morphology development and crystal growth of nuclei on the surface of template at the early stage of template crystallization.

The AFM images of calcium carbonate particles formed on APS SAMs at different stages of process are shown in figure 4.9 to figure 4.11. For each stage, two images with different magnification were shown. All these images are height AFM profiles. One thing need to be mentioned is that z ranges are different for different figures. Z ranges are 20nm, 30 nm and 50 nm for figure 4.9(1hr), figure 4.10(3hr) and figure 4.11 (6hr), respectively. For the nuclei at early stages (1hr and 3hr) on the solid surfaces, the shape of particle is circular, with diameter much bigger than height. It is very similar to the

liquid droplet spreading on solid surface with low contact angle. This indicates the interfacial energy between nuclei and solid surface is very low, which is the thermodynamic basis for the template directed nucleation. At the stage of 6 hr, some big nuclei already showed the hexagonal shape. These big nuclei will develop into the central spots of vaterite crystals as we observed in chapter 3(figure 3.8 and figure 3.14).

One observation from these AFM images is that there are two types of particles at each stage, with one have much bigger particle size than the other. The particle size and frequency at different stages are summarized in table 4.2. For the big particles, both height and diameter of particles increase with time. However, for small particles, the particle size didn't changed much from 1hr to 3 hr. The size of small particles does increase from 3 hr to 6 hr.

Table 4.2 Growth of calcium carbonate crystals on APS SAMs surfaces

Time (hr)		1 hr	3 hr	6 hr
Big particles	Diameter (nm)	372.8	410.2	1113.4
	Height(nm)	22.8	25.3	27.4
	Frequency(number/25 μ^2)	10	49	7
Small particles	Diameter (nm)	302.7	289.5	468.4
	Height(nm)	3.4	3.9	13.1
	Frequency(number/25 μ^2)	332	244	57
Total frequency(number/25 μ^2)		342	293	64

From table 4.2, we found that the total particle frequency at the stage of 3 hr is almost the same as that of 1 hr. This indicates that nucleation only happened at the very beginning of the process and most of nucleus on the surfaces didn't dissolve during this period. However the frequency of bigger particles increased from 10 to 49 during 1 hr to 3 hr, which indicates the growth of a small portion of small particles has surpassed others and become bigger particles. By comparing figure 4.11 to figure 4.10, we found that particle frequency on surface has decreased dramatically during the 3hr to 6hr period. The number of small particles at 6 hr is almost the same as the number of big particles at 3 hr. It seems that most of small particles we observed at 3 hr are dissolved during this time period. The big particles at 3hr became small particles at 6 hr. This was also verified by the fact that the diameter and frequency of small particles at 6 hr is almost the same as that of big particles at 3 hr. Again during this period, a few particles grew faster than others and became big particles at 6 hr, but with even smaller frequency. By this way, a few of nuclei grew into big crystals with size of tens of microns, while most of particles dissolved. The final frequency of vaterite crystals after 18 hr is approximately 143/mm^2. So only one nucleus out of 0.96×10^5 nuclei survived and grew into micron-sized particles during crystal growth process.

Another interesting observation is that there are fewer small particles in the area surrounding the big particles compared to other areas. This is more obvious at 6 hr as

shown in figure 4.11. So it is very obviously that the smaller particles will dissolve while the bigger particles grow, which is very common phenomenon during crystal growth and known as Ostwald ripening process.

As shown in figure 4.9 and figure 4.10, the frequency of nuclei on the functionalized surfaces are extremely high at the early stage of nucleation. This indicates that the energy barrier for nucleation is extremely low. The interaction between amine groups on the surfaces and the anion ion from the solution has dramatically decrease the interfacial energy between the solid surfaces and the crystalline phase nucleated.

4.4 Conclusion

In situ ATR-FTIR was used to study the structure of stearic acid LB, the calcium ions binding to the carboxylate headgroups and the interactions between the templates and the moieties of crystals. The spectra of stearic acid LB film showed that LB monolayer is highly ordered and takes trans-zigzag confirmation. The calcium binding to the stearic acid headgroups when contacted with $CaCl_2$ solution was evident both from the increase of doublet carboxylate asymmetric stretching band intensity and the decrease of carbonyl stretching band intensity. When the supersaturate solution was introduced into flow cell, the carbonate in-plane asymmetric band and out-of-plane bending band were probed by FTIR, which indicates the formation of calcium carbonate crystal on LB film. At high solution pH, the formation of calcium-carboxylate complex is fast and

complete, while at low pH, the headgroups of stearic acid were only partially bound with calcium ions at the beginning of nucleation. This leads the different calcium carbonate crystallization behavior on acid-terminated surfaces at different pH.

Atomic force microscopy (AFM) was used to investigate the morphology development and crystal growth of nuclei on the solid surface at the early stage of template crystallization. Our results showed that nucleation only happened at the very beginning of the process. The frequency of nuclei on the functionalized surfaces is extremely high at the early stage of nucleation. However, only a very small portion of these nuclei (one out of 0.96×10^5) survived and grew into micron-sized particle during crystal growth process.

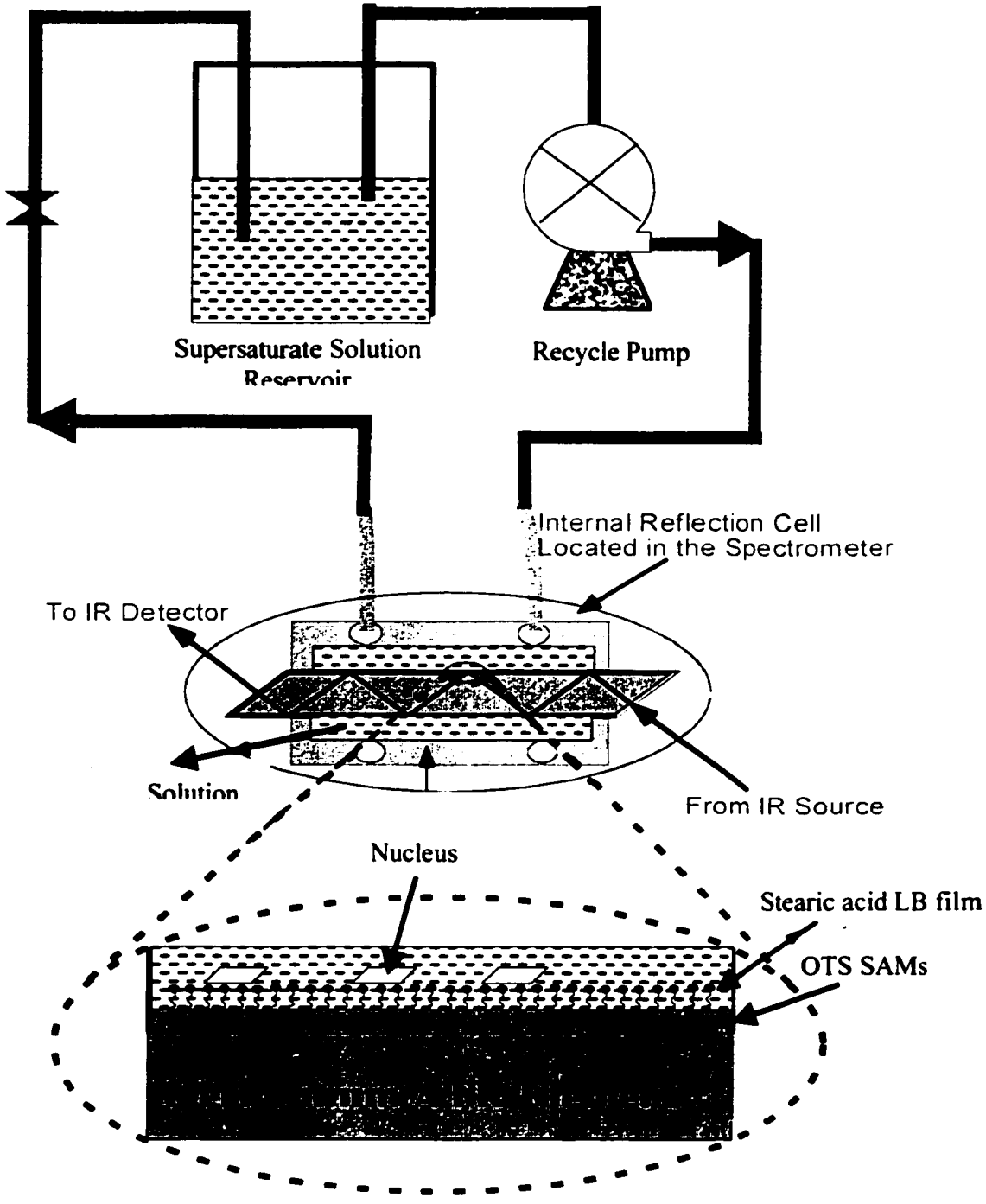

Figure 4.1 Experimental setup for in situ ATR-FTIR measurement of template directed nucleation. The middle figure shows the ATR-FTIR flow cell construction. The bottom figure shows stearic acid LB film deposit on the OTS treated Germanium ATR element. The crystal was nucleated on the top of LB film.

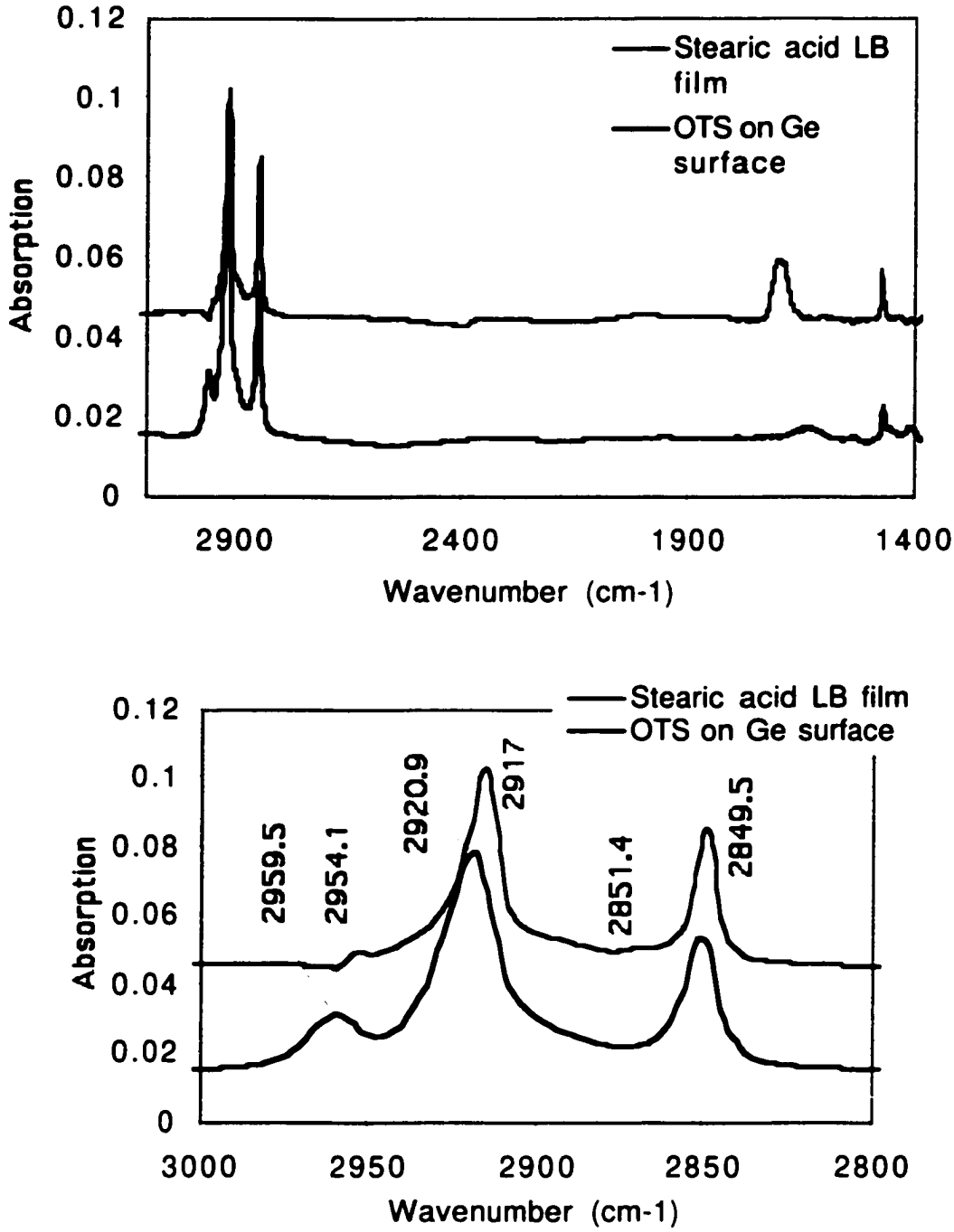

Figure 4.2 FTIR Spectra of OTS SAMs on silicon surfaces and stearic acid LB film. Vibrational bands for hydrocarbon alkyl chain and carbonyl head group are clearly shown in the spectra.

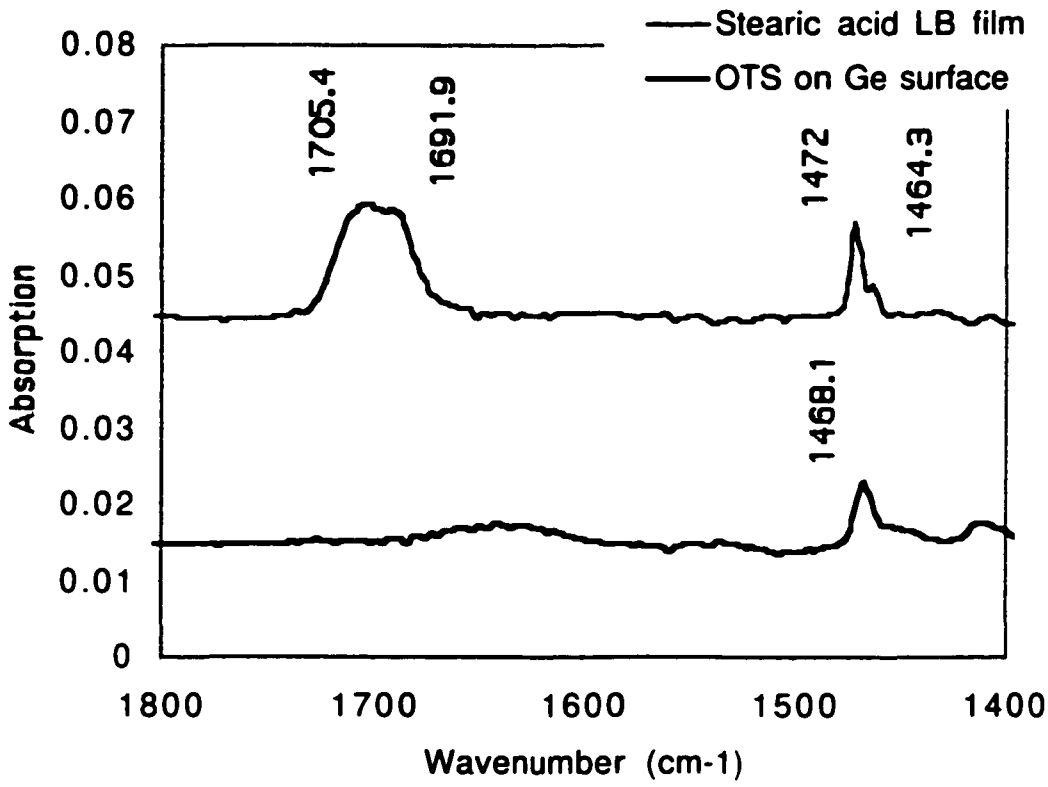

Figure 4.3 FTIR Spectra of OTS SAMs on silicon surfaces and Stearic acid LB film in the range of 1400 cm^{-1} to 1800 cm^{-1}. The peaks at 1705.4 cm^{-1} and 1691.9 cm^{-1} are the carbonyl stretching bands. The bands near 1470 cm^{-1} are for the methylene bending.

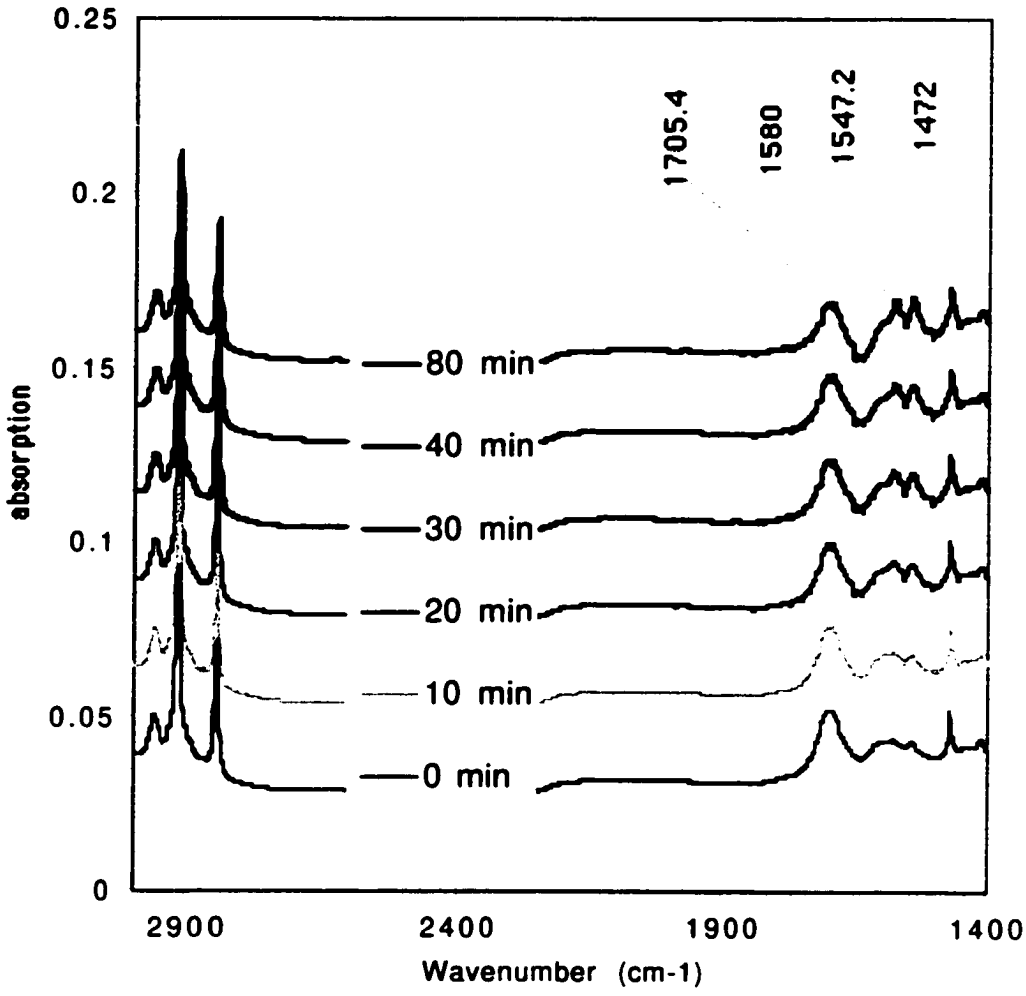

Figure 4.4 FTIR Spectra of stearic acid LB film with contact of 10 mM $CaCl_2$ solution. The bands at 1580 cm^{-1} and 1547.2 cm^{-1} indicate the calcium ion binding to the carbonyl headgroup.

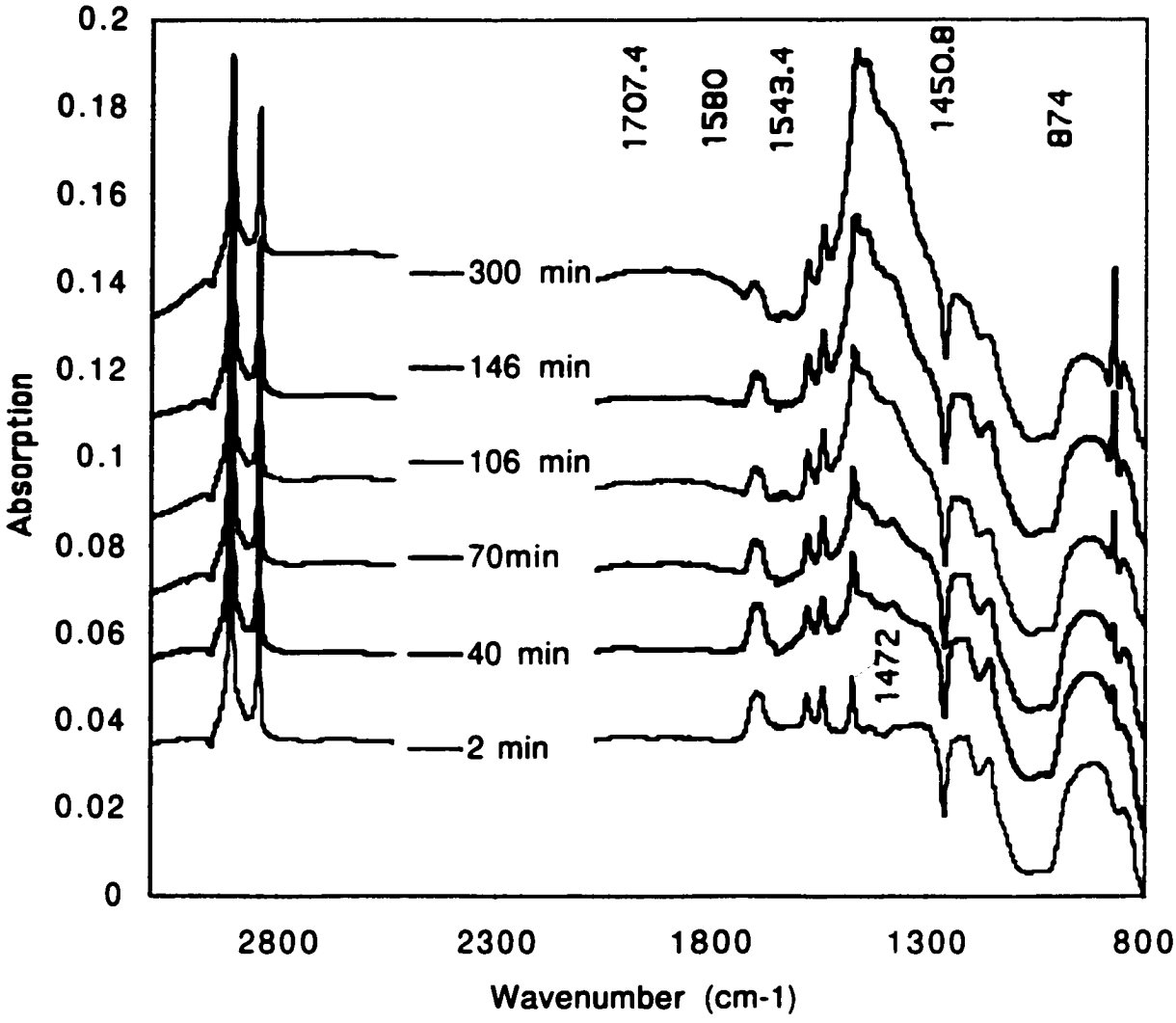

Figure 4.5 *In situ* FTIR Spectra of template directed nucleation of calcium carbonate on stearic acid LB film. The pH of supersaturate solution is 7.5

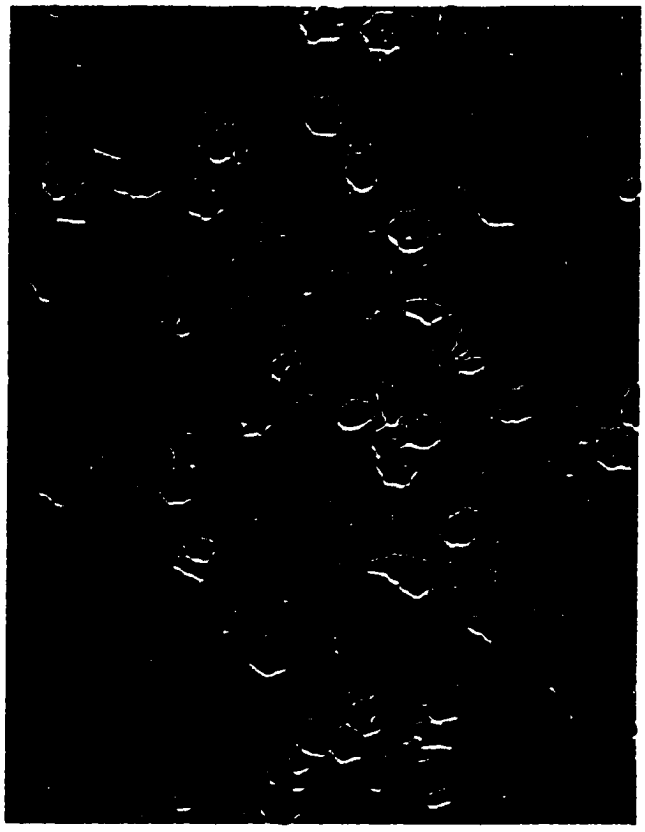

Figure 4.6 Crystals formed on the stearic acid LB film at germanium ATR surfaces at the end of *in-situ* FTIR experiment. Most of crystals observed are vaterite with [00.1] perpendicular to the ATR surface.

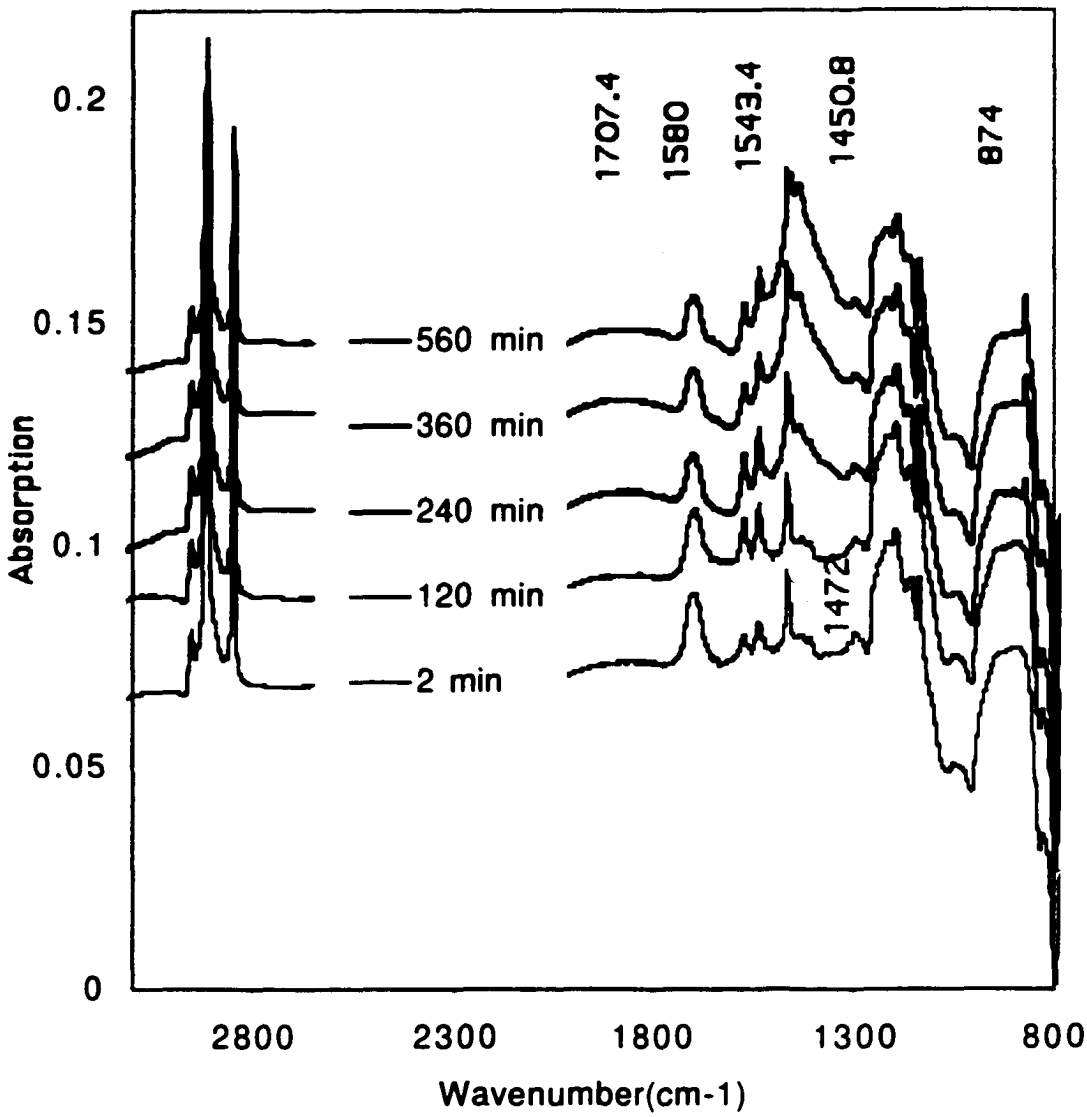

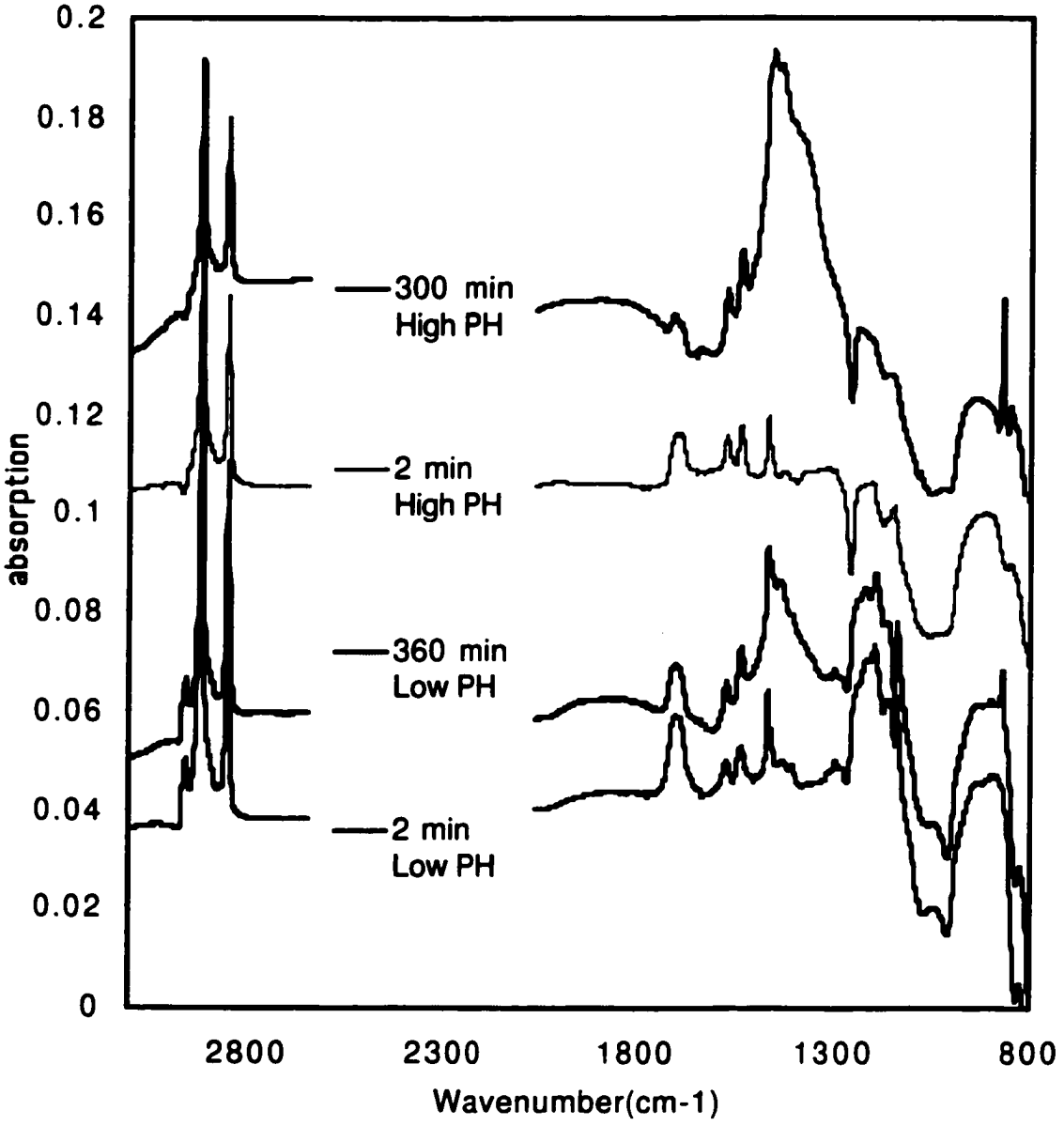

Figure 4.8 Comparison of *in situ* FTIR Spectra of template directed nucleation of calcium carbonate on stearic acid LB film at different pH.

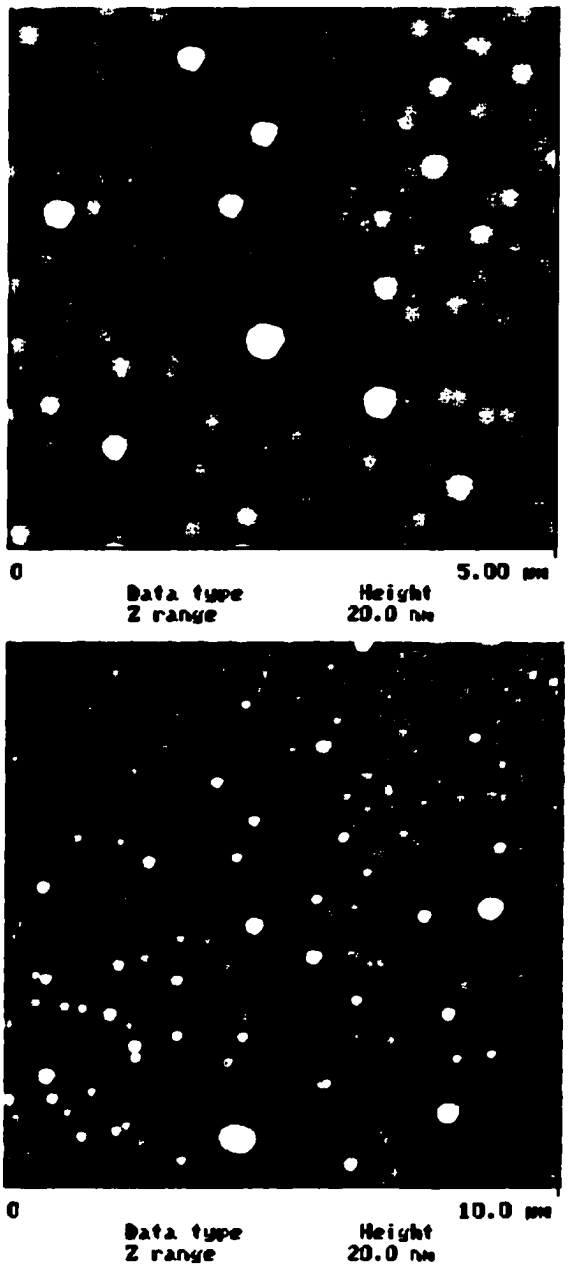

Figure 4. 9. AFM images of $CaCO_3$ nuclei on APS surfaces during template directed nucleation.(1hr)

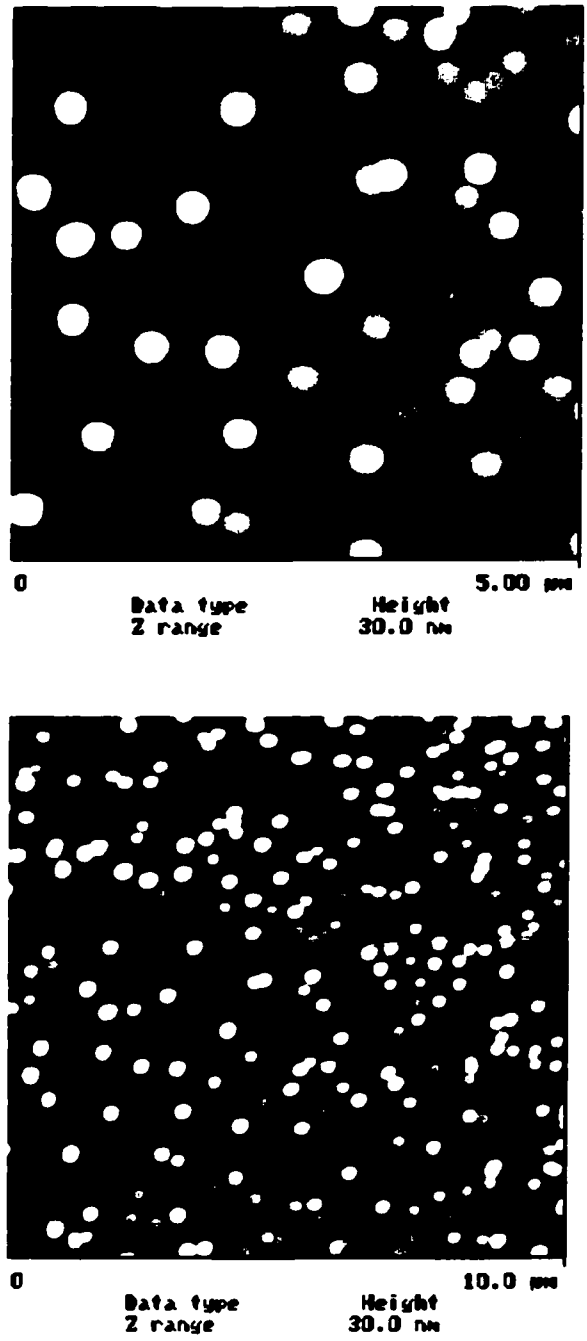

Figure 4.10. AFM images of $CaCO_3$ nuclei on APS surfaces during template directed nucleation.(3hr)

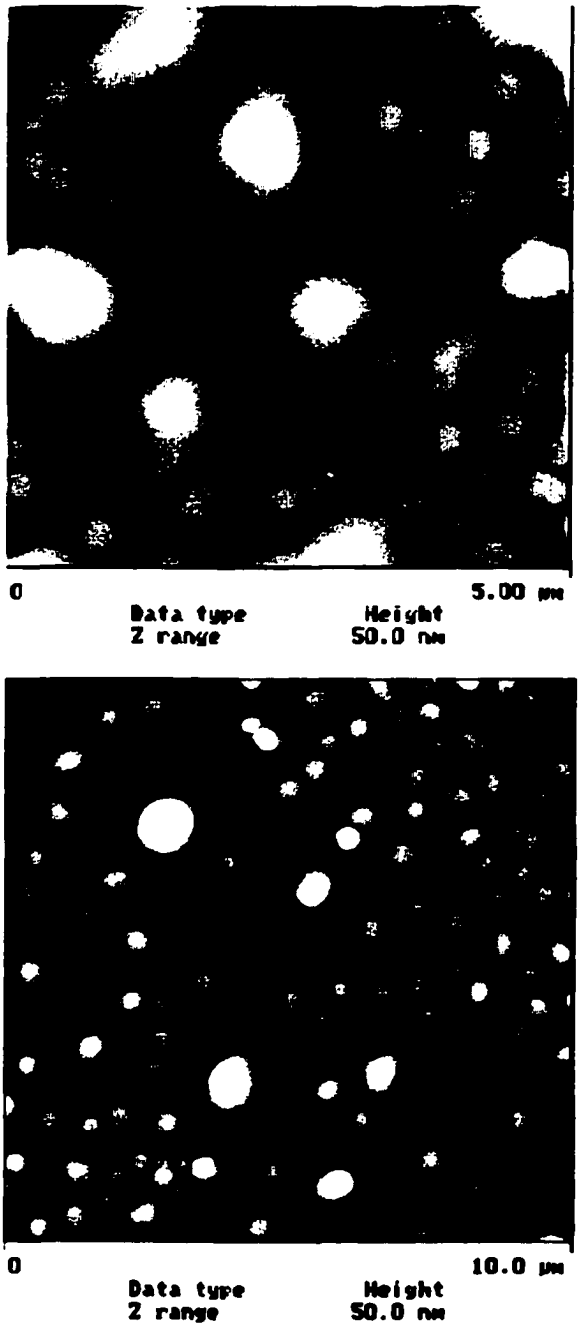

Figure 4.11. AFM images of $CaCO_3$ nuclei on APS surfaces during template directed nucleation.(6hr)

Chapter 5

Conclusions and future work

5.1Conclusions

The size, crystalline phase (polymorphism) and morphology of particles greatly affect the chemical and physical properties of particulate materials. In this research, we have used organized organic assemblies as templates to control the polymorphism of crystals. Calcium carbonate has been chosen as a model crystal system in this research. By using Langmuir monolayers at the air/liquid interfaces and Self-Assembled Monolayers (SAMs) at the solid/liquid interfaces as templates, we have successfully controlled the polymorphism of $CaCO_3$ crystals. Vaterite crystals, which are the thermodynamically unfavored from homogeneous crystallization, have been nucleated by carefully choosing the functional groups of organic assemblies.

Several Langmuir monolayers with various properties have been investigated as templates for polymorph selective crystallization of $CaCO_3$. The crystalline phases of polymorphs of CaCO3 observed under monolayers mainly depend on the dissociation of the headgroup of monolayers instead of the molecular packing density and the properties of the hydrophobic chains. Templating happens only when the functional groups are

completely dissociated and ions of the crystalline component from solution bind to the ionized functional groups.

SAMs of organosilicon on silica surfaces and organosulfur on gold surfaces have been used as template for crystallization. The crystalline phases of $CaCO_3$ nucleated on the functionalized solid surfaces are controlled by the terminal groups of the SAMs, while the substrate used (Au or Si) and the properties of intermediate chain are not very important to the templating process. In both cases, vaterite crystals with [00.1] axis perpendicular to the monolayers were induced by the amine-terminated SAMs. With uncharged alkyl-terminated or alcohol-terminated SAMs, most of crystals are randomly oriented calcite. For acid terminated SAMs, the results depend on the pH of supersaturate solution because the dissociation of acid headgroup is different at different pH. At the solution pH of 5.8, most of crystals obtained on acid-terminated SAMs are calcite, while at pH of 7.5, vaterite crystals with [00.1] axis perpendicular to the substrate were templated.

Our experimental results have clearly shown that the electrostatic interaction and stereochemical correspondence between incipient nuclei and organized organic assemblies are the predominant factors in determining the specific nucleation face and the polymorphism of the crystals, while the exact geometric matching is not necessary for template directed nucleation.

In situ ATR-FTIR have been used to study the structure of stearic acid LB film, the calcium ions binding to the carboxylate headgroups and the interactions between the templates and the crystal moieties. The spectra of stearic acid LB film showed that LB monolayer is highly ordered and assume an all trans confirmation. The calcium ion binding to the stearic acid headgroups was evident from the increase of carboxylate asymmetric stretching band intensity. When the supersaturate solution was introduced into flow cell, the carbonate in-plane asymmetric band and out-of-plane bending modes were probed by FTIR, which indicates the formation of calcium carbonate crystal on LB film. At high solution pH, the formation of calcium-carboxylate complex is fast and complete, while at low pH, the headgroups of stearic acid were only partially bound with calcium ions at the beginning of nucleation. This leads the different calcium carbonate crystallization behavior on acid-terminated surfaces at different pH.

Atomic force microscopy (AFM) was used to investigate the morphology development and crystal growth of nuclei on the solid surface at the early stage of template crystallization. AFM results showed that nucleation only happened at the very beginning of the process. The frequency of nuclei on the functionalized surfaces is extremely high at the early stage of nucleation. However, only a very small portion of these nuclei (one out of 0.96×10^5) survived and grew into micron-sized particle during crystal growth process.

5.2 Future work

In this research we have successfully controlled the polymorphism of calcium carbonate crystals by using organized organic assemblies as template and proved that template directed nucleation is a great approach to control the polymorphism of crystalline materials. However, calcium carbonate was chosen as model crystal system in this study just because the crystal structures and morphologies of its polymorphs are well known. Controlling the polymorphism of calcium carbonate itself does not have much direct practical application. The major application of polymorph selective crystallization will be in pharmaceutical industry. So one direction for the future work will be using this approach to control the polymorphism of drug substance or organic materials, such as glycine and Paracetamol.

In a lot of applications, it not only requires to obtain a desired crystalline phase but also need to control the size of particles. So another direction for the future work will be simultaneous controlling the polymorphism and size of crystals. One way to control the particle size is by confining the particle growth space, such as using reverse emulsions as nano-sized or micron-sized crystallizer. Another way to control both polymorphism and size of crystals is by using patterned SAMs as templates instead of uniform SAMs as we used in our research. Either the materials[68,114 115] or the space available for crystal growth will be limited by using patterned SAMs as templates for crystallization

References

(1) Cullity, B. D. *Element of X-ray diffraction*, 1978.

(2) Glusker, J. P.; Lewis, M.; Rossi, M. *Crystal structure analysis for chemists and biologists*, 1994.

(3) Jenkins, E. W. *The polymorphism of Elements and Compounds*, 1973.

(4) Brittain, H. G.; Byrn, S. R. Structural Aspects of polymorphism. In *Polymorphism in pharmaceutical solids*; Brittan, H. G., Ed., 1999; Vol. 95; pp 73-124.

(5) Beckmann, W.; Nickisch, K.; Budde, U. *Organic Process Research and Development* **1998**, *2*, 298-304.

(6) Nichols, G.; Frampton, C. S. *Journal of Pharmaceutical Sciences* **1998**, *87*, 684-689.

(7) Khoshkhoo, S.; Anwart, J. *J. phys. D: Appl. Phys.* **1993**, *26*, B90-B93.

(8) Chemburkar, S. R.; Bauer, J.; Deming, K.; Spiwek, H.; Patel, K.; Morris, J.; Henry, R.; Spanton, S.; Walter Dziki, W. P., John Quick, Phil Bauer, John Donaubauer, B. A. Narayanan, Mauro Soldani,; Dave Riley, a. K. M. *Organic Process Research & Development* **2000**, *4*, 413-417.

(9) Danesh, A.; X., C.; Davies, M. C.; Roberts, C. J.; Sanders, G. H. W.; Tendler, S. J. B.; Williams, P. M.; Wilkins, M. J. *Langmuir* **2000**, *16*, 866-870.

(10) Guillory, J. K. Generation of polymorphs, hydrates, solvates, and amorphous solids. In *Polymorphism in pharmaceutical solids*; Brittan, H. G., Ed., 1999; pp 183-226.

(11) Lewis, N. *Organic Process Research & Development* **2000**, *4*, 407-412.

(12) McCrone, W. C. Polymorphism. In *Physics and Chemistry of the Organic Solid State*; Fox, L., Weissberger, W., Eds., 1965; Vol. 2; pp 725-767.

(13) Grant, D. J. W. Theory and origin of polymorphism. In *Polymorphism in pharmaceutical solids*; Brittan, H. G., Ed., 1999; Vol. 95; pp 1-33.

(14) *Mineral physics & crystallography*; Ahrens, T. J., Ed.; Washington, DC : American Geophysical Union,:, 1995.

(15) Campbell, A. A. *Current opinionin colloid & interface science* **1999**, *4*, 40-45.

(16) Rieke, P. C. *Journal of Crystal Growth* **1997**, *182*, 472-484.

(17) Mann, S.; Ozin, G. A. *Nature* **1996**, *382*, 313-318.

(18) Ozin, G. A. *Acc. chem. res.* **1997**, *30*, 17-27.

(19) Weiner, s.; Addadi, L. *J. Mater. Chem.* **1997**, *7*, 689-702.

(20) Mann, S. *Nature* **1993**, *365*, 499-505.

(21) Weiner, S.; Addadi, L. *Trends in biochemical sciences* **1991**, *16*, 252-256.

(22) Gorski, J. P. *Calcified Tissue International* **1992**, *50*, 391-396.

(23) Heuer, A. H.; J., F. D.; Laraia, V. J.; Arias, J. L.; Calvert, P. D.; Kendall, K.; Messing, G. L. e.; Rieke, P. C.; Caplan, A. I. *Science* **1992**, *255*, 1098-1105.

(24) Mann, S. *Nature* **1988**, *332*, 119-124.

(25) Aizenberg, J.; Hanson, J.; Koetzle, T. F.; Weiner, S.; Addadi, L. *J. Am. Chem. Soc.* **1997**, *119*, 881-886.

(26) Berman, A.; Addadi, L.; Weiner, S. *Nature* **1988**, *331*, 546-548.

(27) Calvert, P.; Rieke, p. *Chem. Mater.* **1996**, *8*, 1715-1727.

(28) Fritz, M.; Belcher, A. M.; Radmacher, M.; Walters, D. A.; Hansma, P. K.; Stucky, G. D.; Morse, D. E.; Mann, S. *Nature* **1994**, *371*, 49-51.

(29) Hunter, G. K.; Kyle, L. C.; Goldberg, H. A. *Biochem. J.* **1994**, *300*, 723-728.

(30) Hunter, G. K.; Hauschka, P. V.; Poole, A. R.; Rosenberg, L. C.; Goldberg, H. A. *Biochemical Journal* **1996**, *317*, 59-64.

(31) Knobler. *Science* **1990**, *249*, 870-874.

(32) Moore, B. G.; Knobler, C. M. *J. Phys. Chem.* **1990**, *94*, 4588-4595.

(33) Moore, B. G.; Knobler, C. M.; Broseta, D.; Rondelez, F. *Chem. Soc. Faraday Trans.* **1986**, *82*, 1753-1761.

(34) Christodoulou, A. P.; Rosano, h. L. *Molecular association in biological and related system* **1968**, 210-223.

(35) Neuman, R. D. *Journal of colloid and interfacial science* **1975**, *56*, 505-510.

(36) Pezron, E.; Claesson, P. M.; Berg, J. M.; Vollhardt, D. *Journal of Colloid and Interface Science* **1990**, *138*, 245-254.

(37) Pilpel, N.; Enever, R. P. *Trans. Faraday Soc.* **1968**, *64*, 231-237.

(38) Mann, S.; Heywood, B. R.; Rajam, S.; Walker, J. B. A. *J. Phys. D* **1991**, *3*, 154-164.

(39) Landau, E. M.; Popovitz-Biro, R.; Levanon, M.; Leiserowitz, L.; Lahav, M.; Sagiv, J. *Journal of Liquid Crystals* **1986**, *134*, 323-335.

(40) Ulman, A. *Chem. Rev.* **1996**, *96*, 1533-1554.

(41) Swalen, J. D.; Allara, D. L.; Andrade, J. D.; Chandross, E. A.; Garoff, S.; Yu, H. *Langmuir* **1987**, *3*, 932-950.

(42) Brandow, S. L.; Chen, M.-S.; Aggarwal, R.; Dulcey, C. S.; Calvert, J. M.; Dressick, W. J. *Langmuir* **1999**, *15*, 5429-5432.

(43) Krishnan, S. Kinetics of Octadecyltrichlorosilane self-assembly on silicon oxide surfaces: an experimental and numerical study. PhD, City college of New York, 1999.

(44) Bain, C. D.; Whitesides, G. M. *J. Am. Chem. Soc.* **1989**, *111*, 7155-7164.

(45) Bain, C. D.; Whitesides, G. M. *J. Am. Chem. Soc.* **1989**, *111*, 7164-7175.

(46) Belcher, A. M.; Wu, X. H.; Christensen, R. J.; Hansma, P. K.; Stucky, G. D.; Morse, D. E. *Nature* **1996**, *381*, 56-58.

(47) Falini, G.; Albeck, s.; Weiner, S.; Addadi, L. *Science* **1996**, *271*, 67-69.

(48) Walters, D. A.; Smith, B. L.; Belcher, A. M.; Paloczi, G. T.; Stucky, G. D.; Morse, D. E.; Hansma, P. K. *Biophysical Journal* **1997**, *72*, 1425-2433.

(49) Zaremba, C. M.; Belcher, A. M.; Fritz, M.; Li, Y.; Mann, S.; Hansma, P. K.; Morse, D. E.; Speck, J. S.; Stucky, G. D. *Chem. Mater.* **1996**, *8*, 679-690.

(50) Mann, S.; Heywood, B. R.; Rajam, S.; Birchall, J. D. *Nature* **1988**, *334*, 692-695.

(51) Mann, S.; Heywood, B. R.; Rajam, S.; Birchall, J. D. *Proceeding of the Roal Society of London, A* **1989**, *423*, 457-471.

(52) Mann, S.; Heywood, B. R.; Rajam, S.; Walker, J. B. A. *Surface reactive peptides and polymers (book)* **1991**, 29-41.

(53) Lochhead, M. J.; letellier, S. R.; Vogel, V. *J. Phys. Chem. B* **1997**, *101*, 10821-10827.

(54) Litvin, A. L.; Valiyaveettil, S.; Kaplan, D. L.; Mann, S. *Advanced Materials* **1997**, *9*, 124-127.

(55) Landau, E. M.; Levanon, M.; Leiserowitz, L.; Lahav, M.; Sagiv, J. *Nature* **1985**, *318*, 353-356.

(56) Landau, E. M.; Wolf, S. G.; Levanon, M.; Leiserowitz, L.; Lahav, M.; Sagiv, J. *Journal of the American Chemical Society* **1989**, *111*, 1436-1445.

(57) Weissbuch, I.; Berfeld, M.; Bouwman, W.; Kjaer, K.; Als-Nielsen, J.; Lahav, M.; Leiserowitz, L. *J. Am. Chem. Soc.* **1997**, *119*, 933-942.

(58) Heywood, B. R.; Mann, S. *Journal of the American Chemical Society* **1992**, *114*, 4681-4686.

(59) Lin, H.; Seo, W. S.; Kuwabara, K.; Koumoto, K. *Journal of Ceramic Society of Japan* **1996**, *104*, 291-295.

(60) Unuma, H.; Ito, K.; T., O.; Takahashi, M. *J. Am. Ceram. Soc.* **1996**, *79*, 2474-76.

(61) Frostman, L. M.; Ward, M. D. *Langmuir* **1997**, *13*, 330-337.

(62) Swift, J. A.; Pivovar, A. M.; Reynolds, A. M.; Ward, M. *J. Am. Chem. Soc.* **1998**, *120*, 5887-5894.

(63) Letellier, R. S.; Lochhead, M. J.; Campbell, A. A.; Vogel, V. *Biochimica et biophysica Acta* **1998**, *1380*, 31-45.

(64) Kuther, J.; Tremel, W. *Chem. Commun.* **1997**, 2029-2030.

(65) Kuther, J.; Seshadri, R.; Knoll, W.; Tremel, W. *J. Mater. Chem.* **1998**, *8(3)*, 641-650.

(66) Kuther, J.; Tremel, W. *Thin Solid films* **1998**, *327-329*.

(67) Kuther, J.; Seshadri, R.; Nelles, G.; Assenmacher, W.; Butt, H. J.; Mader, W.; Tremel, W. *Chem. Mater.* **1999**, *11*, 1517-1523.

(68) Aizenberg, J.; Black, A. J.; Whitesides, G. M. *Nature* **1999**, *398*, 495-502.

(69) Aizenberg, J.; Black, A. J.; Whitesides, G. M. *J. Am. Chem. Soc.* **1999**, *121*, 4500-4509.

(70) Tarasevich, B. J.; Rieke, P. C.; Liu, J. *Chem. Mater.* **1996**, *8*, 292-300.

(71) Campbell, A. A.; Fryxell, G. E.; Graff, G. L.; Rieke, P. C.; Tarasevich, B. *Scanning Microscopy* **1993**, *7*, 423-429.

(72) Kang, J. F.; Zaccaro, J.; Ulman, A.; Myerson, A. *Langmuir* **2000**, *16*, 3791-3796.

(73) Frostman, L. M.; Bader, M. M.; Ward, M. D. *Langmuir* **1994**, *10*, 576-582.

(74) Ahn, D. J.; Berman, A.; Charych, D. *Journal of Physical Chemistry* **1996**, *100*, 12455-12461.

(75) Berman, A.; Ahn, D. J.; Lio, A.; Salmeron, M.; Reichert, A.; Charych, D. *Science* **1995**, *269*, 515-518.

(76) Lahiri, J.; Xu, G.; Dabbs, D. M.; Yao, N.; Aksay, I. A.; Groves , J. T. *J. Am. Chem. Soc.* **1997**, *119*, 5449-5450.

(77) Xu, G.; Yao, N.; Aksay, I. A.; Groves, J. T. *J. Am. Chem. Soc.* **1998**, *120*, 11977-11985.

(78) Chen, B.-D.; Davey, R. J.; Garside, J. *ICHemE (the 1997 jubilee research event)* **1997**.

(79) Chen, B.-D.; Cilliers, J. J.; Davey, R. J.; Garside, J.; Woodburn, E. T. *J. Am. Chem. Soc.* **1998**, *120*, 1625-1626.

(80) Archibald, D. D.; Qadri, S. B.; Gaber, B. P. *Langmuir* **1996**, *2*, 538-566.

(81) Enever, R. P.; Pilpel, N. *Trans. Faraday Soc.* **1967**, *63*, 781.

(82) Enever, R. P.; Pilpel, N. *Trans. Faraday Soc.* **1967**, *63*, 1559-1566.

(83) Fainerman, V. B.; Vollhardt, D.; Johann , R. *Langmuir* **2000**, *16*, 7731.

(84) Johann, R.; Brezesinski, G.; Vollhardt, D.; Mohwald, H. *J. Phys. Chem. B* **2001**, 2957.

(85) Johann, R.; Vollhardt, D.; Mohwald, H. *Langmuir* **2001**, *17*, 4569.

(86) Xu, S.; Miyano, K.; Abraham, B. M. *Journal of colloid and interface science* **1982**, *89*, 581-583.

(87) Rapaport, H.; Kuzmenko, I.; Berfeld, M.; Kjaer, K.; Als-Nielsen, J.; Popovitz-Biro, R.; Weissbuch, I.; Lahav, M.; Leiserowitz, L. *J. Phys. Chem. B* **2000**, *104*, 1399-1428.

(88) Kitano, Y. *Bull chem. Soc. Japan* **1962**, *35*, 1980-1985.

(89) Skoog, D. A.; West, M. M. *Fundamentals of analytical chemistry*, 1963.

(90) Deamer, D. W.; Cornwell, D. G. *Biochimmica ET Biophysica ACTA* **1966**, *116*, 555-562.

(91) Kissa, E. *Fluorinated surfactants: synthesis, properties, applications*, 1994.

(92) Flath, J.; Meldrum, F. C.; Knoll, W. *Thin solid films* **1998**, *327-329*, 506.

(93) Liu, J.; Kim, A. Y.; Wang, L. Q.; Palmer, B. J.; Chen, Y. L.; Bruinsma, P.; Bunker, B. C.; Exarhos, G. J.; Graff, G. L.; Rieke, P. C.; Fryxell, G. E.; Virden, J. W.; Tarasevich, B. J.; Chick, L. A. *Advances in colloid and interface science* **1996**, *69*, 131-180.

(94) Petri, D. F. S.; Wenz, G.; Schunk, P.; Schimmel, T. *Langmuir* **1999**, *15*, 4520-4523.

(95) Kumar, N.; Maldarelli, C.; Steiner, C.; Couzis, A. *Langmuir* **2001**, *17*, 7789.

(96) Meyer, H. J. *Zeitschrift fur Kristallographie* **1969**, *128*, 183-212.

(97) Kamhi, S. *Acta Cryst.* **1963**, *16*, 770-772.

(98) Hooper, A. E.; Werho, D.; Hopson, T.; Palmer, O. *Surf. Interface Anal.* **2001**, *31*, 809.

(99) Popovitz-Biro, R.; Wang, J. L.; Majewski, J.; Shavit, E.; Leiserowitz, L.; Lahav, M. *J. Am. Chem. Soc.* **1994**, *116*, 1179.

(100) Fujimoto, Y.; Ozaki, Y. *Chemical physics letters* **1992**, *196*, 347.

(101) Gericke, A.; Huhnerfuss, H. *J. Phys. Chem.* **1993**, *97*, 12899.

(102) Du, X.; Shi, B.; Liang, Y. *Langmuir* **1998**, *14*, 3631-3636.

(103) Gericke, A.; Huhnerfuss, H. *Langmuir* **1995**, *11*, 225.

(104) Hasegawa, T.; Nishijo, J.; Watanabe, M.; Umemura, J.; Ma, Y.; Sui, G.; Huo, Q.; Leblanc, R. M. *Langmuir* **2002**, *18*, 4758.

(105) Couzis, A.; Gulari, E. *Langmuir* **1993**, *9*, 3414.

(106) Cheng, S. S.; Scherson, D. A.; Sukenik, C. N. *Langmuir* **1995**, *11*, 1190.

(107) Marshbanks, T. L.; Ahn, D. J.; Franses, E. I. *Langmuir* **1994**, *10*, 276.

(108) Kumar, N. Study of Adsorption of Trisiloxane Surfactants on Air-Water and Hydrophobic Solid-Water Interface: An Attempt to Explain the "Super-Spreading" Behavior. PhD, City College of New York, 2001.

(109) Flach, C. R.; Brauner, J. W.; Mendelsohn, R. *Biophysical Journal* **1993**, *65*, 1994.

(110) Gericke, A.; Huhnerfuss, H. *Thin Solid Films* **1994**, *245*, 74.

(111) Kawai, T.; Umemura, J.; Takenaka, T. *Langmuir* **1990**, *6*, 672.

(112) Kubota, M.; Ozaki, Y.; Araki, T.; Ohki, S.; Iriyama, K. *Langmuir* **1991**, *7*, 774.

(113) Brecevic, L.; Nielsen, A. E. *Journal of crystal growth* **1989**, *98*, 504-510.

(114) Thalladi, V. R.; Whitesides, G. M. *J. Am. Chem. Soc.* **2002**, *124*, 3520.

(115) Zhong, Z.; Gates, B.; Xia, Y.; Qin, D. *Langmuir* **2000**, *16*, 10369.